Master's thesis

NTNU
Norwegian University of Science and Technology
Faculty of Medicine and Health Sciences
Kavli Institute for Systems Neuroscience

Erik Justin Courcelles

Investigation of the topographic organization of feedback projections from perirhinal cortex to primary somatosensory and visual cortices in the mouse

Master's thesis in MSc in Neuroscience
Supervisor: Maximiliano Jose Nigro
May 2023

NTNU
Norwegian University of
Science and Technology

Erik Justin Courcelles

Investigation of the topographic organization of feedback projections from perirhinal cortex to primary somatosensory and visual cortices in the mouse

Master's thesis in MSc in Neuroscience
Supervisor: Maximiliano Jose Nigro
May 2023

Norwegian University of Science and Technology
Faculty of Medicine and Health Sciences
Kavli Institute for Systems Neuroscience

NTNU
Norwegian University of
Science and Technology

Abstract

The perirhinal cortex is a medial temporal lobe area considered part of the parahippocampal formation and has been shown to have prominent interconnectivity with cortices of all sensory modalities in rats and primates. This multisensory nature has been thought to be integral for the functions of perirhinal cortex such as in object recognition memory which requires sensory information for stimulus discrimination. Projections from the perirhinal cortex back to sensory cortices are termed feedback connections and have been described to affect sensory perception by modulating the feedforward sensory signal. Efferents from perirhinal cortex to superficial layers of the mouse barrel cortex have been shown in mice. However, projections from perirhinal cortex to deep layers of mouse barrel cortex as well as to any layer of primary visual cortex have not yet been described in mice. The primary aim of this study is therefore to investigate the feedback projections from perirhinal cortex to the primary somatosensory and primary visual cortices in mice. To describe the topography and laminar distribution of perirhinal cortex feedback neurons, I stereotaxically injected retrograde tracers in layer 6 of the barrel cortex and primary visual cortex in mice. I found that the perirhinal cortex projects to layer 6 of both mouse barrel cortex and primary visual cortex. Furthermore, I show that the neurons in the perirhinal cortex projecting to these cortices are primarily localized in deep layers, consistent with previous descriptions for feedback type neurons. Perirhinal feedback neurons to the mouse barrel cortex primarily originated in rostral perirhinal cortex, while perirhinal feedback neurons to primary visual cortex originated in a rostrocaudal level following the rostrocaudal level of the injection site. This study provides novel findings surrounding the efferent connectivity of perirhinal cortex which can aid in future research of the perirhinal cortex using the mouse as model animal.

Sammendrag

Perirhinal cortex er et medialt temporallappområde som anses som en del av parahippocampiske formasjonen og har vist seg å ha fremtredende sammenkobling med cortex av alle sensoriske modaliteter hos rotter og primater. Denne multisensoriske naturen har blitt antatt å være viktig for funksjonene til perirhinal cortex, slik som i objektgjenkjenningsminne som krever sensorisk informasjon for stimulusdiskriminering. Projeksjoner fra perirhinal cortex tilbake til sensoriske cortex kalles feedback projeksjoner og har blitt beskrevet å påvirke sensorisk persepsjon ved å modulere det feedforward sensoriske signalet. Efferenter fra perirhinal cortex til overfladiske lag av mouse barrel cortex er vist hos mus. Imidlertid er projeksjoner fra perirhinal cortex til dype lag av mouse barrel cortex, og til hvilket som helst av lagene av primær visuell cortex, enda ikke blitt beskrevet hos mus. Hovedmålet med denne studien er derfor å undersøke feedback projeksjonene fra perirhinal cortex til de primære somatosensoriske og primære visuelle cortexene hos mus. For å beskrive topografien og laminær distribusjon av perirhinale cortex feedback nevroner, injiserte jeg stereotaksisk retrograde sporstoffer i lag 6 av mouse barrel cortex og primær visuell cortex i mus. Jeg fant ut at den perirhinale cortex projiserer til lag 6 av både mouse barrel cortex og primær visuell cortex. Videre viser jeg at nevronene i perirhinal cortex som projiserer til disse cortexene, primært er lokalisert i dype lag, i samsvar med tidligere beskrivelser for feedback type nevroner. Perirhinale feedback nevroner til mouse barrel cortex oppsto primært i rostrale perirhinal cortex, mens perirhinale feedback nevroner til primær visuell cortex oppsto i et rostrocaudalt nivå som følger det rostrocaudale nivået til injeksjonsstedet. Denne studien viser nye funn rundt den efferente tilkoblingen til perirhinal cortex som kan hjelpe til med fremtidig forskning av perirhinal cortex ved å bruke musen som modelldyr.

Table of Contents

Figures

Tables

Abbreviations

PER	Perirhinal cortex
A36	Brodmann area 36
A35	Brodmann area 35
CA1	Cornu ammonis 1
STS	Superior temporal sulcus
STG	Superior temporal gyrus
L1-6	Cortical layers 1 to 6
V2	Secondary visual cortex
GABA	γ-aminobutyric acid
PV	Parvalbumin
SST	Somatostatin
VIP	Vasoactive intestinal peptide
5HT3aR	Ionotropic serotonin receptor
FF	Feedforward
FB	Feedback
V1	Primary visual cortex
V3	Visual area 3
V4	Visual area 4
S1	Primary somatosensory cortex
NTNU	Norwegian University of Science and Technology
FOTS	Forsøksdyrsforvaltningens tilsyns- og søknadssystem
CtB	Choleratoxin subunit B
GM1	Monosialotetrahexosylganglioside
AF	Alexa Fluor
wS1	Mouse barrel cortex
Tev	Ventral temporal cortex
PFA	Paraformaldehyde
PB	Phosphate buffer
NaCl	Sodium chloride

KCl	Potassium chloride
$NaHCO_3$	Sodium bicarbonate
NeuN	Neuronal nuclei
NGS	Normal goat serum
LPtA	Lateral parietal association cortex
PTPR	Rostral posterior parietal cortex
ec	External capsule
TeA	Temporal association cortex
LEC	Lateral entorhinal cortex
AP	Anterior-Posterior coordinate
S1DZ	Dysgranular zone of S1
V2M	Medial secondary visual cortex
SD	Standard deviation

1 Introduction

The perirhinal cortex (PER) is a medial temporal lobe area commonly described as part of the parahippocampal formation, and PER has been shown to have interconnectivity to other medial temporal lobe regions such as the entorhinal cortex, amygdala and hippocampus (Kealy & Commins, 2011; Suzuki & Naya, 2014; Witter et al., 2000). The medial temporal lobe areas are essential for declarative memory (Squire et al., 2004), and the connectivity between PER and the various other medial temporal lobe areas further implies how PER should have a role in memory. This has indeed been shown in rats and primates to be the case for mnemonic functions such as recognition memory, fear conditioning and spatial memory (Kealy & Commins, 2011; Suzuki & Naya, 2014). Furthermore, PER receives information from sensory cortices of all modalities and is believed to integrate the multisensory information to perform its roles in functions such as object recognition memory or perceptual discrimination of complex stimuli (Suzuki & Naya, 2014; Winters & Reid, 2010).

Projections from higher order areas to lower order areas in terms of cortical hierarchy are referred to as feedback projections, while feedforward refers to the projections ascending in the hierarchy. Feedback pathways have been described as the only neural system capable of implementing the regulation of neural activity necessary for complex, goal-directed behaviors (Zagha, 2020), and are proposed to do this by modulating the feedforward pathways of lower order areas. The feedback projections from PER are shown to contribute to learning and memory (Doron et al., 2020; Higuchi & Miyashita, 1996), and could also possibly affect sensory processing in primary sensory cortices.

1.1 Basic anatomy of the perirhinal cortex

PER is composed of two rostrocaudally oriented bands of cortex: the dorsal Brodmann area 36 (A36) often also referred to as ectorhinal cortex (Franklin & Paxinos, 2008), and the ventral area 35 (A35) often referred to as simply perirhinal cortex (*Allen Reference Atlas - Mouse Brain*, 2011; Franklin & Paxinos, 2008). In this thesis PER is used to refer to A35 and A36 as a whole. PER is associated with the rhinal fissure for its entire rostrocaudal extent, where rostrally A36 is situated approximately at the fundus of the rhinal fissure while A35 is situated ventral to the fissure (Beaudin et al., 2013). Proceeding from rostral to caudal PER, it rises in position relative to the fundus of the rhinal fissure until both A35 and A36 lie above the fundus. The cytoarchitecture of PER is characterized by how layer 4 (L4) is absent entirely in A35, while in A36 L4 is barely discernable only in sections in the horizontal plane (Beaudin et al., 2013). In rats and monkeys, this cytoarchitecture is noted to be differentiated across the rostrocaudal and dorsoventral or mediolateral axes, respectively for each species (Burwell et al., 1995), which exemplifies how PER is heterogenous as an area.

1.2 Connectivity of the perirhinal cortex

PER has specifically been described to have prominent interconnectivity with cortical areas of several different sensory modalities in primates and rats (Kealy & Commins, 2011; Suzuki & Naya, 2014), as well as intrinsic connectivity shown within PER postulated to integrate this multisensory information (Burwell & Amaral, 1998b; Lavenex et al., 2004). The specific detailing of these cortical interconnections seem to vary from

species to species (Suzuki, 2009; Suzuki & Naya, 2014), which is possibly in part due to the different species' reliance on specific sensory modalities. Furthermore, it has been shown that the topography of cortical inputs to PER vary along its rostrocaudal axis in rodents, cats and primates (Burwell & Amaral, 1998a; Foroughi, 2022; Room & Groenewegen, 1986; Suzuki & Amaral, 1994), as well as for outputs of PER in rats, cats and primates (Agster & Burwell, 2009; Lavenex et al., 2002; Witter & Groenewegen, 1986). The rostrocaudal pattern of connectivity seems to follow a general rule of rostral cortices projecting to rostral PER, with caudal cortices projecting to caudal PER, but this rule is not absolute. This clearly paints a picture of PER as an area which is heterogenous in its connectivity patterns along its rostrocaudal axis. The cytoarchitecturally different A35 and A36 of PER are also shown to further differ in connectivity patterns in rats and primates (Agster & Burwell, 2009; Burwell & Amaral, 1998a; Suzuki & Amaral, 1994) which emphasizes the importance in making this distinction between the two subdomains of PER. To understand the current consensus of PER interconnectivity as well as what has yet to be investigated, a description of the afferent and efferent connectivity of PER is described below.

1.2.1 Afferent connectivity

PER has been described to receive inputs from a wide variety of both cortical and subcortical areas in primates and rats. As for hippocampal and parahippocampal areas, PER receives inputs from CA1 of the hippocampus, subiculum, entorhinal cortex, postrhinal cortex in rats and parahippocampal cortex in primates (Kealy & Commins, 2011; Suzuki & Naya, 2014). Input from subcortical areas that relate to PER's assumed role in multisensory integration and associative memory, these being the amygdala and various thalamic nuclei, have also been described in rats (Pereira et al., 2016; van Groen et al., 1999). As mentioned, PER has been shown to receive input from a wide range of cortical areas, some examples shown in both primates and rats being areas in the frontal lobe, temporal lobe, parietal lobe and insular cortex (Burwell & Amaral, 1998a; Suzuki & Amaral, 1994). As for specifically sensory afferents in primates, regions that relate to somatosensory, visual and auditory information have all been described (Suzuki & Amaral, 1994). In rats, inputs from sensory regions relating to somatosensory, visual, auditory and olfactory information have been described (Burwell & Amaral, 1998a). In this current thesis the sensory interconnectivity of PER is in focus, and thus a concise summary of findings surrounding unimodal sensory afferents to PER in primates, rats, and mice is described below.

Sensory afferents in primates

Primate cortical afferents to PER was investigated by Suzuki & Amaral (1994), where they injected retrograde tracers into different rostrocaudal and dorsoventral levels of PER in macaque monkeys (Suzuki & Amaral, 1994).

Temporal lobe inputs to PER include the unimodal visual areas TE and TEO of the inferotemporal cortex (Suzuki & Amaral, 1994). When comparing retrograde tracer injections into three different rostrocaudal levels of PER, they find that rostral area TE seems to preferentially innervate rostral PER, while caudal TE and TEO seems to preferentially innervate caudal PER. Unimodal visual area input from the ventral bank of the superior temporal sulcus (STS) was also described, with patches of cortex in the rostral regions providing strong input to rostral PER, and caudal PER injections resulting

in less dense labeling and did not show any preference in rostrocaudal distribution in the ventral bank of STS.

As for input from areas that relate to somatosensory information however, PER in primates have not been described to receive this from parietal areas, but are only noted to potentially receive this from the insula (Suzuki & Amaral, 1994; Suzuki & Naya, 2014). The insula is a multisensory area that is described to not only receive somatosensory information, but information from all modalities (Gogolla, 2017), and as such is termed a polymodal area. The pattern of input from the insular cortex to PER seemed to not preferentially innervate either rostral or caudal A36 as well as A35, but rather all projected in a similar manner to PER (Suzuki & Amaral, 1994). Other polymodal sensory areas that input to PER in primates is the dorsal bank of the STS (Suzuki & Amaral, 1994), which seemingly preferentially innervated A35 over A36. The dorsal bank of STS is shown to respond to visual, auditory and somatosensory stimuli in single cell recordings in primates (Bruce et al., 1981), so it is alike the insular cortex a polymodal area. Given the current description of the connectivity of PER in primates, somatosensory information can only input to PER through these various polymodal regions.

As for auditory input to PER, input from the rostral portion of the superior temporal gyrus (STG) was shown (Suzuki & Amaral, 1994). They note that rostral STG responds to both visual and auditory stimuli, and weak labeling in rostral STG was observed as a result of injections into both A36 and A35.

Sensory afferents in rats

In a study by Burwell & Amaral (1998), rat afferents were investigated from many different cortical areas by injecting retrograde tracers into different rostrocaudal levels of PER, postrhinal and entorhinal cortex (Burwell & Amaral, 1998a). In focus here are their results surrounding unimodal sensory afferents to PER.

Olfactory information was defined as traveling through inputs from the piriform cortex and was shown to project to both A35 and 36 (Burwell & Amaral, 1998a). A35 receives more of its total input from piriform cortex than A36, and the input is more heavily weighted to rostral A35 than caudal A35. Furthermore, the projections primarily originate in caudal piriform cortex L2/3 and terminates in superficial layers of PER.

Input from the temporal lobe, where some areas that relate to visual and auditory sensory information reside, was also shown (Burwell & Amaral, 1998a). The auditory regions are described to preferentially innervate rostral A36, while the visual postrhinal cortex preferentially innervates caudal A36. Of note is also how the input originates in L2/3 in the postrhinal cortex, but from L2, L5 and L6 of the other temporal regions.

Input from parietal areas, of which primary and secondary somatosensory cortex are specifically mentioned, is also shown in rats (Burwell & Amaral, 1998a). Primary somatosensory cortex was only found to project specifically to the rostral extreme of PER, and secondary somatosensory cortex is mentioned to input more strongly to rostral than caudal A36. For A35, all rostrocaudal levels are noted to receive input from the parietal areas. The inputs originate from L2, L5 and L6 across the parietal areas.

Input from occipital areas, of which include visual association cortices, is also shown to go to PER in rats (Burwell & Amaral, 1998a). Input from lateral and medial visual areas are both noted to terminate in the extreme caudal level of A36, and little to no input is provided to the rest of A36 or A35. The projections are noted to arise in all rostrocaudal

levels of the medial and lateral visual areas, but projects more strongly from the caudal part of the medial visual areas. The inputs originate from L2, L5 and L6 of the visual areas.

Sensory afferents in mice

In a study done by Foroughi of the Nigro lab at NTNU (Foroughi, 2022), the afferents to mouse PER from sensory areas were investigated by injecting retrograde tracers into different rostrocaudal levels of PER.

Olfactory regions, of which was defined as piriform cortex afferents, was shown to project to PER (Foroughi, 2022). The input was greater to caudal PER than rostral PER, and the retrograde injection that reached into A35 showed a greater proportion of total inputs from piriform cortex than the other injections in A36. This result is in accordance with the rat piriform afferent findings (Burwell & Amaral, 1998a) that show a stronger weighting towards A35 than A36. The projections seem to predominantly originate from caudal piriform cortex relative to rostral piriform cortex, which also is consistent with the rat findings (Burwell & Amaral, 1998a).

Somatosensory information arriving from primary and secondary somatosensory cortex and barrel cortex specifically were all shown to project to PER (Foroughi, 2022). Injections into rostral PER resulted in higher proportional labeling of the somatosensory areas than injections into caudal PER, indicating that somatosensory areas input more strongly onto rostral PER. It was also noted that most of the somatosensory input to PER originates in caudal somatosensory areas.

Auditory information from primary and secondary auditory regions was also shown to project to PER (Foroughi, 2022), however the distribution of this input was noted to be more complex in the study. Rostral auditory cortex seemed to preferentially innervate rostral PER, while caudal auditory cortex seemed to preferentially innervate caudal PER. However, the highest proportion of auditory input was from the injections that hit both A35 and 36 and was largely located to superficial layers while omitting any injection bolus in L6. Conversely, the lowest proportion of auditory input were from the injections that targeted deep layers and were primarily located in A35 while omitting A36.

Visual areas were defined as primary and secondary visual cortex, as well as postrhinal cortex, and was shown to project to PER (Foroughi, 2022). The postrhinal cortex was recognized within the study as receiving information from multiple sensory modalities, but was still defined as a visual area in accordance with the Wang & Burkhalter (2007) definition of postrhinal cortex as a visual area (Wang & Burkhalter, 2007). The input from visual areas was stronger to caudal PER relative to rostral PER. Additionally, injections into deep layers of caudal PER mainly targeting A35 resulted in the highest proportion of visual input. Furthermore, lateral V2 preferentially targeted rostral PER while medial V2 preferentially targeted caudal PER. Input from postrhinal cortex also preferentially targeted caudal PER but elicited the strongest proportion of labeling in PER from injections in superficial layers of PER relative to injections in deep layers.

1.2.2 Efferent connectivity

PER has been shown to provide output to a multitude of cortical areas in primates and rats (Agster & Burwell, 2009; Lavenex et al., 2002), and subcortical areas in rats (Agster et al., 2016). As for cortical areas specifically, projections to piriform, frontal, insular,

temporal, cingulate, parietal and occipital regions have all been shown in rats (Agster & Burwell, 2009). In primates, the temporal, frontal, insular, cingulate and parietal areas have all been shown to receive projections from PER (Lavenex et al., 2002). In rats, PER has also been shown to provide outputs to subcortical areas, such as the basal ganglia, the amygdala, various thalamic nuclei and olfactory structures (Agster et al., 2016). Various hippocampal and parahippocampal areas have been shown to receive projections from PER in rats, such as CA1 of the hippocampus, subiculum, entorhinal cortex and postrhinal cortex (Kealy & Commins, 2011). As for efferents to sensory areas, regions that relate to visual, somatosensory and auditory information have all been shown in primates (Lavenex et al., 2002). In rats, efferents to regions related to somatosensory, visual, auditory and olfactory information have been described (Agster & Burwell, 2009). Following is a summary of findings surrounding sensory efferents from PER in primates, rats, and mice.

Sensory efferents in primates

In primates, efferents from PER to various polymodal and unimodal sensory areas were investigated by Lavenex, et al. (2002) by injecting anterograde tracers into various rostrocaudal and dorsoventral levels of PER in macaque monkeys (Lavenex et al., 2002). However, most of these injections were located in various levels of A36 specifically, with only two of fifteen injections having some spill into A35. The authors do not mention anything specifically for A35 throughout the study, and as such it is to be assumed that only efferents of A36 of PER are described here in primates.

As for projections from PER to the temporal lobe, A36 was found to project heavily to the unimodal visual area TE (Lavenex et al., 2002) with stronger projections to medial relative to lateral area TE. A36 was also found to project to the entire rostrocaudal extent of TEO, another unimodal visual area, as well as to the rostral part of the ventral bank of the polymodal STS. The rostral and medial part of the dorsal bank of the STS also receives projections from A36, as well as the most rostral aspect of the fundus of the STS. For the projections to TE and TEO, they note that these terminate predominantly in L1. For STS, they show that PER innervates all superficial layers, in particular L2/3 with less labeling in L1.

Output from PER to the insular cortex was also described (Lavenex et al., 2002). The insular cortex is an area that for all its regions receives sensory information from all modalities and is postulated to function as an integration hub for this information (Gogolla, 2017). Projections from A36 to granular insula, dysgranular insula and agranular insula as well as the parainsular cortex were all shown (Lavenex et al., 2002). The rostrocaudal distribution of outputs in PER lead to slightly different labeling in the insular cortex. Rostral PER seems to innervate granular, dysgranular and agranular insula, while caudal PER seems to only innervate dysgranular and agranular insula and only slightly the parainsular cortex. They note that input from PER to granular insular cortex preferentially innervates L1, while for the parainsular cortex it preferentially innervates L2/3 with less observed labeling in L1.

Output from PER to somatosensory parietal areas was not found in primates (Lavenex et al., 2002). This is consistent with the afferent input to PER, where there was found to be no input from somatosensory parietal areas to PER (Suzuki & Amaral, 1994). This means that PER has not been found to provide any efferent output to any unimodal somatosensory region in primates, and as such all output to regions that relate to somatosensory information would be to polymodal areas.

Sensory efferents in rats

In a study done by Agster & Burwell in rats (2009), they investigated PER efferents to several cortical areas by injecting anterograde tracers into various rostrocaudal levels of both A35 and A36 (Agster & Burwell, 2009).

Piriform areas relating to olfactory information were shown to receive projections from PER (Agster & Burwell, 2009). The labeling was weak but consistent across the entirety of piriform cortex. They further show that the injection that resulted in the strongest labeling in the piriform cortex was into midrostrocaudal A36 and hit all layers. The rostral A36 deep layer injection as well as the rostral A35 injection that hit all layers both resulted in a slightly weaker labeling. The injections which resulted in the weakest labeling of all were the ones into caudal A35 and 36 and that hit all layers. Overall, this indicates that midrostrocaudal to rostral PER are the rostrocaudal levels where PER output neurons to piriform cortex preferentially reside, with no apparent preference for either A35 or A36. A difference in topography is noted in that injections into A35 resulted in labeling in all rostrocaudal levels of piriform cortex, while rostral A36 injections preferentially labeled rostral piriform cortex and caudal injections preferentially labeled caudal piriform cortex. Labeled fibers were found in all layers of the piriform cortex and were heaviest in L1 and L3.

PER was also shown to project to temporal areas of which unimodal auditory areas are found in rats (Agster & Burwell, 2009). Both ventral auditory cortex which is considered auditory association cortex, as well as primary auditory cortex were both labeled by injections into both A35 and 36. The projections to these auditory areas were slightly stronger from A36, and L1-3 and L6 were preferentially labeled.

Primary and secondary somatosensory cortex of the parietal lobe, which relate to somatosensory information, as well as the polymodal posterior parietal cortex were also shown to receive prominent projections from PER (Agster & Burwell, 2009). Rostral PER injections resulted in stronger labeling of primary and secondary somatosensory cortex, especially so for rostral A36 injections specifically. Labeling was greatest in L1-3, and in caudal somatosensory cortex. The largest labeling following rostral PER injections was in primary somatosensory cortex, which was noted to be unexpected as the secondary somatosensory cortex provides the most afferent input to PER (Burwell & Amaral, 1998a) and the projections were believed to be reciprocal. As for the polymodal posterior parietal cortex, labeling was greater as a result of A36 injections relative to A35 injections and was found primarily in superficial layers (Agster & Burwell, 2009).

Occipital regions of which relate to visual information were shown to receive projections from PER (Agster & Burwell, 2009). The primary visual cortex, as well as lateral and medial secondary visual cortex were investigated. Caudal PER injections lead to strongest labeling of all occipital areas, including the primary and secondary visual cortices. Projections to lateral secondary visual cortex were more dense than medial secondary visual cortex and primary visual cortex, and projections from A36 were slightly stronger than from A35 although the difference was quite small. The projections from PER were noted to preferentially innervate superficial layers.

Substantial projections to insular cortex from PER were also shown (Agster & Burwell, 2009). Injections into rostral PER resulted in highest density of labeled fibers in all insular regions, and there was no notable difference in density between A35 and A36 injections. A35 injections resulted in labeling in L2-5 of the entire insular cortex. For A36 injections,

fibers to the rostral part of the dorsal agranular insular cortex were primarily labeled in L1-3 but shifted to L5 and L6 caudally. In the posterior agranular insular cortex, A36 injections preferentially labeled L5 and L6. They do note that labeled fibers in visceral and gustatory regions of insular cortex were observed in both deep and superficial layers, with either L1 or L6 being labeled the heaviest.

Sensory efferents in mice

In mice, no large study on perirhinal cortex efferents has been performed yet. However, there are some recent studies of PER that elucidate some of the efferents of PER in mice as part of their study.

In a study performed by Doron et al. (2020), they investigated how perirhinal input to neocortical L1 controls learning (Doron et al., 2020). They show that PER in mice projects to L1 of S1 specifically by injecting retrograde tracers into L1 of S1, and they note that this labeled cells in deep layers of PER. They also inject an adeno-associated virus containing channelrhodopsin and yellow fluorescent protein into deep layers of PER and found that this densely labels axons in L1 of S1. These results confirm that PER projects to L1 of S1 in mice.

Another study in mice which give us a more detailed look at what cell types receive this efferent input from PER in L1 of S1 was performed by Naskar et al. (2021), investigating cell-type-specific recruitment of GABAergic interneurons in the primary somatosensory cortex by long-range inputs (Naskar et al., 2021). The nomenclature they follow is of ectorhinal cortex and perirhinal cortex as two distinct areas, referring to A36 and A35 respectively. As mentioned previously, in this thesis these two areas in combination are referred to as perirhinal cortex. They first identify that PER projects to the supragranular L1-3 of S1 through injection of retrograde viral tracers into these layers of S1. The interneurons were categorized based on whether they expressed parvalbumin (PV), somatostatin (SST), vasoactive intestinal peptide (VIP) or were non-VIP 5HT3aR interneurons, four groups that altogether are believed to account for nearly all interneurons in the neocortex (Tremblay et al., 2016). The long-range efferents from PER to supragranular layers of S1 did not preferentially innervate any inhibitory interneuron subtype over pyramidal neurons but were found to provide significantly much weaker input to SST interneurons relative to pyramidal neurons (Naskar et al., 2021). This paints a picture of PER output to S1 supragranular layers as innervating all four types of GABAergic interneurons as well as pyramidal neurons.

1.3 Function of the perirhinal cortex

The main behavioral function attributed to PER as part of the parahippocampal formation is its role in recognition memory (Kealy & Commins, 2011; Suzuki & Naya, 2014), but PER has also been shown to play a role in other mnemonic functions such as in fear conditioning and spatial memory (Kealy & Commins, 2011). PER has been implicated in object recognition memory, a form of recognition memory that intuitively relies on visuotactile information, especially so for rats and mice that rely quite strongly on information from their whiskers for such a task. An example study exemplifying PER's role in object recognition in rats is by Winters & Reid (2010) investigating crossmodal object recognition (Winters & Reid, 2010). Rats were tasked to investigate a Y-maze and explore objects using tactile and/or visual information. During the first trial the rats are placed into the long end of the Y-maze and could explore two objects, one in each end of

the forked end of the maze. During the second trial one object is replaced with a novel object while the other is replaced with an identical object as the one previously placed there. If an object is novel, rats are expected to spend more time exploring it (Ennaceur & Delacour, 1988), and Winters & Reid (2010) quantified this time spent by the rats exploring each object to determine if object recognition memory was retained as a result of bilateral PER lesions (Winters & Reid, 2010). During tactile-only trials, PER lesioned rats performed similar to controls in discriminating between a familiar and novel object. However, during visual-only trials lesioned rats were significantly impaired in their ability to recognize the novel object. Furthermore, during crossmodal trials where the objects were first explored using only tactile information and the rats were tasked to recognize the object using only visual information afterwards, the lesioned rats were significantly impaired in their ability to recognize the object. These results show that not only does bilateral PER lesions impair purely visual object recognition in rats, but also impairs crossmodal object recognition memory between the tactile and visual modalities in rats. This study shows how PER uses multisensory information when performing its role in object recognition memory, and furthermore shows why it is important to study the multisensory connectivity and integration of PER.

PER has also been described to play a role in non-mnemonic perception as well, where this is described as largely revolving around PER's overarching function of discriminating between sensory stimuli (Kealy & Commins, 2011). Eacott et al. (2001) investigated the performance of rats in a visual discrimination learning task following lesions of PER (Eacott et al., 2001). In this experiment, the rats were tested in discriminating visual stimuli that increase in complexity. They found that the performance of PER lesioned rats was similar to control for simple visual form discrimination, but was impaired during discrimination of complex stimuli with overlapping features. The explanation for this impairment is not due to a deficit in recognition memory of a specific discriminant as all the discriminants were highly and equally familiar. This implicates PER in being directly involved with the sensory processing of highly complex visual information, and not just the memory of these multifeature objects.

1.4 Feedback connections

In the cortical hierarchy of the brain, feedforward (FF) connections refer to ascending projections from lower order to higher order cortical areas, while feedback (FB) connections refer to the descending projections from higher order to lower order cortical areas (Felleman & Van Essen, 1991). As PER is well described as an area high up in the cortical hierarchy (Felleman & Van Essen, 1991), projections going from PER to these areas would be categorized as FB connections. FB neurons are pyramidal cells, and have been shown to innervate both GABAergic and pyramidal neurons in the recipient cortex (Zagha, 2020).

1.4.1 Anatomy of feedforward versus feedback projections

To describe the current understanding of the specific anatomy of feedback projections, some light will be shed on feedforward projections as well to compare the differences in the two distinct pathways.

Feedforward and feedback pathways are commonly defined as such based on the origin of the output neuron and the layers that are innervated in the receiving cortex (Felleman

& Van Essen, 1991). Felleman & Van Essen (1991) describe FF ascending pathways as predominantly originating from supragranular layers and innervating the granular L4, while FB pathways predominantly originate in infragranular layers and innervate both the supragranular and infragranular regions. They also note that a few pathways originate in a bilaminar pattern, meaning of roughly equal supragranular and infragranular origin, yet still innervate in either the FF or the FB motif (Felleman & Van Essen, 1991). However, they also show that the occurrence of these bilaminar output neurons is greatly restricted to areas of the closest two levels in the hierarchy, and as such would presumably not be occurring often between PER and primary sensory cortices as the hierarchical distance is much larger in primates.

As a refinement of the early findings of laminar organization of FF and FB pathways, Markov et al. (2014) investigated the anatomy of cortical hierarchy in primates and sheds some light on the laminar location of FF and FB neurons in the visual cortex (Markov et al., 2014). They note that although FF and FB neurons predominantly originate in the supragranular and infragranular regions respectively and this has been well described previously (Felleman & Van Essen, 1991), there is a notable population of FF and FB neurons in the opposite region as well. Markov et al. (2014) injected retrograde tracers into various visual areas, and find that FF and FB neuron origins become increasingly concentrated to the supragranular and infragranular layers respectively as the distance between the regions in terms of steps in the cortical hierarchy increases (Markov et al., 2014). This in turn implies that areas closer in the cortical hierarchy show much less of defined laminar origin for FF and FB neurons and would explain the bilaminar output neurons close in the cortical hierarchy described by Felleman & Van Essen (1991). PER was one of the areas assessed, and they note that the FB neurons to primary visual cortex (V1) were almost exclusively localized to infragranular layers, which coincides with what is acknowledged as the hierarchical distance between A36 and V1 in the visual system of primates (Felleman & Van Essen, 1991; Markov et al., 2014).

Markov et al. (2014) also investigated whether the FF and FB neuron origins are anatomically distinct within the supragranular and infragranular layers (Markov et al., 2014). Based on injections of retrograde tracers into V1 and V4, they assess the laminar localization of FF and FB neurons in V2 and V3. Within the supragranular layers, V2/3 FB neurons projecting to V1 were concentrated in L2/3A while V2/3 FF neurons projecting to V4 were concentrated in L3B. In the infragranular layers, FB neurons were located in L6 and the bottom of L5 of V2/3, while FF neurons were spread diffusely throughout the entirety of L5-6 of V2/3. They further confirm these findings by assessing the laminar localization of FF and FB neurons at different hierarchical levels and finding the same laminar segregation.

As for the specific lamina that are innervated by FF and FB projections in the recipient cortex, Markov et al. (2014) summarize their findings with previous knowledge to create a schematic of the current understanding of the organization of FF and FB pathways in primates (Markov et al., 2014). FF neurons to close levels in the hierarchy originate in both L3B and L5-6 and innervate L4, while long-distance FF pathways primarily originate in L3B and innervate L4 of upstream areas. In the same way as the lamina of origin for FB neurons vary by the hierarchical distance, so does the lamina of which FB projections innervate. Both long and short-distance FB pathways originate in L6 and innervate both L6 and L1 of downstream areas, while sharpening its pattern of innervation to only L1 as distance increases. For short-distance FB pathways however, they are noted to originate

in L2/3A and primarily innervate L1 apical dendritic tufts. Of note here is how the FF neurons in L3B and L5 are noted to have apical dendritic tufts in the local L1, and thus receive innervation by the FB projections at this site of interaction between the two pathways. Figure 1 shows a summary schematic of the anatomical description of feedforward and feedback pathways adapted from Markov et al. (2014).

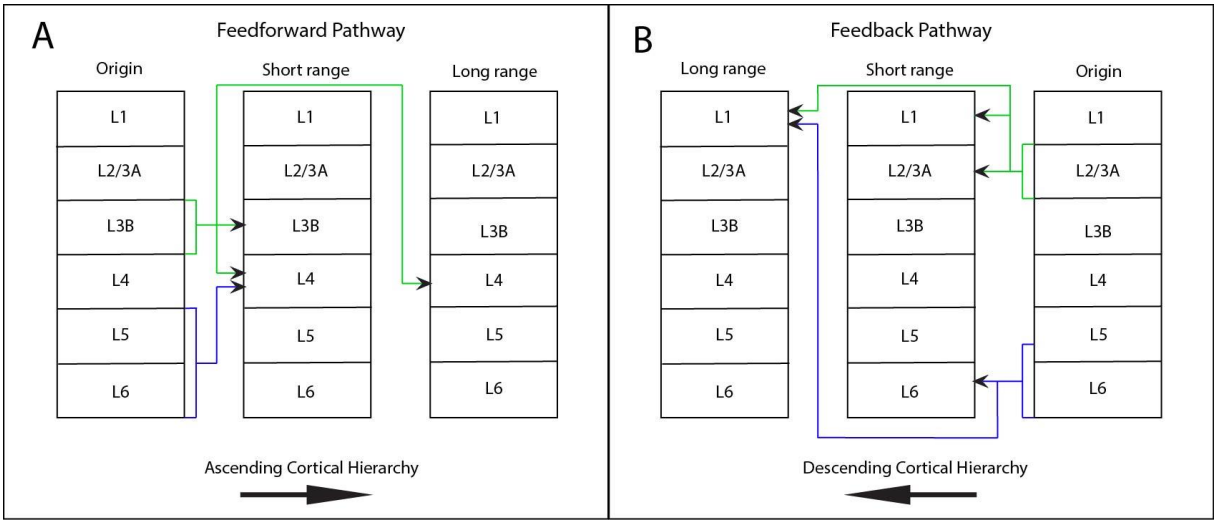

Figure 1: Simplified summary schematic for feedforward and feedback pathways in the cortex of primates. Adapted from Markov et al. (2014) using findings from the visual system in primates, with an emphasis on lamina of origin and innervated lamina for the respective pathways. Green lines indicate pathways originating from superficial layers L1-3, blue lines indicate pathways originating from deep layers L5-6. Green and blue lines do not indicate the anatomical path the axons travel through when reaching their target. A: Feedforward pathway from cortex of origin to short range and long range cortical targets. Superficial pathway FF neurons originate in L3B and innervates short range L3B, L4 and long range L4. Deep pathway FF neurons originate diffusely in L5/6 and innervates short range L4 only. B: Feedback pathway. Superficial pathway FB neurons originate in L2/3A and innervates short range L1, L2/3A and long range L1. Deep pathway FB neurons originate in L6 and bottom of L5, and innervates short range L6 as well as long range L1.

1.4.2 Function of feedback connections

The proposed function of FB projections to downstream areas is largely understood as modulating the feedforward signal (Zagha, 2020). Proposed functions of which FB neurons may contribute to, depending on involved regions of the brain, include motor planning, impulse control, spatial attention, corollary discharge, predictive coding and sensory perception (Zagha, 2020).

The role of FB projections in affecting sensory perception has been described as a possible dynamic interplay between feedback prediction of sensory signals and feedforward sensory evidence (Zagha, 2020). PER could possibly be affecting the sensory processing in primary sensory cortices by positively or negatively regulating activity in the target region, and thereby increase or decrease sensory evoked responses in the target area respectively (Zagha, 2020). Angelucci & Bressloff (2006) postulate that FB projections from extrastriate cortex to V1 in primates could contribute with generating the center-surround receptive field of V1 neurons (Angelucci & Bressloff, 2006). In a similar way as this, PER might impact the receptive fields of primary sensory cortices in

mice such as the whisker representation in the barrel cortex or visual scenery representation in the primary visual cortex.

FB pathways have also been proposed to contribute with mnemonic processes such as memory formation, consolidation and/or readout (Felleman & Van Essen, 1991). Lesions of PER and entorhinal cortex in primates have shown to inhibit the ability of inferotemporal cortex neurons to represent association between picture pairs (Higuchi & Miyashita, 1996), which supports this claim for neurons of parahippocampal regions to lower order areas. In mice, a study by Doron et al. (2020) investigating how PER efferents to L1 of primary somatosensory cortex controls learning supports the mnemonic contribution of PER FB pathways specifically (Doron et al., 2020). They set up an experiment which involved a cortical microstimulation task where rats and mice were trained to report short electrical microstimulation pulses delivered through a microelectrode implanted in L5 of S1. Their rationale is that pyramidal neurons in L5 have distal tuft dendrites that innervate L1, and that these will both receive the pulses delivered in L5 and input from PER at their dendrites in L1. The authors describe that specific inhibition of the perirhinal projections to L1 of S1 impairs the learning of the microstimulation detection task in a way that is similar to deactivating the entirety of PER with lidocaine. They further show that this PER input to L1 during learning modulates the activity and enhances burst firing in S1 L5 pyramidal neurons. This study implicates the PER projections to L1 of S1 as in some way contributing with a memory-related function as part of the parahippocampal formation.

1.5 Aims of current study

Mice are quite useful as a model in neuroscience due to the vast repository of genetic lines, usable techniques of which have reliable protocols, the capability of mice to exhibit complex behaviors, and more. As such, elucidating the connectivity of PER in mice is of great importance to aid in further research. To summarize, only PER output to L1 and other supragranular layers of primary somatosensory cortex has been described in mice (Doron et al., 2020; Naskar et al., 2021). There has not yet been a study to investigate the PER efferents to infragranular layers of primary somatosensory cortex in mice, or feedback efferents from PER to any layers of other sensory cortices in mice. As feedback efferents should innervate both supragranular and infragranular layers (Markov et al., 2014), it remains to be shown if PER provides feedback efferents to the infragranular layers of S1 and V1 in mice.

The primary aims of the study are therefore to investigate the feedback projections from PER to the primary somatosensory and primary visual cortices, to investigate the topography of PER output neurons to L6 of these sensory cortices, and to investigate the layer of origin of the feedback projections from PER.

The secondary aims of the study are to investigate whether the same output neurons in perirhinal cortex innervates both sensory cortices, to investigate the anatomy of projections from contralateral PER to these cortices, and whether there are marked differences in topography in PER between feedback projections to L1 and L6 of these cortices.

2 Methods

2.1 Animals

All animals used for this study were adult mice of the C57BomTac +/+ line, 3 male and 7 female, with ages ranging from 80 days to 283 days old at the date of sacrifice. The animals were bred at the Kavli Institute for Systems Neuroscience at the Norwegian University of Science and Technology (NTNU). The animals were permitted unrestricted access to food and water in enriched cages where they were housed alone for at least 7 days prior to surgery. The mice are housed alone beforehand to habituate them to living alone in a new cage, and furthermore ensures that after surgery they recover optimally without the presence of external stressors in the form of cohabitants in the same cage. The cages were in a room with a reversed light/dark cycle for 12 hours from 8 am to 8 pm. All experiments were performed during daytime, thus in the dark cycle for the mice. This research has been approved by the FOTS authorities under the application 25405. All experiments and procedures were performed at the Kavli Institute for Systems Neuroscience at NTNU.

2.2 Retrograde tracer

For the experiments performed in this study, choleratoxin subunit B (CtB) conjugated to Alexa Fluor 555 (C34776 from Invitrogen by Thermo Fisher Scientific) and 647 (C34778 from Invitrogen by Thermo Fisher Scientific) were used as retrograde tracers. The choleratoxin protein complex is composed of one A subunit and five B subunits, where the B subunits have the capability to bind to GM1 gangliosides on the cell surface of neurons (Conte et al., 2009; De Haan & Hirst, 2004; Kenworthy et al., 2021), a characteristic which is taken advantage of for this specific retrograde tracing technique. CtB, which is a synthetic molecule composed of only these five B subunits and not the A subunit which has enzymatic activity, is conjugated to a fluorescent molecule yielding the CtB-Alexa Fluor (CtB-AF). The B subunits of CtB-AF binds the GM1 gangliosides, and the entire molecule is transported back to the endoplasmatic reticulum in the cell body of the target cell (Conte et al., 2009; De Haan & Hirst, 2004; Kenworthy et al., 2021). CtB555 and CtB647 used in this study, which are specific products of CtB-AF, will then fluorescently stain the cytoplasm and not the nucleus of the cell, giving the cells a distinct fluorescent profile for easier identification and the possibility to quantify cells directly in PER as a means to investigate the topography of FB neurons in PER. Injection of the tracer into a given brain region will have it bind GM1 in the membrane of synaptic terminals (Conte et al., 2009) and the tracer will retrogradely travel to the soma of neurons that innervate the injection area. CtB is here injected through pressure injection, which has been described along with iontophoresis as possible methods of delivering CtB (Conte et al., 2009). After injection the survival period for the mice in this study was of 7-8 days, a time period which has been shown to be sufficient for good results from this retrograde tracer (Conte et al., 2009) given that too short a post-operative survival time will likely not allow for enough transport of the tracer to the cell bodies of target cells while too long a time could possibly lead to problems such as tracer degradation or loss of fluorescence.

2.3 Injection coordinates

The brain area targets for CtB injection were L6 and L1 of mouse barrel cortex (wS1) and V1 of the right hemisphere as these are the layers of which are described to receive feedback connections from other cortical areas (Zagha, 2020), and as such, are predicted to be the layers perirhinal feedback projections innervate. The preliminary coordinates for L6 of wS1 and V1 were determined by using the Franklin & Paxinos mouse brain atlas (Franklin & Paxinos, 2008). The anterior-posterior coordinate is measured as distance from bregma, medial-lateral coordinate is measured as distance from sagittal sinus, dorsal-ventral coordinate is measured as distance from surface of the brain. Based on the success of a given injection coordinate, adjustments in any of the three axes were made if deemed necessary for later injections to the same site. Further adjustments were based on measured distance from preferred injection area indicated in fluorescence images taken by a slide scanner.

It has been shown that efferents from PER to areas such as Tev and piriform cortex in rats originate in different rostrocaudal levels of PER based on the rostrocaudal level of the innervated cortex (Agster & Burwell, 2009). To control for potential patterns such as this, I therefore target several different rostrocaudal levels wS1 and V1. Specifically, one rostral, one midrostrocaudal, and one caudal injection site coordinate was used for both wS1 and V1. For the primary somatosensory cortex, I chose to further aim specifically for wS1 because it is the most studied of the primary somatosensory areas and tactile exploration with whiskers is very important in rodents.

L1 injection coordinates for V1 and wS1 were based on existing already functional anterior-posterior coordinates for each region. Results gathered from the L6 injections in wS1 indicated the caudal region as the most reliable, while the V1 injection was chosen to be midrostrocaudal because no clear indication could be retrieved by the time of L1 injection surgery start. The medial-lateral and dorsal-ventral coordinates were determined based on measured distance from L1 in the L6 injection fluorescence images taken by a slide scanner. For the precise injection coordinates used for each mouse and the results of said injection, please see Table 1 (see below). For the histology of each of the injection sites, please see Fig. 5-7 and Appendix A1.

Mouse ID	**Injection Target 1 (CtB555)**	**Injection coordinate (AP, ML, DV)**	**Result**	**Injection Target 2 (CtB647)**	**Injection coordinate (AP, ML, DV)**	**Result**
66702	wS1 midrc L6	(-0.82, 2.5, 1.15)	Caudal wS1 L6b + ec (AP: -1.22)	V1 rostral L6	(-2.5, 2.25, 0.7)	Hippocampus + ec. (AP: -2.18)
104375	wS1 rostral L6	(0.14, 2.7, 1.37)	Rostral wS1 L6b + S1DZ L5 (AP: 0.38)	V1 midrc L6	(-3.5, 2.0, 0.7)	V2M L1-6 + ec (AP: -2.80)
104376	wS1 caudal L6	(-1.82, 2.75, 0.95)	Caudal wS1 L6b + ec	V1 caudal L6	(-4.5, 2.5, 0.85)	Midrc V1 L6 + ec (AP: -4.16)

			(AP: -1.58)			
104379	wS1 midrc L6	(-0.82, 2.5, 1.05)	Midrc wS1 L4-6 (AP: -0.70)	V1 rostral L6	(-2.5, 2.25, 0.7)	LPtA L5-6 + PTPR L6 + ec (AP: -1.94)
104380	wS1 rostral L6	(0.14, 2.8, 1.27)	rostral wS1 L6b + S1FL L6b + S1DZ L6 + ec (AP: -0.10)	V1 midrc L6	(-3.5, 2.0, 0.65)	Midrc V1 L1-6 + ec (AP: -3.80)
103825	wS1 caudal L6	(-1.82, 2.75, 0.8)	Caudal wS1 L3-5a, some spill in L1-2. (AP: -1.46)	V1 caudal L6	(-4.5, 2.5, 0.75)	Midrc V1 L1-6 (AP: -3.88)
103824	wS1 caudal L6	(-1.82, 2.75, 0.8)	Caudal wS1 L6 (AP: -1.82)	V1 rostral L6	(-2.8, 2.4, 0.7)	Rostral V1 L5-6 + ec. Possibly some L1 as well. (AP: -2.30)
103823	V1 rostral L6	(-2.8, 2.4, 0.7)	Rostral V1 L6b + ec (AP: -2.80)	V1 caudal L6	(-4.5, 2.35, 0.7)	Caudal V1 L1-6 + V2M L1-6 (AP: -4.36)
103822	wS1 caudal L1	(-1.82, 3.2, 0.03)	Miss.	V1 midrc L1	(-3.5, 2.0, 0.03)	Miss.
103821	wS1 caudal L1	(-1.82, 3.2, 0.03)	Miss.	V1 midrc L1	(-3.5, 2.2, 0.03)	V2M L1-6. Stronger in superficial layers. (AP: -2.54)

Table 1: Injection status for each mouse. Includes the injection target area, injection coordinate used for that area, and the results of each injection.

2.4 Injection surgery

The mice are habituated to nutella for at least seven days prior to surgery to ensure that the mouse will consume post-operative Nutella mixed with an oral tablet of Buprenorphine hydrochloride (Oral Temgesic from Invidior).

Just before surgery, an anesthesia induction chamber is filled with 4% isoflurane. After some minutes when the chamber has had time to fill with isoflurane, the mouse is moved into the chamber and isoflurane is reduced to 3%. After visual confirmation that anesthesia is induced in the animal, the mouse is moved to a stereotaxic frame where it is head fixed by inserting its incisors into the stage and placing ear bars into the mouse's ear canals. 2% isoflurane is then given through a mask moving forward with the procedure, and eye salve (Simplex) is applied. To ensure deep anesthesia, surgical

forceps were used to pinch between the toes of the mouse to assess its reflexes. Once reflexes to the toe-pinch method are absent, Bupivacaine hydrochloride (Marcain from Astra Zeneca; concentration = 0.5 mg/ml; dose = 0.06-0.18 ml/30g bodyweight), is given subcutaneously above the scalp. Meloxicam (Metacam from Boerringer Ingelheim Vetmedica; concentration = 1 mg/ml; dose = 0.15 ml/30g) is given subcutaneously in loose skin on one side of the abdomen. An injection of Temgesic (Invidior; concentration = 0.03 mg/ml; dose = 0.09 ml/30g) is given subcutaneously on the other side of the abdomen. The head of the mouse is shaved, washed with saline and disinfected with chlorhexidine before access to scalp is cut using a scalpel (blade no. 10). The periostium is carefully scraped off so as to gain access to the skull. After about 30 minutes, isoflurane is adjusted to 1.5%. If surgery still persists after 3 hours, or if the circumstances of the surgery required it, isoflurane is then adjusted to 1%. The skull was fixed in a flat position by measuring the dorsoventral coordinate of both bregma and lambda on the skull and having them be within 0.5 mm of each other. The sagittal sinus was exposed by drilling (0.9 mm or 0.5 mm drill tip from Fine Science Tools) through the skull, and is the landmark used as reference point for the medial-lateral coordinates. The anterior-posterior coordinate is measured from bregma. Pressure injections were performed with a glass capillary (20-30 µm tip size) attached to an injector (Nanoliter 2020, World Precision Instruments) controlled by a microsyringe pump controller (Micro2T SMARTouch controller, World Precision Instruments). Once the stereotaxic frame has been adjusted to position the injector just above the injection site, the skull is drilled into so as to gain access to the brain and the injector is inserted into the brain according to the dorsal-ventral coordinate for the given injection measured from the surface of the brain. 30 nl (50 nl for mouse 66702) of CtB555 is pressure injected 10 nl/min into the first injection site, and a few minutes pass after the injection is done before it is retracted. The stereotaxic frame is adjusted to move the injector to the second injection site, access to the brain is drilled into the skull, and 30 nl of CtB647 (50 nl for mouse 66702) is injected 10 nl/min into this injection site. After injections, the head wound is sutured, cleaned with saline and disinfected with chlorhexidine. 1 ml of saline is given subcutaneously in loose skin on the side of the abdomen for hydration. The mouse is moved to a heat chamber to recover, and when it has regained movement capabilities it will then be transferred back to its cage.

Post-operatively, the mouse is given additional food in the form of baby porridge and a wettened pellet. 6-8 hours after Temgesic was given during start of surgery, oral Temgesic is crushed and mixed with Nutella (0.2 mg Temgesic / 1 g nutella) and fed to the mouse (dose = 150 mg/30g). Approximately 12 hours after this Temgesic/Nutella dose is given, another dose will be given with the same dosage and concentration. Alternatively, for some mice if Temgesic/Nutella was not ingested when given, a Temgesic injection of the same dose and concentration as during surgery is then given subcutaneously instead. The following third dose of Temgesic to be given must then be within 6-8 hours of this second dose. Approximately 24 hours after Metacam was given during surgery, another Metacam injection of the same dose as under surgery is given subcutaneously while the mouse is anesthetized from 4% isoflurane in an induction chamber. The mice are weighed every day after the operation until the weight has stabilized.

2.5 Perfusion and microsectioning

The mice were perfused 7-8 days after surgery. Post-fixative (4% Paraformaldehyde in phosphate buffer, PFA; diluted in 0.125M Phosphate buffer (PB)) solution and Ringer (0.85% NaCl, 0.025% KCl, 0.02% $NaHCO_3$) solution or phosphate buffer solution (Sigma-Aldrich, pH=7.4) is prepared beforehand. The mouse is anesthetized in an induction chamber with 4% isoflurane before a lethal 0.1 ml dose of pentobarbital (Apotekerforeninger) is given intraperitoneally. The mouse is then checked for an absent toe-pinch reflex before it is moved to the operation table. The arms and legs are taped down, an incision is made just below the breastbone, muscle and skin is cut laterally, then cuts are made across the rib bones up towards the base of the arms. A cut is made across the diaphragm and the heart is exposed. Ringer solution ventilated with bioxide to maintain a pH of 7.4 or PBS (mouse 103821) is pumped through the mouse circulatory system transcardially using a peristaltic pump (Peri-star Pro from World Precision Instruments Inc.) by inserting a cannula in the left ventricle of the heart at the same time as the right atrium is clipped open to permit blood to flow out of the body. This was continued until areas such as the toes and lips of the mouse turned pale, and the liquid that was leaking out of the right atrium was transparent. At that point, the peristaltic pump was changed to then pump PFA through the circulatory system until the tail of the animal and the liver was deemed sufficiently stiffened by the fixative solution. The mouse was then decapitated, and its brain was carefully extracted from the skull. The brain was then put into a brain cup filled with 4% PFA for three hours, then moved to a 15% sucrose in 0.125M phosphate buffer (PB) solution for cryoprotection. The day after, the brain was moved to a 30% sucrose solution and left in it for two days.

After two days of incubation in 30% sucrose solution, the brain is ready to be sectioned by use of a microtome (Microm HM 430 by Thermo Scientific). In preparation for sectioning, a platform of 30% sucrose in 0.125M PB was created on top of a freezing stage (Physitemp BFS-MP Freezing Stage). The brains were cut into the left hemisphere using a scalpel blade no. 10 for easier identification of hemispheres after immunohistochemistry, then carefully mounted on top of the sucrose platform with the dorsal end of the brain facing the microtome blade. The brain is frozen completely by encasing it in dry ice and sectioning commenced. All brains were sectioned into 50 µm thick coronal sections, and each section was carefully lifted using a thin paint brush and placed into either a series of 5 (n=5) or a series of 6 (n=5) tubes containing antifreeze (30% glycerol, 30% ethylene glycol, 40% PBS). The brains were all sectioned from just past the olfactory bulbs until the cerebellum was reached. All tubes were then stored in -20° C.

2.6 Immunohistochemistry

Once the brains are sectioned into different series, two of these series per brain were used for further immunohistochemical treatment. Examples of immunoprotocols are in Appendix C. One series was to be counterstained for neuronal nuclear protein (NeuN) while the other was to be counterstained for PV, and these were run simultaneously. The two series are first placed into separate multiwells on an orbital shaker, where all steps moving forward take place, and are then treated to three 10-minute washing steps using 0.125 M PB before being taken through a blocking step lasting one hour. The blocking solution contains 10% Normal Goat Serum (NGS) (Abcam) and 0.01% Triton X-100 (Merck), diluted with 0.125M PB. After this blocking stage it is then placed in a primary

antibody solution of either Guinea Pig anti-NeuN (Sigma Millipore, #ABN90P) for the NeuN treated series or Rabbit anti-PV (Swant, #P3088) for the PV treated series, both diluted 1:1000. Both primary antibody solutions also contain 1% NGS, 0.1% Triton X-100 and are diluted with 0.125M PB. The series were left in this primary solution overnight at 4°C. The day after, the series are treated to three 20-minute washing steps in 0.125M PB before being placed in a secondary antibody solution either at 4° C overnight or in room temperature for 4 hours. The secondary antibody solution contains either Goat anti-Guinea Pig A488 (Thermo Fisher Scientific, #A11073) for the NeuN treated series or Donkey anti-Rabbit A488 (Thermo Fisher Scientific, #A21206) for the PV treated series, both diluted 1:500. Both secondary antibody solutions also contain 1% NGS, 0.01% Triton X-100 and are diluted with 0.125M PB. When the secondary antibody step is finished, the series are treated to three 10 minute washing steps in 0.125M PB before the sections are mounted onto slides (SuperFrost; Thermo Fisher Scientific) using 0.125M PB. The slides are left to dry for at least a couple of hours before they are washed in distilled water, then dry for a couple more hours before they are coverslipped (Fluoromount-G by Southern Biotech), then dry for a couple more hours before they are sealed with nail polish (Abalico High Dry).

2.7 Microscopy

The slides were imaged for fluorescence using a confocal microscope (Zeiss LSM 880 Confocal Laser Scanning Microscope) and a slide scanner (Zeiss Axioscan.Z1 Slide Scanner). Confocal microscopes are able to create high-resolution 3-D images of the sections (Nwaneshiudu et al., 2012), which allows for a much higher accuracy in the counting of CtB-AF labeled cells than in normal fluorescence images. Such a high resolution was not required for the images of the entire sections used to confirm the injections and for assistance in delineation of PER, so a fluorescence microscope slide scanner was sufficient and thus used for this purpose. For the confocal imaging, the entire rostrocaudal extent of the perirhinal cortex was imaged. A 20x objective was used (Plan-Apochromat 20x/0.8) for image acquisition, a pinhole size of 1 Airy unit, and each section was imaged with bi-directional tile scanning using lasers for three wavelengths: 488 for NeuN/PV, 561 for the CtB555 and 633 for the CtB647. The laser strength for lasers 488, 561 and 633 was 2.0, 4.0 and 4.0, respectively. The gain used was also adjusted for each laser, with 610, 700 and 700 used respectively. The entire thickness of each section was imaged with a 0.81 µm z-stack interval. For the slide scanning, the entirety of all slides was imaged using a 20x objective (Plan-Apochromat 20x/0.8), and using lasers for the wavelengths 488, 555 and 647.

2.8 Delineations and cytoarchitecture

Delineations were based on the Franklin & Paxinos atlas of the mouse brain (Franklin & Paxinos, 2008) in combination with relevant literature describing cytoarchitectural landmarks of the various regions (Beaudin et al., 2013; van Groen, 2001). All delineations were performed in either Neurolucida (MBF Bioscience) or Zen Desk (Zeiss) directly on fluorescence images of the tissue created from either confocal microscopy or a slide scanner, respectively. Both ipsilateral and contralateral PER relative to the injection site were imaged in a confocal microscope and delineated for quantification of PER output neurons stained by CtB-AF. Images were also made of the injection sites using the slide

scanner, with areas surrounding the injection bolus also delineated. The marker NeuN is a reliable marker for most types of neurons in the neocortex save some few exceptions such as Cajal-Retzius cells (Gusel'nikova & Korzhevskiy, 2015). NeuN stained tissue is commonly used in histology, and was used here to visibly determine the cytoarchitecture of the cortical areas to be delineated and was also used to identify the different lamina of PER. Several counterstained series for PV, a marker for fast-spiking basket and chandelier cells (Tremblay et al., 2016), were used to assist in delineating the perirhinal cortex which has been shown to stain very lightly for PV (Beaudin et al., 2013; van Groen, 2001) (Fig. 2B, D).

Delineations of the wS1, V1, mediomedial V2 (V2M), lateral parietal association cortex (LPtA) and rostral posterior parietal cortex (PTPR) for the images of the injection sites were based on the Franklin & Paxinos mouse brain atlas of 2007 (Franklin & Paxinos, 2008). For wS1 specifically, the identification of barrels in L4 was used to help delineate the borders of wS1. Delineation of cortical lamina in wS1, V1, V2M, LPtA and PTPR is based on the following procedure of delineation: First, L1 is identified as a layer with very sparse soma labeling by NeuN, appearing as a dark band at the cortical surface. Next, L4 is identified as a dense layer containing small somas, just above L5. L5 is the layer just below L4 which is very sparse in cell density and contains neurons with larger somas. L2/3 is identified as the area between L1 and L4. L6 is the layer below layer 5 which stretches until just past the striated lower L6, and until the external capsule (ec) is reached.

2.8.1 Delineation of PER

PER is commonly separated into two areas, A36 as the dorsal region and A35 as the ventral region (Beaudin et al., 2013). PER is associated with the rhinal fissure along its entire rostrocaudal extent, but the association changes as one moves towards more caudal PER. In rostral PER in mice, A36 is situated approximately at the fundus of the rhinal fissure while A35 is situated ventral to the fissure. As one moves further caudally, A36 and A35 rise until they both lie above the fundus of the rhinal fissure (Beaudin et al., 2013). Sections relevant for locating PER are first identified using the Paxinos mouse brain atlas and then imaged using a confocal microscope. Of note here is how the ectorhinal cortex in the Franklin & Paxinos mouse brain atlas of 2007 corresponds to only A36, while perirhinal cortex in the atlas corresponds to specifically A35. The delineation of PER in this study is based cytoarchitectural landmarks described by Beaudin, et al. 2013 (Beaudin et al., 2013). PV staining was used to assist in delineating PER, which shows lighter neuropil and cell staining for PV than regions at its ventral and dorsal borders (Beaudin et al., 2013) (Fig. 2). The series stained here for PV contains adjacent sections to the sections in the series stained for NeuN, and is used in addition to cytoarchitectural criteria to confirm whether the area delineated is PER by comparing the adjacent sections (Fig. 2).

Rostral and caudal borders of PER

PER is bordered rostrally by insular cortex which overlies the claustrum (Beaudin et al., 2013). The rostral border of PER used in this study is thus when the claustrum is no longer present in PER underneath the cortex but is positioned ventrally, and additionally when the LEC ventral to PER is clearly identified (see below) (Beaudin et al., 2013). PER is bordered caudally by the postrhinal cortex, which appears at the caudal end of the angular bundle (Beaudin et al., 2013). The main criteria used in this study for setting the

caudal border of PER is therefore based on if the section still contains the angular bundle, where an absent angular bundle means we have proceeded past PER and reached postrhinal cortex.

Dorsal border of PER

The regions of which A36 of PER borders dorsally vary across its rostrocaudal axis. Rostral A36 borders to secondary somatosensory area, midrostrocaudal A36 borders to posterior auditory association cortices and caudal A36 borders to temporal association cortex (TeA) (Beaudin et al., 2013). L4 is completely missing in A35 while it is detectable but much more evident in horizontal sections of A36 (Beaudin et al., 2013; Kealy & Commins, 2011). In coronal sections, L4 is completely missing in both areas, and the dorsal border is defined as approximately where L4 disappears. The absence of L4 in PER in coronal sections is the main cytoarchitectural criteria used to set the dorsal border, as all cortices that border A36 dorsally have a more discernable L4 (Beaudin et al., 2013). Additionally, TeA has been described to have a broader L5 (Beaudin et al., 2013), but this was not as easily confirmed in the sections gathered in this study. For the more midrostrocaudal and caudal sections, the lighter PV staining in PER relative to dorsal cortices (Beaudin et al., 2013; van Groen, 2001) in addition to the stronger PV staining in deep layers of the dorsal cortices (Beaudin et al., 2013) was used to confirm the dorsal border initially set using cytoarchitectural landmarks (Fig. 2).

Ventral border of PER

A35 of PER borders to the lateral entorhinal cortex (LEC) ventrally across its entire rostrocaudal extent (van Groen, 2001). The difference between the two is most easily distinguished by the difference in L2, where L2 in LEC is much thicker and larger (van Groen, 2001) than in A35. Additionally for more caudal sections, there is a cell sparse zone between L2 and L3 in LEC (van Groen, 2001). Furthermore, L2a of LEC is superficial and protrudes into L1, with larger, densely packed neurons that tend to cluster into islands (Ohara et al., 2021). LEC L6 is described to be more narrow than L6 in A35 (Beaudin et al., 2013), but this was not easily determined in the sections in this study. For deep layers, the presence of lamina dissecans in LEC is a good landmark to also confirm for the ventral border. PV staining was used here as well to confirm the borders, as PER stains lighter for PV than LEC (Beaudin et al., 2013; van Groen, 2001) and LEC has a stronger PV staining in superficial layers specifically (van Groen, 2001) (Fig. 2).

A35 vs A36

The difference between A35 and A36 is most evident in L2, where cells in L2 of A36 are described to be large, round and are more compactly clustered together (Beaudin et al., 2013) while cells in L2 of A35 show a vertical organization. The difference between L2 of A35 and A36 has also been described as L2 of A35 being more disorganized than L2 of A36 (Beaudin et al., 2013). Other cytoarchitectural characteristics include how L6 is narrower in A35 than A36, and how the cortical depth of A35 tends to be narrower than A36 especially towards more caudal PER (Beaudin et al., 2013).

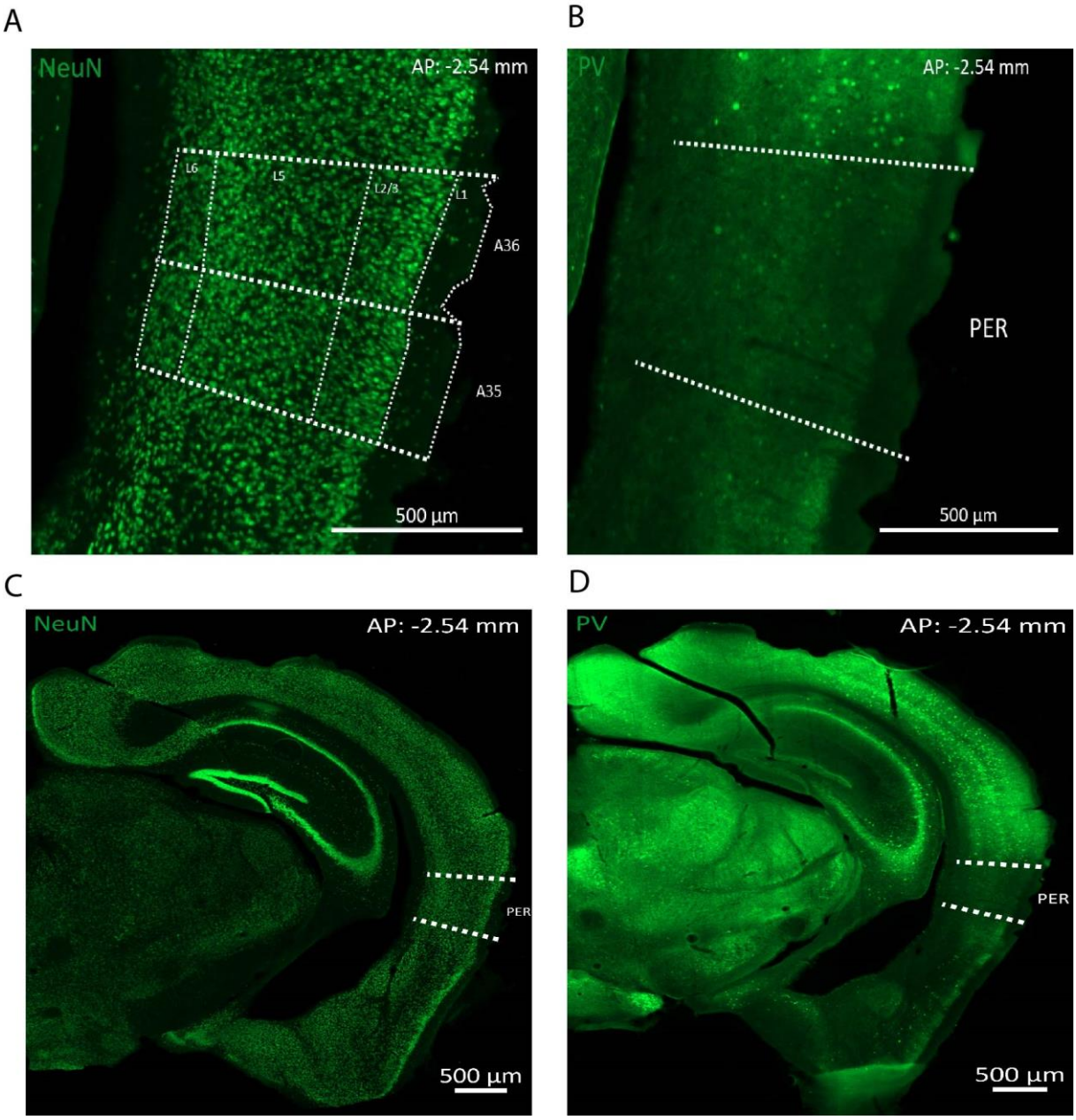

Figure 2: Delineation of PER. A: Image of PER delineated into A36, A35, and the various cortical lamina according to Beaudin et al. (2013). B: Parvalbumin stained image of adjacent section used to assist in delineating PER. C: Expanded view of right hemisphere with PER delineated in NeuN stained section shown in 2A. D: Expanded view of right hemisphere with PER delineated in PV-stained section shown in 2B.

2.9 Quantification

The software Neurolucida (MBF Bioscience) was used for the quantification of CtB-AF labeled cells in the fluorescence images generated by confocal microscopy. First, PER A36 and A35 was delineated based on the criteria described (Fig. 2A), and then all cells within the delineated region were assessed for CtB-AF staining. The CtB-AF stained cells will

fluorescently stain the cytoplasm and not the nucleus of the cell (Conte et al., 2009; De Haan & Hirst, 2004; Kenworthy et al., 2021), which at times makes it quite difficult to discern CtB-AF labeled cells from noise. To account for this, all visually identified possible CtB-AF labeled cells were crosschecked with the NeuN labeling of the cell as NeuN is quite reliable at staining nearly all neurons in the neocortex (Gusel'nikova & Korzhevskiy, 2015). If the pattern of CtB-AF staining aligned with the NeuN labeling, and this was consistent for several of the z stacks, the cell was counted (Fig. 3). The sections are separated by 250/300 µm for the series of 5 and 6 sections per tube respectively and as such there is no concern for overcounting in the z-axis. Some series indicate an error in sectioning where two subsequent sections were placed into the same tube, and manual correction was applied to these to ensure no overcounting of cells.

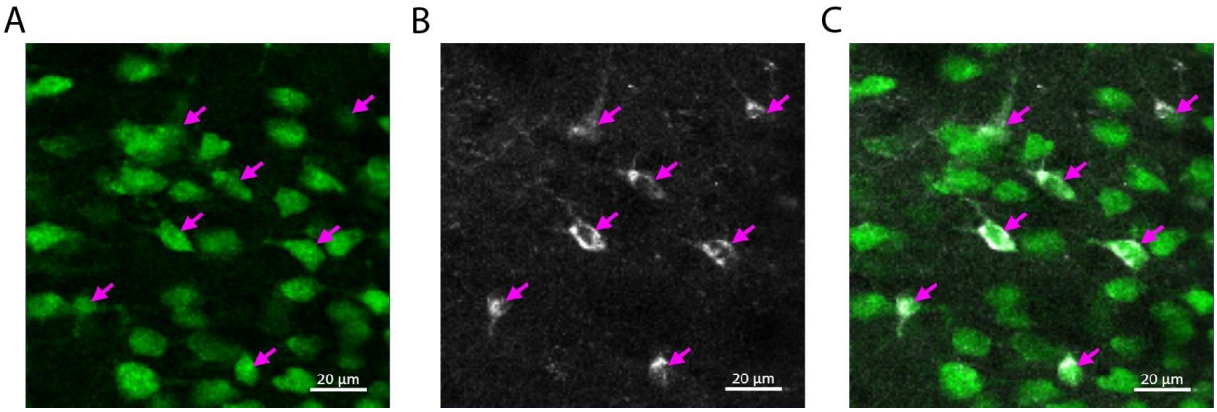

Figure 3: Example quantification of CtB-AF labeled cells colocalized with NeuN counterstaining. Pink arrows indicate counted cells. A: NeuN labeled cells. B: CtB-AF labeled cells. C: CtB-AF labeled cells colocalized with NeuN staining.

2.10 Analysis

Immunofluorescence for PV is stronger in more rostral parts of PER, then becomes much weaker towards caudal PER (Beaudin et al., 2013). To bin PER across its rostrocaudal extent using a meaningful molecular landmark that defines PER and as an attempt to avoid arbitrarily assigning different portions of PER into certain bins, I quantified the PV+ cells in PER at different rostrocaudal levels. The data of PV counted cells across the entire rostrocaudal extent of PER was quantified in three mice (103823, 103824, 103825). Through visual investigation of the total counts and density of PV+ cells across the rostrocaudal levels of PER, and in addition plotting the KMeans clustering of the total counts and density, a division into two groups was defined as appropriate in this thesis (Fig. 4, Appendix B1). The rostral bin of PER is thus defined here as stretching from -1.94 to -3.08 mm from bregma and the caudal bin from -3.16 mm to -4.24 mm from bregma. These specific coordinates are based on comparison with the Franklin & Paxinos atlas to determine the rostrocaudal levels of each section quantified in PER for this study and dividing the entire sampled rostrocaudal extent into two halves (Franklin & Paxinos, 2008). This was tested on the data and was found to be reasonable to show relationships between rostral and caudal PER. One could however argue that binning based on the neuropil stained by PV in addition to the PV+ cells, where there is a visually identifiable sharp drop off in PV staining as one proceeds caudally could be better (Fig. 4B-D). However, this would be biased to the subjective visual determination done by any one

person, and as such simply splitting PER into a first and second half was chosen for this study. Figure 4A shows the quantification of PV cells across the rostrocaudal extent of PER, with Figure 4B-D showing three sections at approximately where one could visually determine the drop in fluorescence of PV labeled cells and neuropil. Given the example PV-stained sections shown (Fig. 2B, Fig. 4B-D) one could make an argument for how splitting PER into three bins could be more appropriate as there is already strong loss of fluorescence occurring earlier than -3.08 mm from bregma. However, one could also make a case for there being a noteworthy drop in fluorescence occurring between the two sections at -2.80 to -3.28 mm from bregma (Fig. 4C, D) making it difficult to define precisely exactly how to bin the rostrocaudal extent of PER. Two bins were used for the results in this study, but those same figures have also been remade using three bins and added to Appendix B2.1 and B3.1.

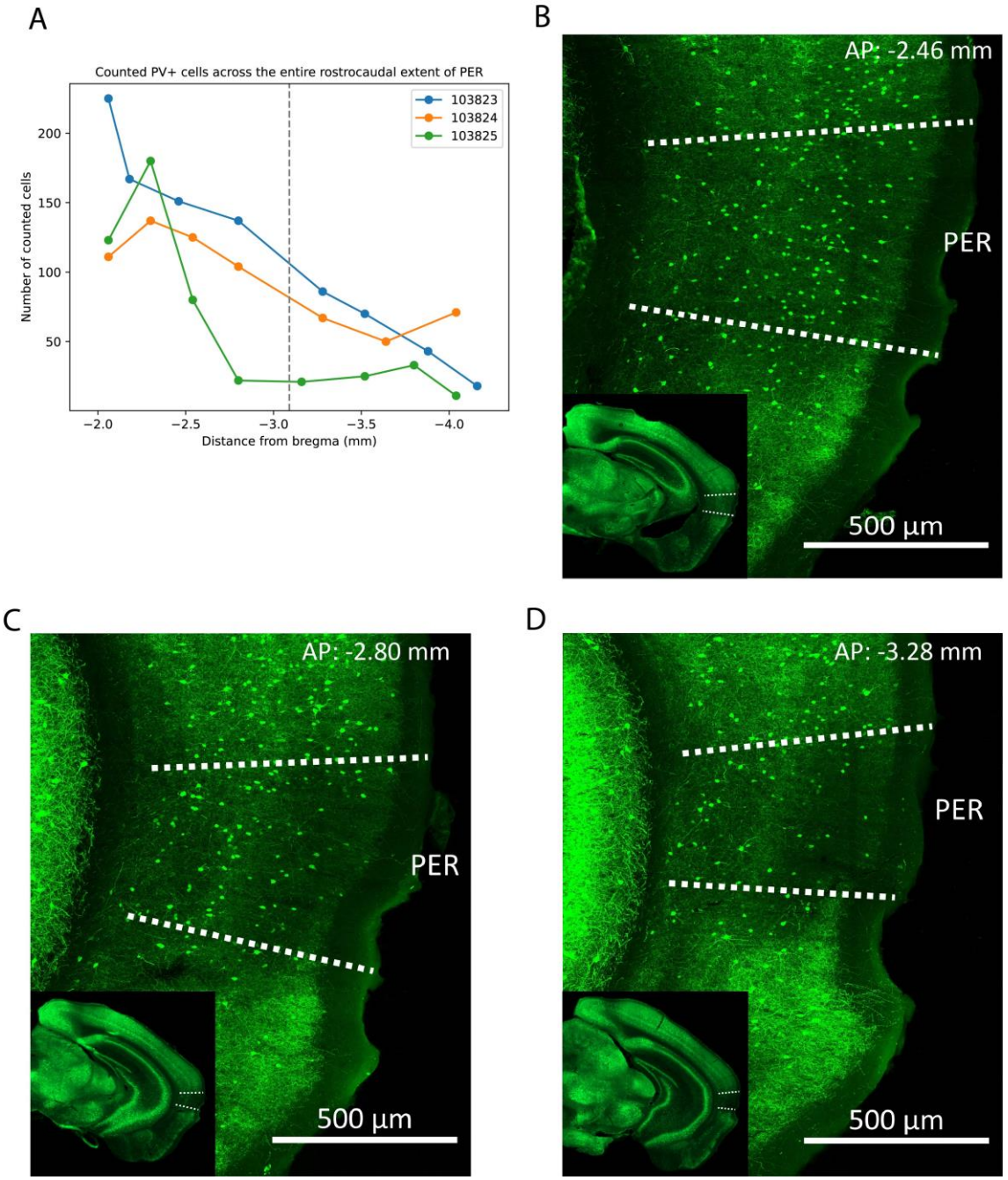

Figure 4: PV expression across the rostrocaudal axis of PER. A: Line graph of quantified PV+ neurons across the rostrocaudal extent of PER in three mice. Each point is the PV+ cell count at a section in the series. AP coordinate of each section is based on comparison with the Franklin & Paxinos mouse brain atlas (Franklin & Paxinos, 2008). Dotted line at AP = -3.09 indicates the split between the rostral and caudal bins used in further in this study. B-D: Histology of example sections at three rostrocaudal levels of PER in mouse 103823. Expanded views of PER are maximal intensity projections made from confocal images of the tissue, image indicating right hemisphere are images made by slide scanner. Sections included are approximately where the reduction in PV labeled neuropil and PV+ cells can be visually identified.

What is defined in this thesis as rostral, midrostrocaudal and caudal wS1 and V1 is based on comparison with the Franklin & Paxinos mouse brain atlas (Franklin & Paxinos, 2008) and splitting the entire rostrocaudal extent indicated by the atlas for the cortices into roughly three portions. For wS1, if the injection was determined to be located in a section of which compared to the Paxinos atlas was between 0.50 mm and -0.31 mm from bregma, the injection is considered in rostral wS1. Midrostrocaudal wS1 is defined in this study as between -0.30 and -1.12 mm from bregma, and caudal wS1 is defined as between -1.12 mm and -1.94 mm from bregma. As for V1, rostral is defined as between -2.18 mm and -3.20 mm from bregma, midrostrocaudal as between -3.20 mm and -4.20 mm from bregma, and caudal as between -4.20 mm and -5.20 mm from bregma.

After delineation of PER and counting of cells in Neurolucida 360, the file for a given section was run through Neurolucida Explorer to get a Microsoft Excel file of all possible analyses performed by Neurolucida. The data of how many cells were counted in each layer and subdivision of PER was stored and analysed in a larger Excel file and figures were generated using both Excel and Python (See Appendix D). To account for the difference in bolus amount concentrated in L6 between the different injections, all cell counts were normalized to the total amount of cells counted in that brain for that given injection.

Two injections into mouse 104380 hit L6b of wS1 as well as L1-6 of V1 but contained so few quantifiable sections due to damage to PER that it was excluded from the study. The very few quantifiable sections due to damage to PER influenced the proportional cell counts to such a degree that they no longer were a reliable way of assessing the topography of the FB neurons in PER. See Appendix A1.2 for histology of these injection sites for this mouse, and Appendix A1.3 for an example histology of a section with damage to PER making the mouse excluded from analysis.

103823 had two injections into V1, one rostral injection using CtB555 (103823r) and one caudal injection using CtB647 (103823c).

3 Results

3.1 Description of injection sites

A summary of the coordinates used for injections and the results of those injections are listed in Table 1 (see above). Seven injections were aimed to hit various midrostrocaudal levels of wS1 L6, nine aimed to hit V1 L6, two aimed to hit wS1 L1 and two aimed to hit V1 L1. Of the ones targeting specifically L1, all either missed or did not specifically hit their target.

Of the quantifiable injections targeting L6 of wS1, five injections hit at least some part of L6 (Fig. 5A-E), though two had spill into the external capsule (ec), which contains axonal fiber tracts (66702, 104376; Fig. 5A, C). Three hit specifically L6b (66702, 104375, 104376; Fig. 5A-C) while two hit the entirety of L6 (104379, 103824; Fig. 5D, E). As for the rostrocaudal distribution of these injections into wS1 L6, one hit rostral wS1 (104375; Fig. 5B), one hit midrostrocaudal wS1 (104379; Fig. 5D), and three hit caudal wS1 (66702, 104376, 103824; Fig. 5A, C, E). Even though the injections targeting L1 of

wS1 and V1 missed, one injection targeting L6 of wS1 did instead hit layers 1-5a of caudal wS1 (103825; Fig. 5F) although the injection bolus is strongest in L3-5a.

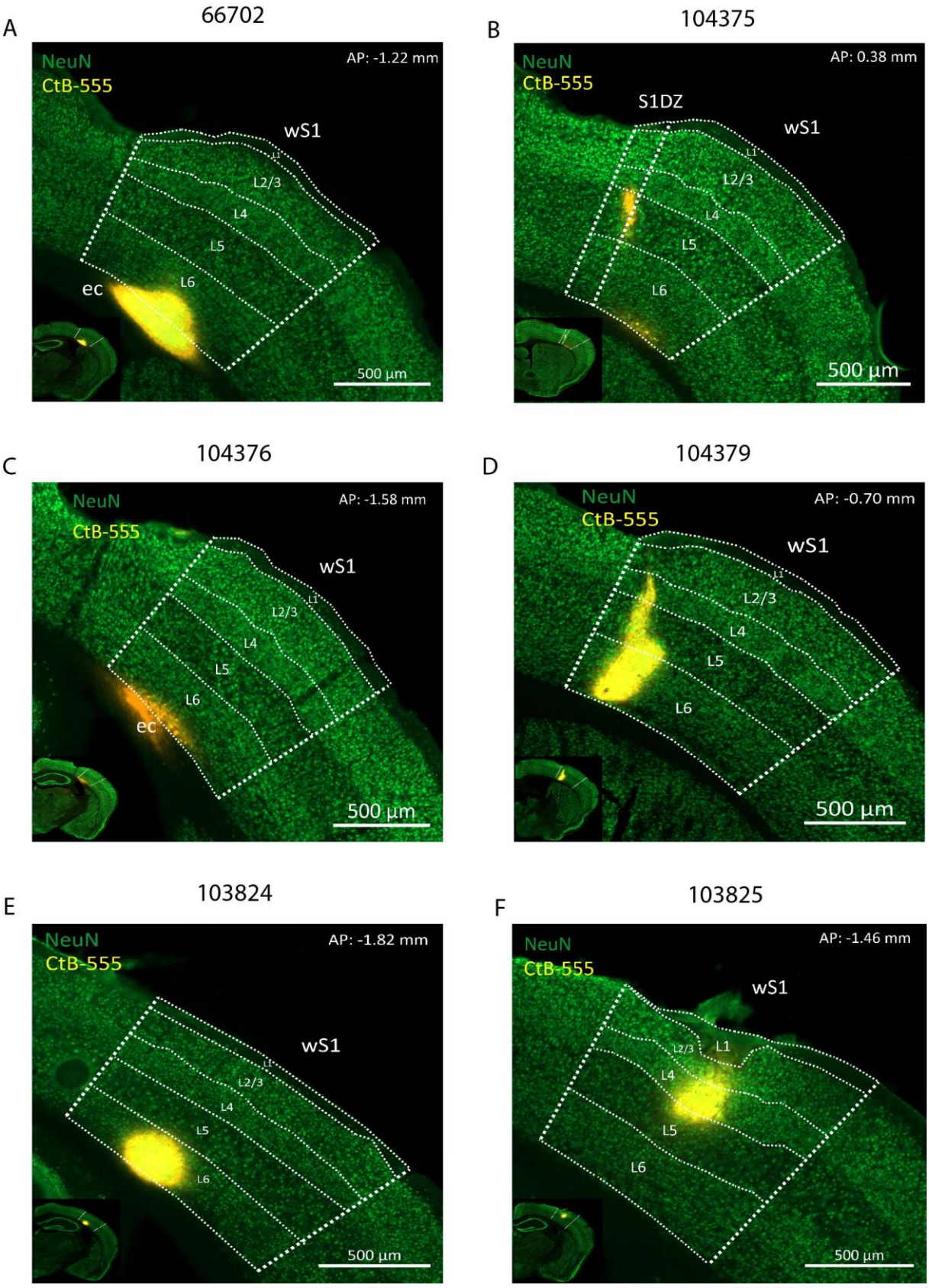

Figure 5: Histology of retrograde tracer injection sites in wS1. Expanded view of right hemisphere at the bottom left corner for each image. Tissue is stained for NeuN in green. Delineations of wS1 based on Franklin & Paxinos mouse brain atlas (Franklin & Paxinos, 2008). A: Mouse ID 66702. Injection hit L6b and ec. AP: -1.22 mm from bregma. B: Mouse ID 104375. Injection hit L6b of wS1 as well as L5 of the dysgranular zone of S1.

AP: 0.38 mm from bregma. C: Mouse ID 104376. Injection hit L6b and ec. AP: -1.58 mm from bregma. D: Mouse ID 104379. Injection hit primarily L6 of wS1 with some spill into L4-5. AP: -0.70 mm from bregma. E: Mouse ID 103824. Injection hit L6 of wS1. AP: -1.82 mm from bregma. F: Mouse ID 103825. Injection hit L1-5a of wS1. AP: -1.46 mm from bregma.

Of the quantifiable injections targeting L6 of V1, five injections hit at least some part of L6 (Fig. 6) though three had some spill into ec (104376, 103824, 103823r; Fig. 6A, C, D). One hit the entirety of L6 (104376; Fig. 6A), while one hit L6b specifically in addition to ec spill (103823r; Fig. 6D). The two injections with no spill into ec did not specifically hit L6, but had spill distributed across the entire cortical column hitting L1-6 (103825, 103823c; Fig. 6B, E). Of note is also how one of these injections also had notable spill into V2M L1-6 (103823c; Fig. 6E). As for the rostrocaudal level of the injections, there were two rostral V1 injections (103824, 103823r; Fig. 6C, D), two midrostrocaudal injections (104376, 103825; Fig. 6A, B), and one caudal injection (103823c; Fig. 6E).

There were three mice with quantifiable sections and successful injections in both wS1 and V1. The first had injections that hit caudal wS1 L6b + ec and midrostrocaudal V1 L6 + ec (104376; Fig. 5C, 6A). The second hit caudal wS1 L1-5a and midrostrocaudal V1 L1-6 (103825; Fig. 5F, 6B). The third hit caudal wS1 L6 and rostral V1 L5-6 + ec (103824; Fig. 5E, 6C).

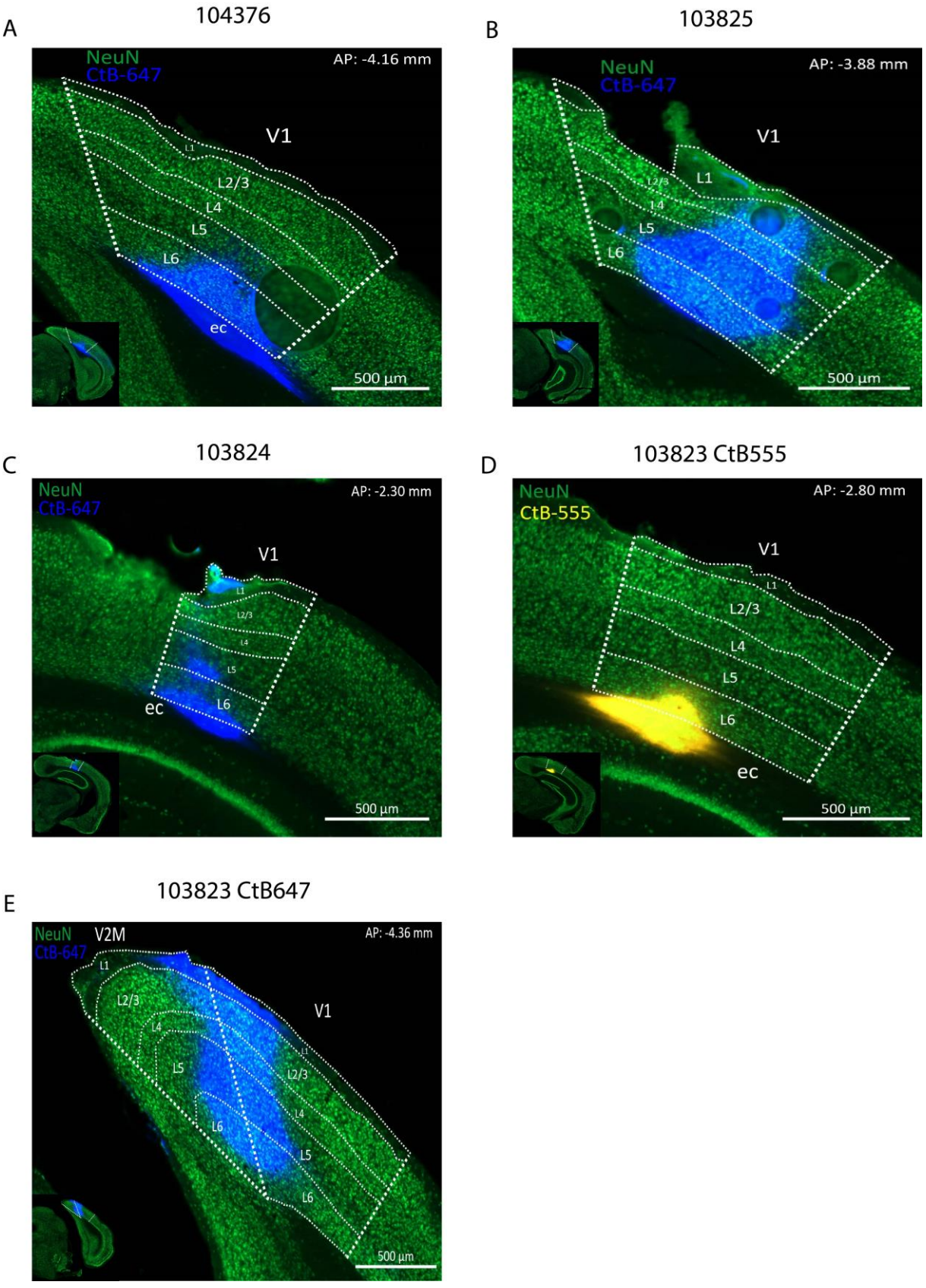

Figure 6: Histology of retrograde tracer injection sites in V1. Expanded view of right hemisphere at the bottom left corner for each image. Tissue is stained for NeuN in green. Delineations of V1 and V2M based on Franklin & Paxinos mouse brain atlas (Franklin & Paxinos, 2008). A: Mouse ID 104376. Injection hit L6 and ec. AP: -4.16 mm from bregma. B: Mouse ID 103825. Injection hit L1-6. AP: -3.88 mm from bregma. C: Mouse

ID 103824. Injection hit L5-6 and ec. Possibly some spill into L1. AP: -2.30 mm from bregma. D: Mouse ID 103823, CtB555 injection. Injection hit primarily L6b of V1 with spill into ec. AP: -2.80 mm from bregma. E: Mouse ID 103823, CtB647 injection. Injection hit L1-6 of V1 as well as L1-6 of V2M. AP: -4.36 mm from bregma.

Some injections targeting wS1 and V1 inadvertently hit other areas than wS1 and V1 (Fig. 7). Two injections hit the entire cortical column of the medial secondary visual cortex (V2M) (104375, 103821; Fig. 7A, B). One injection hit lateral parietal association cortex (LPtA) L5-6 and rostral posterior parietal cortex (PTPR) L6 with some spill into ec (104379; Fig. 7C).

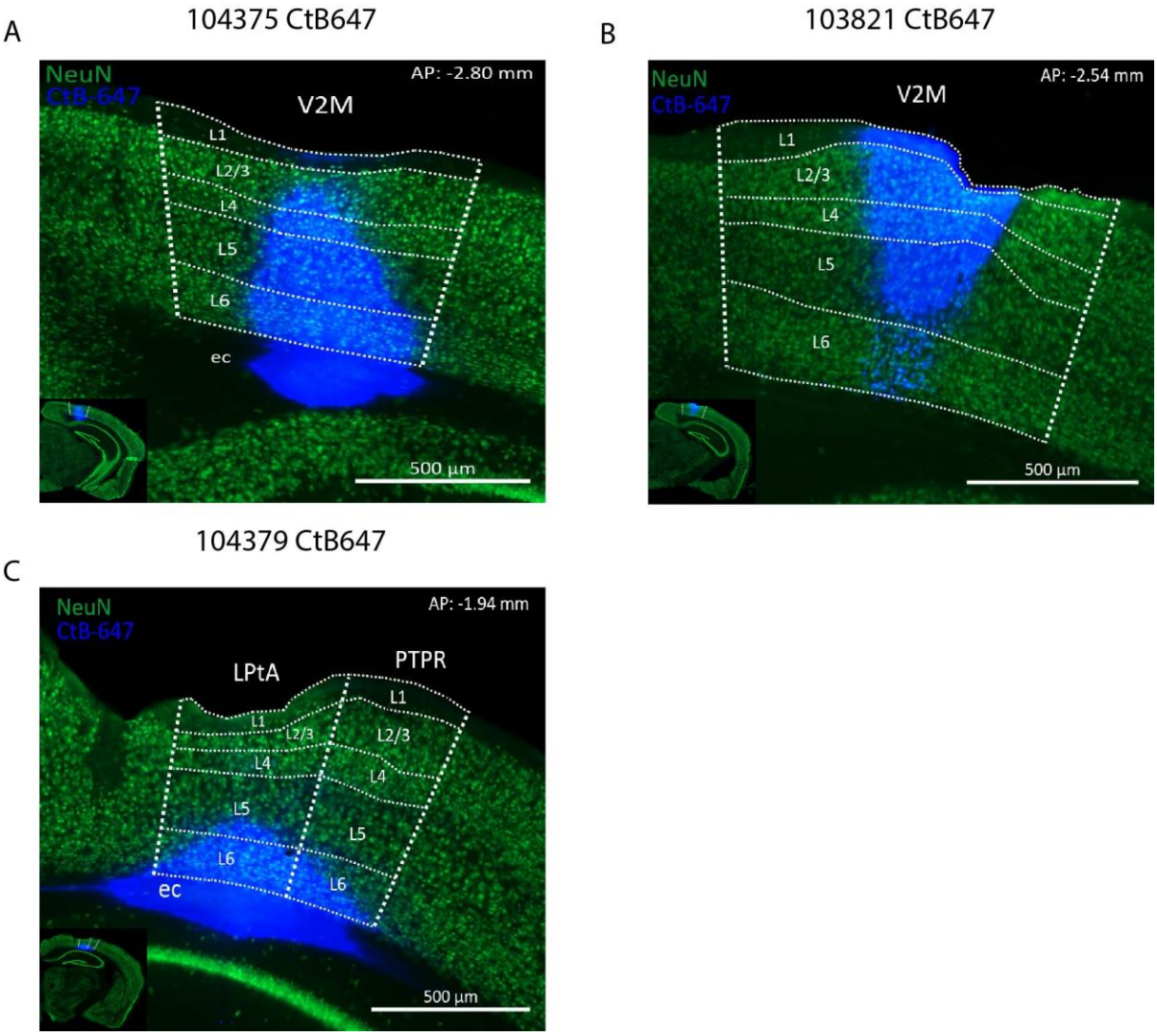

Figure 7: Histology of retrograde tracer injection sites in V2M and LPtA+PTPR. Expanded view of right hemisphere at the bottom left corner for each image. Tissue is stained for NeuN in green. Delineations of V2M and LPtA+PTPR based on Franklin & Paxinos mouse brain atlas (Franklin & Paxinos, 2008). A: Mouse ID 104375. Injection hit V2M L3-6 with spill into ec, and possibly L1 and L2. AP: -2.80 mm from bregma. B: Mouse ID 103821. Injection hit V2M L1-6. AP: -2.54 mm from bregma. C: Mouse ID 104379. Injection hit L5-6 of LPtA, L6 of PTPR, with spill into ec. AP: -1.94 mm from bregma.

For each of the injections above, the entire rostrocaudal extent of PER was investigated for CtB-AF labeled cells and quantified in a way such as shown in Figure 8. For the proportional cell counts per section for each of the injections shown above (Fig. 5-7), please see Appendix B2-5.

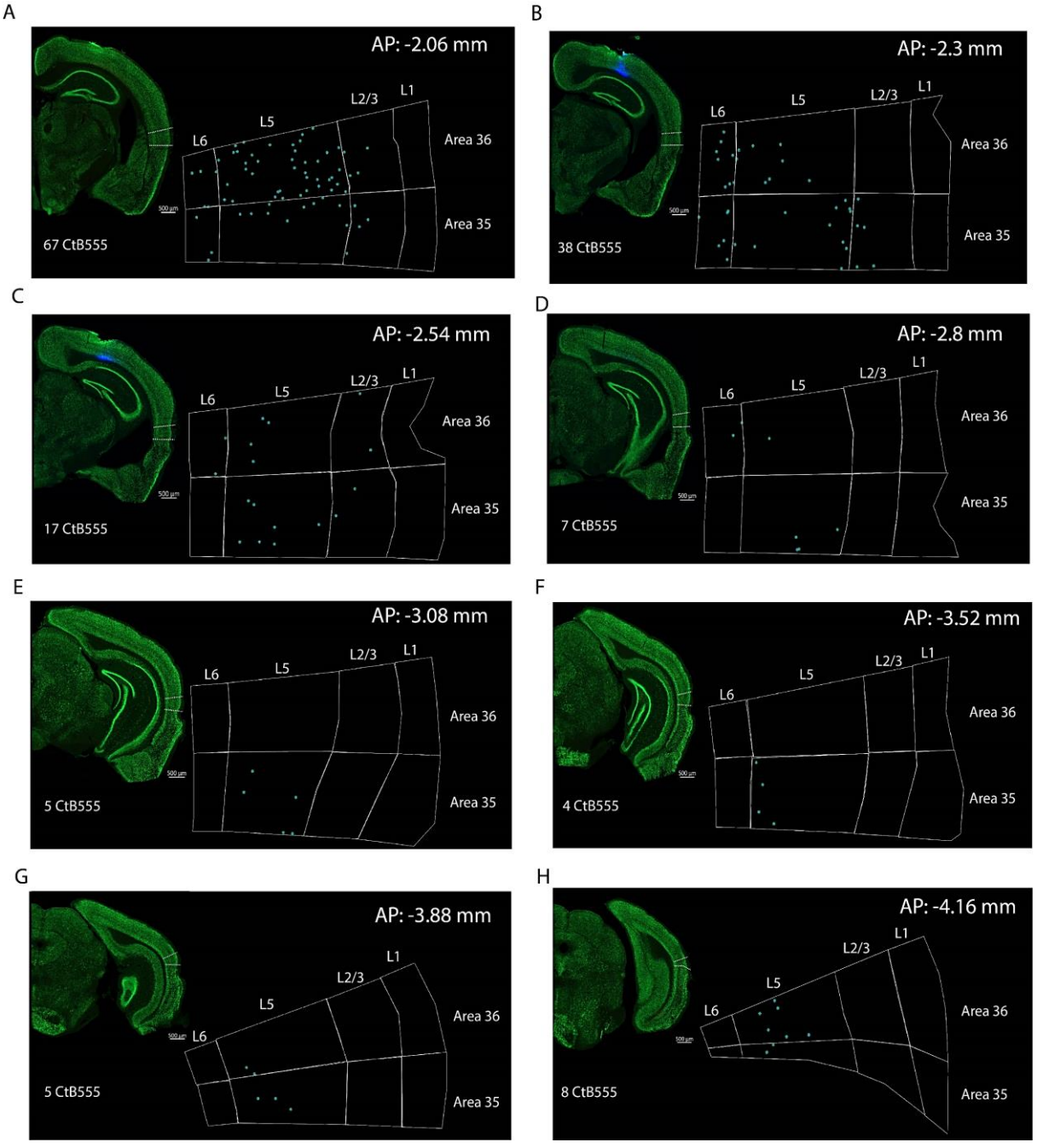

Figure 8: Example quantification of labeled cells across the rostrocaudal extent of PER from the CtB-555 injection in 103824. CtB555 injection marker in light blue is for the wS1 L6 injection (Fig. 5E), the counted cells for the CtB647 injection in this mouse (Fig. 6C) are not included in this example. Green staining is for NeuN. Expanded view of histology of right hemisphere at the top left for each image, with indicated PER delineation and scalebar for 500 µm. The number of CtB555 labeled neurons in each section is reported in the lower left corner. Each section was given an approximate AP

coordinate based on comparison with the Franklin & Paxinos mouse brain atlas (Franklin & Paxinos, 2008). Each section is 50 µm thick and was investigated for labeled cells across the entire z axis.

3.2 Topography of perirhinal feedback neurons to whisker barrel cortex

The rostrocaudal topography of FB neurons in ipsilateral PER to wS1 is strongly weighted towards rostral PER (Fig. 8, 9A). The peaks for all of the distributions were around -2 mm to -2.25 mm from bregma and decreasing sharply when proceeding caudally (Fig. 8, 9A). When binning the first and second half of the rostrocaudal extent of PER into two bins according to the PV labeling (See Methods, Fig. 4), the sum proportion of counted cells for the rostral half is much greater than in the caudal half for all injections (Fig. 9B). The injections with spill into ec did not exhibit a particularly different rostrocaudal pattern compared to the injections that accurately hit only cortical layers and are thus shown and included in the rostrocaudal analysis (Fig. 9A, B).

For the investigation of the laminar distribution of ipsilateral PER FB neurons to wS1, the injections with spill into ec tended to have a slightly higher proportion of counted cells in superficial layers (means: 21.72% vs 16.05%; SD: 12.62% vs 10.63% when including and excluding injections with ec spill, respectively. See Appendix B2.2), and as such were excluded in the analysis of laminar origin (Fig. 9C). The laminar distribution of ipsilateral PER FB neurons to wS1 is heavily weighted towards L5, with some proportion of the counts in L2/3 and L6 (Fig. 9C).

PER FB neurons to wS1 L6 were found in roughly equal proportions in A36 and A35 with a slight trend towards A36 (Fig. 9D). When ordered by rostrocaudal injection site, the data hints to a slight increase in relative proportion towards A36 as the injection site into wS1 proceeds caudally although this is difficult to verify with certainty. Furthermore, PER FB neurons in the injection to L1-5a of wS1 trended more strongly to A36 relative to A35 than the L6 injections (103825; Fig. 5F, 9D).

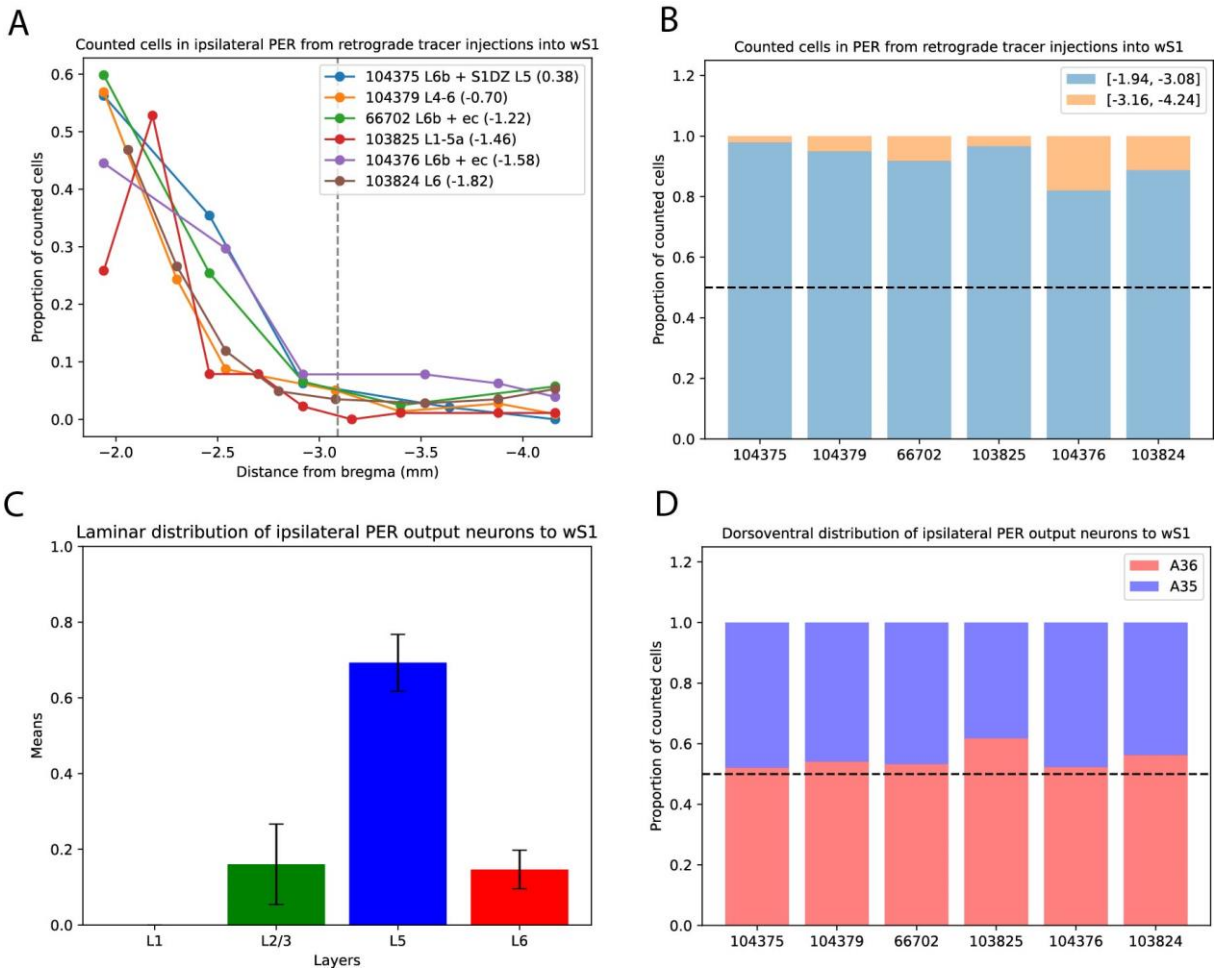

Figure 9: Topography of ipsilateral PER FB neurons to wS1. A: Line graph of counted FB neurons in ipsilateral PER from wS1 retrograde tracer injections. Each point is the cell count at a section in the series. AP coordinate of each section is based on comparison with the Franklin & Paxinos mouse brain atlas (Franklin & Paxinos, 2008). Dotted line at AP = -3.09 indicates the split between the rostral and caudal halves of PER. Series ordered in legend by the AP coordinate of injection site indicated in parenthesis. B: Stacked chart of the rostrocaudal distribution of ipsilateral PER FB neurons for each wS1 injection. Sum proportion of counts in each half of the rostrocaudal extent of PER. Legend indicates the ranges of distance from bregma which is included into each half. Dotted line at proportion = 0.5. C: Bar graph of laminar distribution of ipsilateral PER FB neurons to wS1. Injections with spill into ec are excluded from this figure. Error bars = SD. D: Stacked chart of dorsoventral distribution into A36 and A35 of ipsilateral PER FB neurons to wS1. The series are ordered by the rostrocaudal level of the injection site in wS1, from rostral to caudal.

3.3 Topography of perirhinal feedback neurons to V1

The rostrocaudal topography of PER FB neurons to V1 varied based on the specific rostrocaudal level of the injection site in V1 (Fig. 10, 11A, B). Rostral injection sites into V1 resulted in a higher proportion of labeled cells in rostral PER, while as the injection site proceeds caudally so does the distribution of labeled cells in PER (Fig. 10, 11A). When looking at the summed proportions for the rostral versus the caudal half of the rostrocaudal extent of PER for each of the injections ordered from rostral to caudal V1, this pattern becomes more evident (Fig. 11B). The most caudal injection did not follow

this pattern, but of note is how this injection had notable spill into V2M L1-6 (103823c; Fig. 6E).

When investigating the laminar origin of PER FB neurons to V1 it was found that injections with spill into ec resulted in a higher proportion of labeled neurons in superficial layers (See Appendix B3.2), a pattern that was also found during the investigation of laminar distribution of ipsilateral PER FB neurons to wS1 (Fig. 9C). However, when excluding the three V1 injections with spill into ec and looking strictly at the two injections with no spill (103825 & 103823c; Fig. 6B, E) one of these two injections also contains notable spill into V2M (103823c; Fig. 6E). Nevertheless, when looking at the laminar distribution of FB neurons in PER from these two injections, it is found that almost all the labeled neurons localized to the deep layers, with a higher proportion in L5 than L6 (Fig. 11C). The injection which hit V1 L1-6 with spill into V2M L1-6 (103823c; Fig. 6E) had no labeled cells in L2/3, while the injection which hit V1 L1-6 only (103825; Fig. 6B) had very weak labeling in L2/3 (proportion = 0.07285).

The labeled PER FB neurons to V1 mostly trended towards A36, except for the most rostral injection investigated (Fig. 11D) which trended towards A35. The injections with spill into ec (103824, 103823r, 104376) distributed variably into A36 and A35. The injection with notable spill into V2M (103823c) as well as the injection into V1 L1-6 (103825) both preferentially distributed only slightly towards A36 over A35.

When investigating whether the same FB neurons in PER provide efferents to both wS1 and V1, the three mice with successful injections into both wS1 and V1 were examined. The amount of doublelabeled cells in PER was found to be extremely low (3 doublelabeled cells vs 1078 singlelabeled cells across three brains).

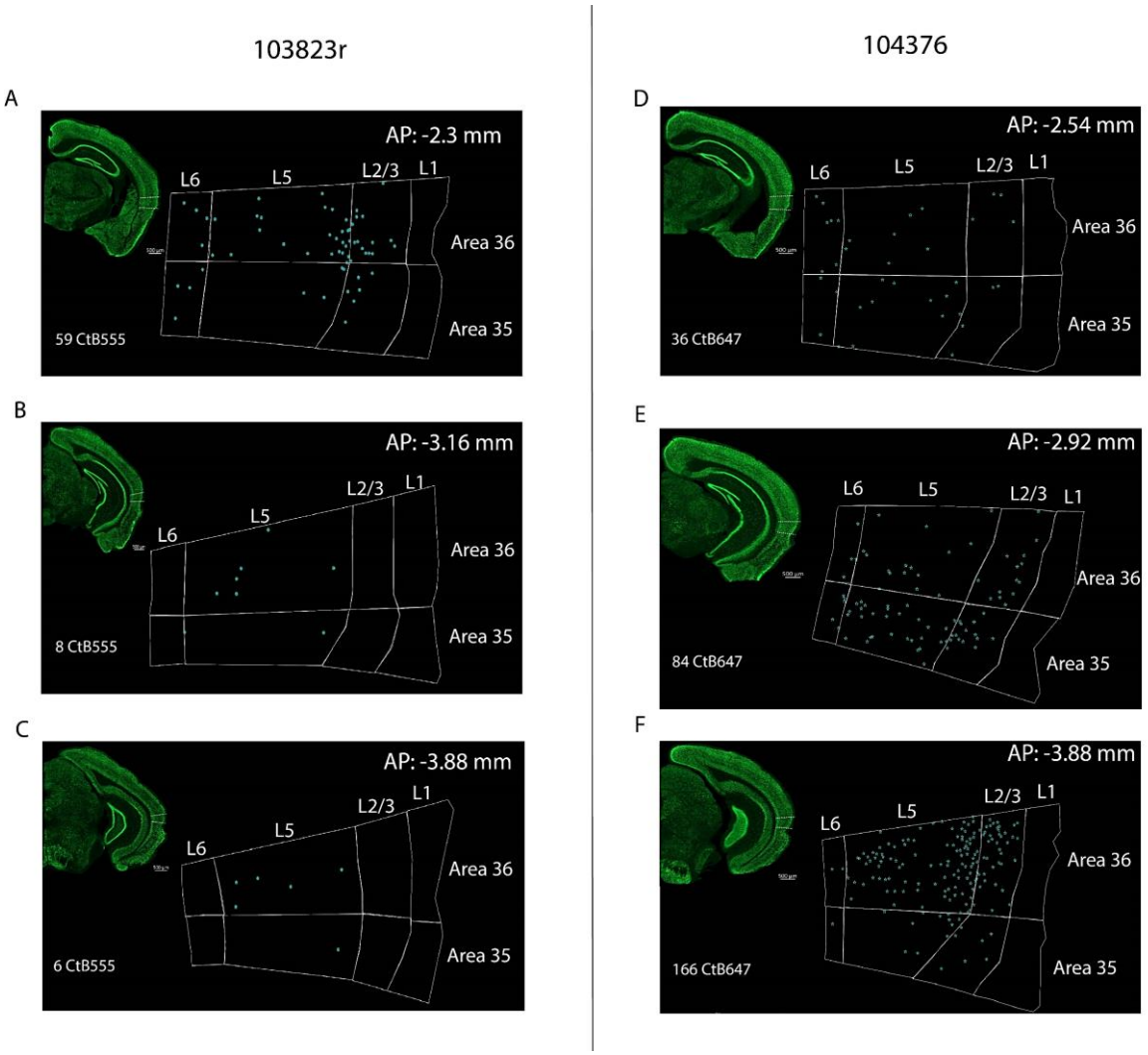

Figure 10: Example quantification of labeled cells across three rostrocaudal levels of PER from CtB-AF injections into V1 in mice 103823r and 104376. The CtB555 injection in mouse 103823 is in rostral V1 L6b + ec (Fig. 6D). The CtB647 injection in mouse 104376 is in midrostrocaudal V1 L6 + ec (Fig. 6A). Bottom left of each image is the quantified number of cells labeled for the CtB-AF injections per section shown in the two mice. Sections of comparable rostrocaudal level were chosen for the two mice. Expanded view of histology of right hemisphere at top left for each image, with indicated PER delineation and scalebar for 500 µm. Green staining is for NeuN. Each section was given an approximate AP coordinate based on comparison with the Franklin & Paxinos mouse brain atlas (Franklin & Paxinos, 2008). Each section is 50 µm thick and was investigated for labeled cells across the entire z axis. A: Peak of the distribution for 103823r. F: Peak of the distribution for 104376.

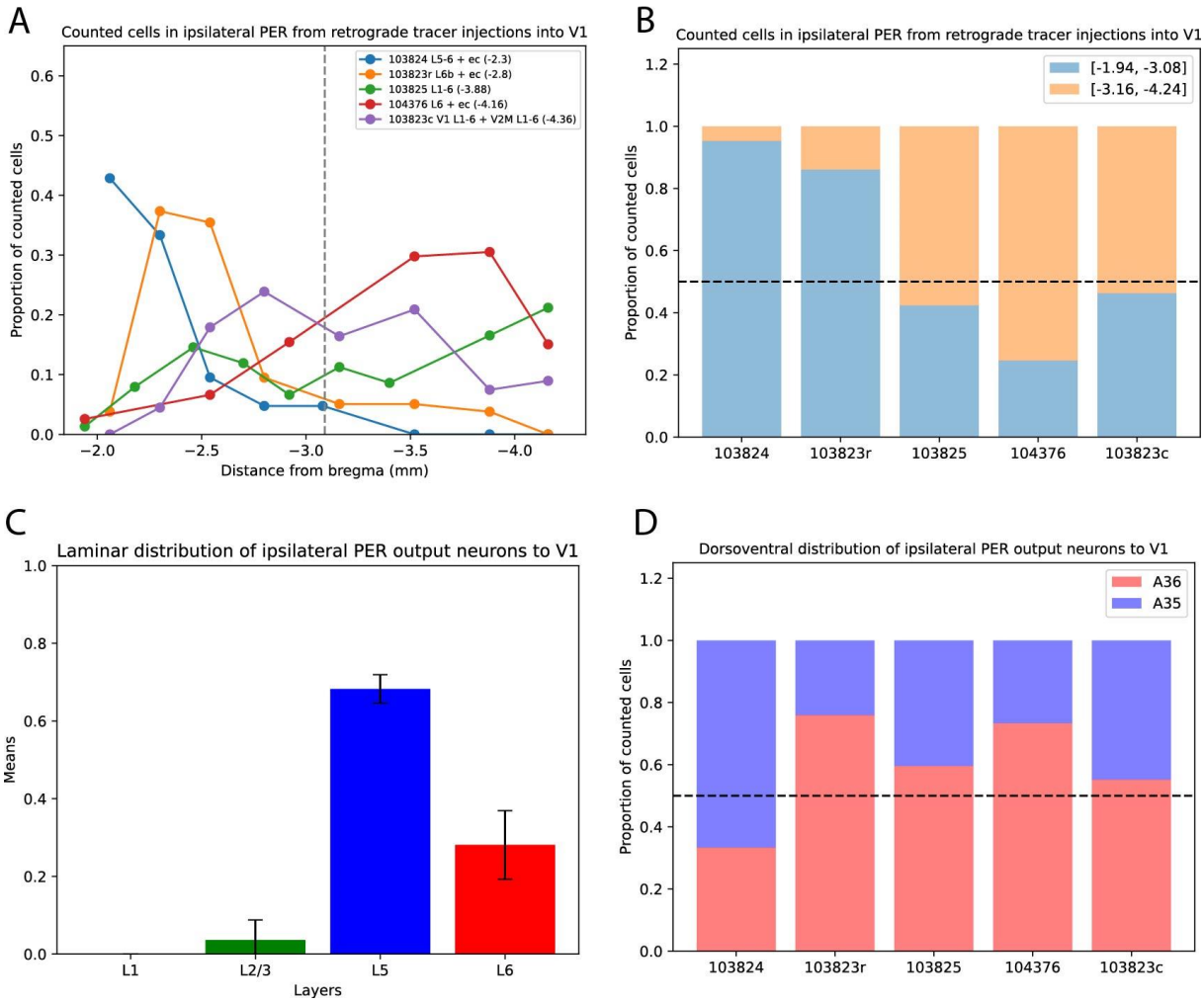

Figure 11: Topography of ipsilateral PER FB neurons to V1. A: Line graph of counted FB neurons in ipsilateral PER from V1 retrograde tracer injections. Each point is the cell count at a section in the series. AP coordinate of each section is based on comparison with the Franklin & Paxinos mouse brain atlas (Franklin & Paxinos, 2008). Dotted line at AP = -3.09 indicates the split between the rostral and caudal halves of PER. Series ordered in legend by the AP coordinate of injection site indicated in parenthesis. B: Stacked chart of the rostrocaudal distribution of ipsilateral PER FB neurons for each V1 injection. Sum proportion of counts in each half of the rostrocaudal extent of PER. Legend indicates the ranges of distance from bregma which is included into each half. Dotted line at proportion = 0.5. C: Bar graph of laminar distribution of ipsilateral PER FB neurons to V1. Injections with spill into ec are excluded from this figure. Error bars = SD. D: Stacked chart of dorsoventral distribution into A35 and A36 of ipsilateral PER FB neurons to V1. The series are ordered by the rostrocaudal level of the injection site in wS1, from rostral to caudal.

3.4 Contralateral PER FB neurons

When investigating the labeling of neurons in contralateral PER from the various injections in wS1 and V1, an interesting difference arose between the cortices. For wS1 L6 injections, irrespective of whether there was considerable ec spill or not, there was a considerable number of labeled neurons although weaker than ipsilaterally (n=266 neurons across five injections contralaterally, vs n= 605 neurons ipsilaterally). However, for the one injection which hit only wS1 L1-5a with most of the injection bolus in L3-4 (103825; Fig. 5F), there was barely any labeling in contralateral PER (n=3 neurons). For

the V1 injections performed for this study, contralateral PER was labeled strongly if there was considerable spill into ec (n=530 neurons across two injections) whereas accurate injections into only the cortex resulted in extremely few labeled cells (n=17 neurons across three injections) making it difficult to provide meaningful analysis. Because of this, labeled neurons in contralateral PER to V1 and L1-5a of wS1 are excluded from this analysis and only the contralateral PER FB neurons to wS1 L6 will be analyzed.

When investigating the rostrocaudal distribution of contralateral PER FB neurons for each injection individually (Fig. 12A), the peaks for each distribution were variably distributed between -2 mm and -2.75 mm from bregma. The rostrocaudal distribution of contralateral PER FB neurons to wS1 L6 was weighted very strongly to the rostral half of the rostrocaudal extent of PER (Fig. 12B).

The laminar origin of contralateral PER FB neurons when excluding the injections with ec spill distributed almost exclusively to L5 of contralateral PER (Fig. 12C). There were no counted cells in L6 of contralateral PER for any of the injections, while a very small proportion of cells originate in L2/3 (mean = 2.70%; SD = 2.58%).

Interestingly, contralateral PER FB neurons to wS1 L6 trended toward A35 for all injections except one of the injections into caudal wS1 L6b with spill into ec (104376; Fig. 5C) which trended toward A36 (Fig. 12D). The injection which hit wS1 L6 exclusively (103824; Fig. 5E) did however result in labeling of contralateral PER exhibiting no particular trend towards A36 or A35.

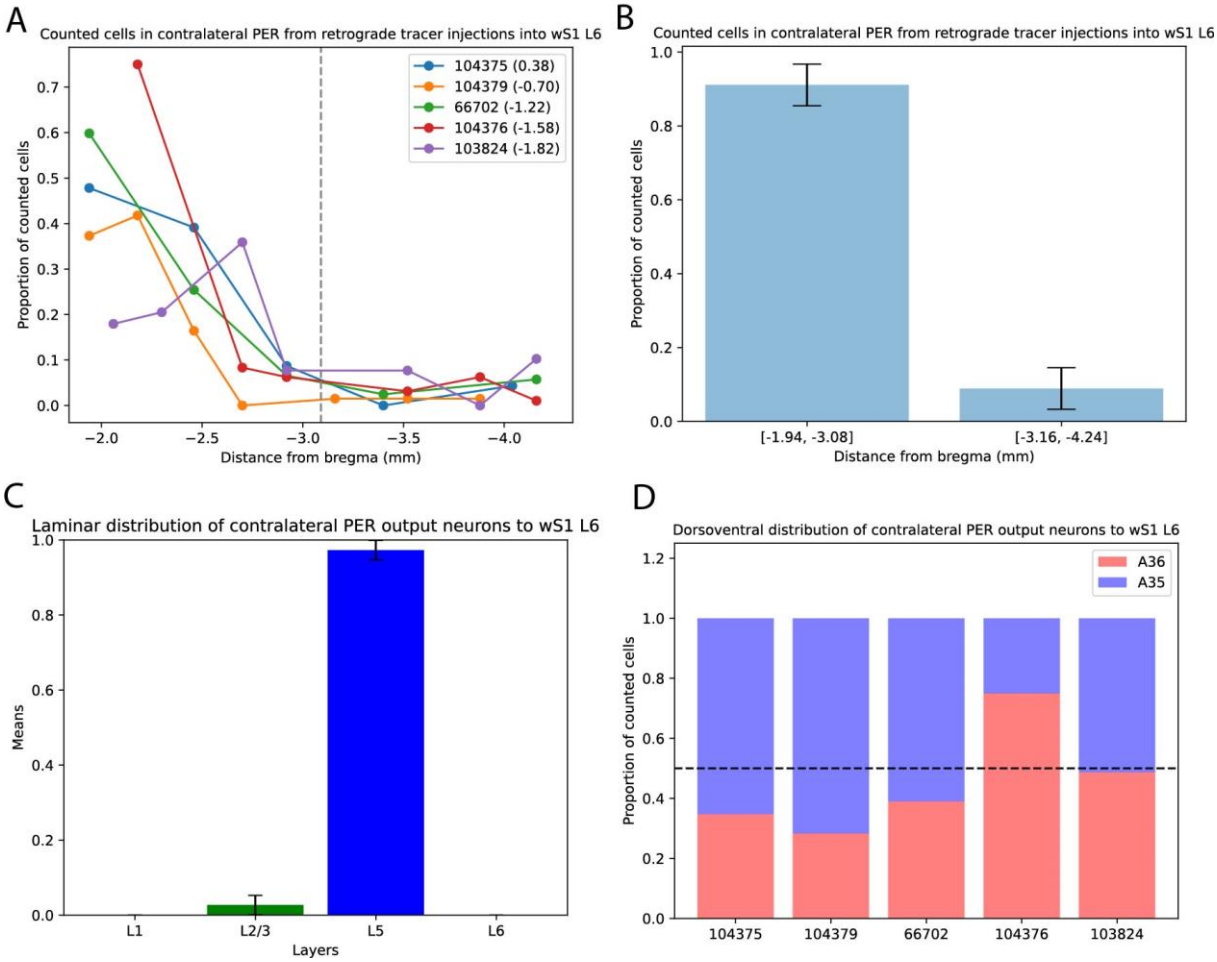

Figure 12: Topography of contralateral PER FB neurons to wS1 L6. A: Line graph of counted FB neurons in contralateral PER from wS1 L6 retrograde tracer injections. Each point is the cell count at a section in the series. AP coordinate of each section is based on comparison with the Franklin & Paxinos mouse brain atlas (Franklin & Paxinos, 2008). Dotted line at AP = -3.09 indicates the split between the rostral and caudal halves of PER. Series ordered in legend by the AP coordinate of injection site indicated in parenthesis. B: Bar graph of the rostrocaudal distribution of contralateral PER FB neurons to wS1 L6. The mean of the sum cell count proportions in contralateral PER from wS1 L6 injections (n=5) is shown for the two halves of the rostrocaudal extent of PER. X-axis labels indicate the ranges of distance from bregma which is included into each half. Error bars = SD. C: Bar graph of laminar distribution of contralateral PER FB neurons to wS1 L6. Injections with spill into ec are excluded from this figure. Error bars = SD. D: Stacked chart of dorsoventral distribution into A35 and A36 of contralateral PER FB neurons to wS1 L6. The series are ordered by the rostrocaudal level of the injection site in wS1, from rostral to caudal.

3.5 Topography of PER FB neurons to V2M and LPtA+PTPR

When aiming for wS1 and V1 injections into L1 and L6, two injections inadvertently hit V2M while one injection inadvertently hit LPtA+PTPR (Fig. 7). The injections into V2M result in labeling of PER FB neurons trending towards rostral PER, while the injection into LPtA+PTPR also trended towards rostral PER (Fig. 13A). As for the laminar distribution of PER FB neurons to these regions, there is a consistent trend towards L5 for both PER FB neurons to V2M and LPtA+PTPR (Fig. 13B, C). Of note is how two of the three injections have spill into ec (104375, 104379; Fig. 7A, C), while the injection which hit V2M but had no spill into ec resulted in quite weak labeling (103821; Fig. 7B) (n=24 cells across 8

sections). Both injections with ec spill shows more proportional cell counts in superficial layers (104375 L2/3 proportion = 0.32; 104379 L2/3 proportion = 0.27), while the injection with no spill has no counted cells in superficial layers of PER. Injections into V2M and LPtA + PTPR all resulted in distributions more strongly weighted towards A36 than A35 (Fig. 13D), more so for the two injections with ec spill than the injection with weak labeling.

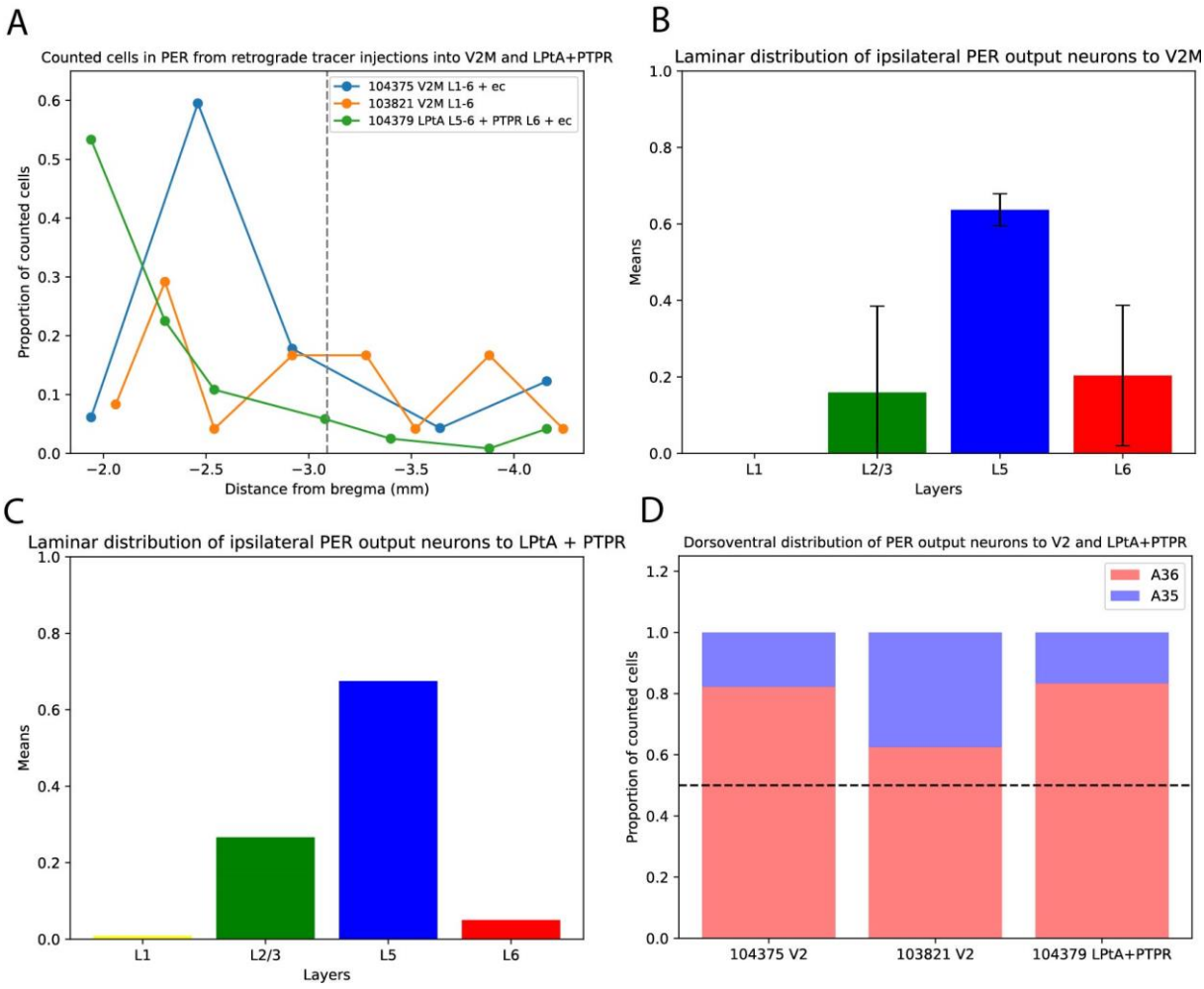

Figure 13: Topography of ipsilateral PER FB neurons to V2M and LPtA+PTPR. A: Line graph of counted FB neurons in ipsilateral PER from retrograde tracer injections into V2M and LPtA+PTPR. Each point is the cell count at a section in the series. AP coordinate of each section is based on comparison with the Franklin & Paxinos mouse brain atlas (Franklin & Paxinos, 2008). Dotted line at AP = -3.09 indicates the split between the rostral and caudal halves of PER. B: Bar graph of laminar distribution of ipsilateral PER FB neurons to V2M. Error bars = SD. C: Bar graph of laminar distribution of ipsilateral PER FB neurons to LPtA+PTPR. D: Stacked chart of dorsoventral distribution into A36 and A35 of ipsilateral PER FB neurons to V2M and LPtA+PTPR.

4 Discussion

PER integrates multisensory information through its afferent connectivity from the various sensory cortices of the brain (Burwell & Amaral, 1998a; Foroughi, 2022; Suzuki & Amaral, 1994). This sensory integration is crucial for PER to perform its role in functions

such as object recognition memory that use sensory information to discriminate between objects. Winters & Reid (2010) exemplify this by showing that perirhinal lesioned rats perform worse in purely visual as well as crossmodal visuotactile object recognition tasks (Winters & Reid, 2010). The efferents from PER to lower order cortices would be referred to as feedback projections and function in modulating the feedforward sensory signal (Zagha, 2020). As for the specific laminar anatomy of FB projections, FB efferents should originate in L6, lower L5 and L2/3A of PER and innervate L1 or L6 of the target cortex depending on the hierarchical distance between the two areas (Markov et al., 2014) (Fig. 1B). Efferent connectivity from PER to specifically wS1 L6 or any layer of V1 has not yet been shown in mice. In this thesis, the retrograde tracer CtB-AF was injected into various rostrocaudal levels of wS1 L6 and V1 L6, and the rostrocaudal, laminar, and dorsoventral distribution of feedback neurons in PER was investigated.

4.1 PER FB neurons project to wS1 L6 and V1 in mice

One of the primary aims of this study was to investigate the feedback projections from PER to the primary somatosensory and visual cortices. This study provides a novel finding in confirming that PER provides FB innervation to wS1 L6 in mice (Fig. 9), as there are several retrograde tracer injections which hit wS1 L6 that give rise to prominent labeling in PER (Fig. 5A-E). My results also show that PER projects to V1 in mice (Fig. 10, 11), a finding which has been shown previously in rats and primates (Agster & Burwell, 2009; Markov et al., 2014). I also find that PER projects to specifically L6 of V1 by the labeling in PER from several injections into V1 L6 (Fig. 6A, C, D).

Furthermore, my results do also to some extent confirm the findings of PER projecting to superficial layers of S1 in both mice and rats by the one injection into wS1 L1-5a (103825; Fig. 5F, Fig. 9) (Agster & Burwell, 2009; Doron et al., 2020; Naskar et al., 2021). Markov et al. (2014) propose that termination of feedback efferents should be localized primarily to L6 but also up to the lower part of L5, just above the border between L5 and L6 (Markov et al., 2014). According to this, the part of the injection bolus in L5a should not be labeling the deep layer innervating efferents of PER (Markov et al., 2014) (Fig. 1B), and the labeling of PER as a result of this injection could be considered due to the injection hitting superficial layers of wS1.

Topography of PER FB neurons to wS1

My aim was to investigate the rostrocaudal origin of PER FB neurons to wS1, and by injecting retrograde tracers into various rostrocaudal levels of wS1 I find that ipsilateral PER FB neurons to wS1 predominantly originate in rostral PER (Fig. 9A, B). This was found to be the case irrespective of the rostrocaudal level of the injection site in wS1, whether the injection had notable spill into ec, or whether the injection hit L6 or was towards more superficial wS1. Agster & Burwell (2009) investigated PER efferents in rats by injecting anterograde tracers into different rostrocaudal levels of A35 and A36, and they note that labeling in S1 was strongest as a result of rostral PER injections (Agster & Burwell, 2009), providing the same indications as my finding of rostral PER being the region which provides most output to S1.

When investigating the aim surrounding the laminar origin of ipsilateral PER FB neurons to wS1, I find that they were greatly restricted to deep layers though not exclusively (Fig. 9C). This was found by excluding injections with spill into ec, as injections into wS1 with spill into ec consistently labeled a higher proportion of neurons in L2/3 of PER (See

Appendix B2.2). Markov et al. (2014) propose that in the supragranular layers FB neurons should originate in L2/3A, while in the infragranular layers FB neurons should originate in L6 and lower L5 (Markov et al., 2014) (Fig. 1B). As the hierarchical distance increases, the FB neurons should gradually originate in only the infragranular layers, and the infragranular originating FB neurons should innervate L6 of wS1 as well as L1. The supragranular FB neurons should only innervate L1, yet I find a small population of supragranular FB neurons as a result of the injections into wS1 L6 (Fig. 9C). This might be due to a peculiarity of PER as a region without L4 in coronal sections making the precise border between L3 and L5 more difficult to define, but even so the proportion of counted cells in L2/3 is consistently too high to be due to miscounting as a result of a few micrometers error in defining the border. Alternatively, the description by Markov et al. (2014) is based on studies in the visual system of primates so it might be due to a species difference between mice and primates. Nevertheless, as the vast majority of FB neurons were found in deep layers, my results do confirm the major indication of FB neurons to L6 originating in deep layers by Markov et al. (2014). Felleman & Van Essen (1991) describe feedback neurons originating in both supragranular and infragranular layers as greatly restricted in the closest two levels in the hierarchy, and a similar indication is in the Markov et al. (2014) framework. However, the proportion of FB neurons to wS1 originating in supragranular layers of PER is very small relative to the proportion originating in infragranular layers. As such, this finding would according to the Markov et al. (2014) framework indicate that the hierarchical distance is not directly adjacent in level but also not very far between wS1 and PER, as there are cells counted in the supragranular layers and not only infragranular layers of PER (Markov et al., 2014).

As for the dorsoventral origin of the FB neurons to wS1, my results indicate a slight trend towards FB neurons preferentially originating in A36 relative to A35 (Fig. 9D). Agster & Burwell (2009) find that labeling was strongest in S1 as a result of anterograde tracer injections into A36 in rats (Agster & Burwell, 2009). My results in mice indicate only a slight preference of origin for PER FB neurons in A36 over A35, which is consistent with the finding in rats even though the difference is not as strong as indicated in their study (Agster & Burwell, 2009).

In rats, caudal S1 was the region with greatest labeling by anterograde tracers into PER in the study by Agster & Burwell (2009). However, they come to this conclusion by directly comparing the amount of labeling in S1 as a result of each of their anterograde tracer injections into PER (Agster & Burwell, 2009). In my study, each injection into wS1 has a varying amount of injection bolus into the lamina of interest while some could be lost to spill or leakage, which ultimately impacts the strength of the labeling in PER. Because of this I cannot directly compare the number of labeled cells between each injection and confirm whether the caudal wS1 injections resulted in the most labeling in PER.

Topography of PER FB neurons to V1

One of the primary aims of this study was to investigate the topography of PER output neurons to V1. My findings indicate a rostrocaudal origin of PER FB neurons to V1 which varied greatly for the various injections into V1 (Fig. 11A). No clear pattern explaining this difference was found when investigating the specific layers hit by each injection or when comparing the injections with spill into ec to the injections without spill. However, one possible explanation for this pattern is the rostrocaudal level of the injection site in

V1. This is more evident when ordering the quantified rostrocaudal extents of PER by the rostrocaudal level of the injection site (Fig. 11B). It seems that the more rostral injection into V1 results in labeling of rostral PER, while as the injection site proceeds caudally so does the labeling of neurons in PER. In other words, my results indicate that the PER FB neurons to V1 originate in a rostrocaudal level that closely follows the rostrocaudal level of the injection site. The most caudal injection deviates from this pattern, but this injection does have around half of its bolus in V2M L1-6 (103823c; Fig. 6E). This deviation from the pattern could be explained by comparing the rostrocaudal origin of PER FB neurons for this caudal V1 injection with the other V2M injections which result in FB neurons preferentially originating in rostral PER (Fig. 13A). It is possible that the most caudal V1 injection results in FB neurons in PER originating more rostrally than the second most caudal V1 injection because of this V2M spill specifically. This rostrocaudal pattern for PER FB to neurons to V1 has been shown here (Fig. 11A) has been described for other areas such as PER efferents to piriform cortex in rats (Agster & Burwell, 2009), but has not been described for V1 in either rats or primates. Agster & Burwell (2009) describe that stronger innervation of all occipital areas including V1 originates from caudal PER in rats, which indicates a different rostrocaudal distribution than indicated by my results. When comparing the labeling of visual areas from their rostral injections with their caudal injections, one could make an argument for their data also indicating a similar rostrocaudal pattern as indicated by my results (Agster & Burwell, 2009). However, the authors make no mention of this specifically.

As for the aim of the study to elucidate the laminar origin of PER FB neurons to V1, I find that the neurons originate almost exclusively in deep layers (Fig. 11C). According to the Markov et al. (2014) framework, the counted cells in L2/3 of PER should be due to the injection in V1 L1, and the counted cells in infragranular layers of PER should be due to the injection in V1 L1 and L6 (Markov et al., 2014). It is however important to note that my findings for wS1 L6 described above show a discrepancy in this framework by labeling neurons in L2/3 of PER as a result of L6 injections, and as such it is not possible to conclude with certainty what neurons labeled in PER is due to what layers of V1 have injection bolus. Nevertheless, the very low proportion of counted FB neurons in supragranular layers of PER indicates according to the Markov et al. (2014) framework that the hierarchical distance between PER and V1 is quite far. This is consistent from what Markov et al. (2014) describe for their own results for the FB projections from PER to V1 in primates, where FB cells were found almost exclusively in deep layers (99.28% of cells were counted in deep layers) (Markov et al., 2014).

When investigating the dorsoventral pattern of origin for PER FB neurons to V1, I find that they preferentially originate in A36 over A35 (Fig 11D). Agster & Burwell (2009) investigate PER efferents to visual areas in the occipital lobe of rats and show that A36 is the subdomain of PER that produced more labeled fibers in occipital regions (Agster & Burwell, 2009). In their study, they do not distinguish V1 from V2 but rather group them together with all visual areas of the occipital lobe, indicating that V1 and V2 should result in the same dorsoventral pattern. These findings in rats, combined with how most of the injections in V1 I performed in this study result in preferential labeling of neurons in A36, supports the case for PER FB neurons to V1 preferentially originating in A36 over A35.

PER FB neurons to both wS1 and V1

When investigating the secondary aim regarding whether the same output neurons in PER innervates both sensory cortices, I find extremely few doublelabeled cells in PER for

mice with successful injections into both wS1 and V1. Of the three injections into wS1 and V1 with quantifiable sections, 3 neurons were doublelabeled while 1078 neurons were labeled only to one of the two retrograde tracer injections. Given the indicated rostrocaudal distribution of PER FB neurons to wS1 and V1 in this study, one could make the argument that only rostral V1 injections would be useful for comparison with wS1 injections as these would overlap in where they distribute in PER. One of these injections hit caudal wS1 L6 and specifically rostral V1 L5-6, and even this injection only resulted in 1 labeled neuron while 170 neurons were labeled for only one of the two injections (103824; Fig. 5E, 6C). These results strongly indicate that there are distinct non-overlapping cell populations that project to either the primary somatosensory or primary visual cortices, or in other words that the same FB neuron in PER does not project to both cortices.

Contralateral PER FB neurons to wS1 and V1

A secondary aim of this study was to investigate the anatomy of projections from contralateral PER to wS1 and V1. I find that the injections into V1 without spill into ec as well as the wS1 L1-5a injection resulted in very weak labeling of contralateral PER, indicating that these areas receive negligible innervation by contralateral PER. The remainder of the wS1 injections all were aimed at L6, and produced a labeling in rostral PER that closely follows what was found for ipsilateral PER to wS1 (Fig. 9A, B, Fig. 11A, B). This was the case irrespective of spill into ec for the rostrocaudal distribution, however spill into ec strongly impacted the laminar distribution of labeled cells and as such were excluded from that specific analysis.

When investigating the laminar origin of contralateral PER FB neurons to wS1 L6, I find that the labeled neurons were almost exclusively originating in L5 (Fig. 12C). No cells were counted in contralateral PER L6 for any of the wS1 L6 injections even when including spill, and an extremely low proportion was counted in L2/3 for the three injections into wS1 L6 without spill into ec (Fig. 12C).

The dorsoventral distribution of contralateral PER FB neurons to wS1 L6 seemed to trend more towards A35 than A36 (Fig. 12D). However, this was not as clear as for ipsilateral PER since not all the injections result in the same indications. The injection with roughly equal parts A35 and A36 labeling (103824; Fig. 5E) was clearly into only L6 of wS1 and would thus be the injection most indicative of contralateral PER FB neurons to wS1 L6. Yet, most of the injections resulted in labeling of primarily A35 while one injection was more strongly towards A36 making it difficult to come to a clear conclusion. Altogether, these results do indicate that contralateral PER FB neurons to wS1 L6 trends more towards A35 than A36 (Fig. 12D), which is different from ipsilateral PER which trends slightly towards A36 (Fig. 9D).

PER FB neurons to V2M and LPtA+PTPR

When targeting wS1 and V1 L6, two injections inadvertently hit V2M and one injection hit LPtA+PTPR (Fig. 7). As there are no notable problems with these injections except the occurrence of ec spill for one V2M injection (Fig. 7A) and the LPtA+PTPR injection (Fig. 7C), they were analyzed in a similar manner as for wS1 and V1.

When investigating the rostrocaudal origin of PER FB neurons to V2M, I find that the neurons preferentially originate in rostral PER in both cases (Fig. 13A). It is however not possible with my data to say whether this labeling in rostral PER for the V2M injections is due to these two injections being quite rostral, or if the FB neurons in PER to V2M will

originate in rostral PER no matter the rostrocaudal level of the injection in V2M. Agster & Burwell (2009) indicate in their findings in rats that injections in caudal PER lead to the strongest labeling of visual areas of the occipital lobe. However, in the same way as discussed above their data might indicate a rostrocaudal origin that follows the rostrocaudal level of the injection site for visual areas. It is therefore difficult to say with certainty if my findings for PER to V2M in mice is inconsistent with their findings in the rat (Agster & Burwell, 2009).

The LPtA+PTPR injection also predominantly labels neurons in rostral PER (Fig. 13A). Agster & Burwell (2009) describe the projection from PER to posterior parietal cortex to follow a rostrocaudal pattern of origin which follows the level of the injection site. As my injection has bolus in rostral posterior parietal cortex it is therefore consistent with their finding in rats (Agster & Burwell, 2009).

One of the aims of this study was to investigate the laminar origin of the PER FB neurons, and I find that the origin of PER FB neurons to V2M and LPtA+PTPR trend strongly to deep layers (Fig. 13B, C). There is however a considerable limitation to the investigation of the laminar origin for these injections, as one of the two V2M injections as well as the LPtA+PTPR injection have considerable spill into ec. This has been found to increase the proportion of supragranular labeled neurons in PER in the analyses of wS1 and V1 (See Appendix B2.2, B3.2). I find a higher proportion of supragranular labeled neurons in PER for the injections with spill into ec, but the one injection into V2M with no spill has no counted cells in supragranular layers. According to the Markov et al. (2014) framework this indicates that PER and V2M are quite distant in terms of hierarchical levels. The injection into LPtA+PTPR with spill into ec cannot be used to indicate the hierarchical distance based on the Markov et al. (2014) framework, but does give the same indication as all the other analyses of laminar distribution performed in this study of L5 being the main layer of origin for FB neurons in PER.

As for the dorsoventral distribution of PER FB neurons to V2M and LPtA+PTPR, all three indicate a preferential origin in A36 over A35 (Fig. 13D). This is consistent with findings from Agster & Burwell (2009), where they find that A36 injections lead to stronger labeling of both posterior parietal cortex as well as visual cortices in the occipital lobe (Agster & Burwell, 2009).

Because there is a low sample size of V2M and LPtA+PTPR injections in this study as well as two of these injections having notable spill into ec, making any definitive conclusions about the topography and laminar distribution of PER FB neurons to V2M and LPtA+PTPR is difficult. Nevertheless, investigating these three injections has been fruitful for the indications given for the general laminar distribution of PER FB neurons trending towards L5 and deep layers, as well as using the V2M injections to compare to the rostrocaudal distribution of the one V1 injection with V2M spill (103823c; Fig. 6E).

4.2 Topographical relationship between input and output of PER

One of the ways feedback efferents from a higher order to a lower order cortical area are noted to perform their function is by modulating the feedforward sensory input received by the lower order cortex (Zagha, 2020). As such, one could expect that the output of PER closely follows the input to PER. However, PER has been noted previously to have

asymmetrical reciprocity with several cortical regions in primates and rats (Agster & Burwell, 2009; Lavenex et al., 2002; Suzuki & Naya, 2014). In other words, PER was found to not always project to areas it receives input from, and not always did PER receive input from areas it projects to. As such, I will compare and contrast my findings on PER output to wS1 and V1 in mice with previous studies investigating the input to PER from S1 and V1.

According to my findings, PER FB neurons to wS1 preferentially originate in rostral PER (Fig. 9A, B). When comparing this to previous work done on the input from S1 to PER in mice, it is suggested that primary somatosensory input arrives to rostral PER (Foroughi, 2022) which indicates reciprocity in rostral PER (Fig. 14A). Furthermore, I find that PER FB neurons to wS1 originate slightly preferentially in area 36 over area 35 (Fig. 9D). No dorsoventral distribution was noted in the study of PER afferents in mice, though there were no injections targeting rostral A35 in their study (Foroughi, 2022). Studies of afferent connectivity in rats by Burwell & Amaral (1998) indicate a slight preference for parietal areas to project to A36 over A35, though this difference was not very strong (Burwell & Amaral, 1998a). One could argue that the slight trend towards A36 that I note in the efferents of PER to wS1 is in fact so small that concluding with no particular dorsoventral difference is reasonable, and that the efferents and afferents both distribute roughly equally to A36 and A35. Overall, the afferent and efferent connectivity of PER to S1 in mice seems to overlap and both preferentially occur in rostral PER, and somewhat more debatable is whether the reciprocal connectivity is roughly equally distributed to A36 and A35 or if it trends slightly to A36.

My results indicate that the output of PER to V1 varies in the rostrocaudal level of origin depending on the rostrocaudal level of the injection site in V1 (Fig. 10, 11A-B, 14B). The study of PER afferents in mice by Foroughi (2022) shows that retrograde tracer injections in PER result in similar labeling across the rostrocaudal extent of V1. It is however not noted whether the labeling in V1 follows the rostrocaudal level of the injection site in PER, or if there was stronger labeling of a certain rostrocaudal level of V1 irrespective of the level of the injection site. If there was stronger labeling of for example caudal V1 irrespective of the injection site, it is possible that the relationship of output and input between PER and V1 is a case of asymmetrical reciprocity such as previously detailed for PER and other areas in rats and primates (Agster & Burwell, 2009; Lavenex et al., 2002; Suzuki & Naya, 2014). It is also possible that the connectivity between V1 and PER is indeed reciprocal but follows a pattern where the connectivity is aligned across the rostrocaudal extent of each area.

I find that PER FB neurons to V1 arise mainly from A36 over A35 (Fig. 10D). Foroughi (2022) notes a possible preferential innervation of A35 (Foroughi, 2022). This trend towards A35 however is also noted by Foroughi (2022) to be due to an injection to deep layers of A35, which resulted in the strongest labeling due to the layers the injection hit rather than reflecting a dorsoventral gradient (Foroughi, 2022). Other than this, no particular dorsoventral gradient was noted in the study. In a study of PER afferents in rats by Burwell & Amaral (1998) they indicate that V1 projects mostly to A36 (Burwell & Amaral, 1998a). My findings are consistent with the indications in the rat afferent study by Burwell & Amaral (1998) as both show a trend towards A36. One notable difference however is that they find afferent projections from V1 to almost exclusively A36, while my findings indicate only a trend towards A36 over A35 for the origin of the efferents from PER to V1. Overall, my results indicate an asymmetrical reciprocity in the dorsoventral axis when compared to the indications from mice afferents (Foroughi,

2022), but symmetrical reciprocity when compared to indications from rat afferents (Burwell & Amaral, 1998a).

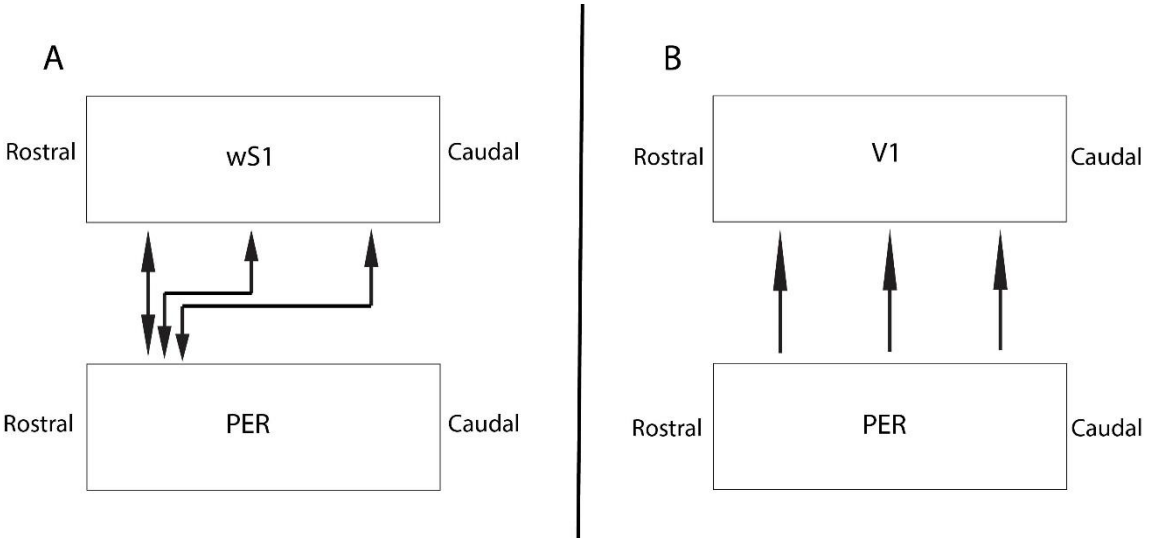

Figure 14: Simplified summary schematic of the topography of FB projections from PER to wS1 and V1. The rectangle sizes do not indicate equivalent rostrocaudal lengths for the three areas. A: Reciprocal connectivity in rostral PER and the entire length of wS1. Arrows from wS1 to PER are FF projections, added from data by Foroughi (2022). Arrows from PER to wS1 are FB projections, using data from the current study. B: Efferent projections from PER to V1 originate in a rostrocaudal level of PER that closely follows the rostrocaudal level innervated in V1. The pattern of origin for inputs from V1 to PER has not been clearly elucidated and is therefore not included in the figure.

4.3 Potential circuitry in L6 of barrel cortex innervated by PER

My results have indeed shown that PER projects to wS1 L6 in mice, but precisely what cell types in L6 of wS1 receive these efferents from PER and the surrounding circuitry has yet to be investigated. Some indications for what cell types in L6 of wS1 receive projections from PER can be gathered by a study performed by Naskar et al. (2021), investigating PER projections to superficial layers of wS1. They find that PER projects to all types of GABAergic interneurons in the superficial layers when defined by the molecular marker they express in the neocortex, as well as pyramidal neurons (Naskar et al., 2021; Tremblay et al., 2016).

Feedback projections from PER could indirectly inhibit pyramidal neurons in the target area by innervating PV and SST interneurons, or lead to disinhibition of pyramidal neurons by targeting VIP interneurons that target other interneurons (Zagha, 2020). PV interneurons, SST interneurons, VIP positive and VIP negative 5HT3aR interneurons can all be found in L6 of wS1 (Perrenoud et al., 2013; Tremblay et al., 2016). PV interneurons specifically are the largest interneuron population in L6 and have been described to preferentially reside in L6a (Perrenoud et al., 2013). Frandolig et al. (2019) shed more light on this by finding differences in PV interneurons between upper L6a ($L6_U$) and lower L6a ($L6_L$) of wS1 in mice (Frandolig et al., 2019). They show that $L6_U$ contains mostly interlaminar as well as some locally ramifying PV interneurons, while $L6_L$ contains almost exclusively PV interneurons of which ramify locally (Frandolig et al.,

2019). As such, feedback efferents from PER could inhibit local neurons in L6 as well as neurons in the various other lamina of wS1 by targeting PV interneurons of L6a.

Feedback projections from PER could also lead to increased excitation by directly innervating pyramidal neurons in L6 of wS1. As for pyramidal neurons, neocortical L6 has been described to contain corticocortical, corticothalamic, and claustrum-projecting neurons (Thomson, 2010). However, primary somatosensory cortex has been found to barely project to the claustrum (Wang et al., 2017) and as such this class of pyramidal neurons can be omitted from the analysis of wS1 L6. Of the corticothalamic neurons, Frandolig et al. (2019) find that the corticothalamic neurons in wS1 $L6_U$ of mice project to VPM, while the corticothalamic neurons in $L6_L$ project to VPM and POm (Frandolig et al., 2019). These corticocortical and corticothalamic neurons of L6a also innervate the interlaminar and local PV interneurons (Frandolig et al., 2019). These are all possible indirect targets as a result of PER providing feedback efferents to the pyramidal neurons of wS1 L6.

4.4 Limitations

The most notable limitation to this study is the frequent incidence of injections with spill into the ec, a white matter tract containing axonal fibers. CtB-AF, the retrograde tracer used in this study, will bind to GM1 gangliosides of the axons and travel along these axons to label the nuclei of these cells. The expectation is that this will cause imprecise labeling of PER efferents targeting other areas, and thereby impact the usability of these injections. From what is indicated in this study, spill into ec impacts the laminar distribution of the FB neurons in PER by increasing the number of superficial neurons labeled. This is consistent for the injections with spill into ec targeting wS1, V1, V2M and LPtA+PTPR, where all of the laminar distributions also have a higher proportion of superficially labeled neurons compared to injections without spill in ec. Of note however, is how injections without spill into ec targeting wS1 also find superficially labeled neurons though the proportion is not as strong. The rostrocaudal distribution of quantified PER FB neurons did not seem to be impacted by spill into ec, and it might have had an impact on the dorsoventral distribution of FB neurons in PER to V1, V2M and LPtA+PTPR. The impact of these spills makes it more difficult to make meaningful conclusions for some of my results, as discussed above.

One limitation to this study which would have more clearly indicated the actual rostrocaudal pattern of FB neurons to V1 involves including injections into the most caudal extents of V1. According to the Franklin & Paxinos mouse brain atlas, V1 proceeds much further caudally than injections included in this study (AP: -5.2 mm from bregma) (Franklin & Paxinos, 2008). As such there is a lack of sampling of the caudal end of V1, which makes it more difficult to say with certainty that the rostrocaudal pattern of FB neurons to V1 is indeed true for mice.

One of the secondary aims of this study was to investigate whether there are marked differences in topography in PER between feedback projections to L1 and L6 of wS1 and V1. This aim is not possible to be answered in a meaningful way by my results as I have a lack of injections hitting only L1 of wS1 and V1. It is also not possible to quantify the number of neurons in PER labeled by injection bolus in L1 or L6 separately when the injection hits the entire cortical column of L1-6.

Another limitation involves how this study cannot indicate any differences that would be due to the sex of the mice. Of the mice used for analysis in this study, only two were male while six were female. Of note is how the two males only had usable injections for wS1 (66702 & 104379; Fig. 5A, D), but the low sample size for each sex makes it difficult to conclude with any differences due to sex. As for the visual injections, all mice were female and as such one cannot say with certainty that the pattern would be the same if investigated in male mice. However, previous research on perirhinal connectivity has mostly used male mice and rats (Agster & Burwell, 2009; Burwell & Amaral, 1998a; Foroughi, 2022), and as such there are no previous indications to assume differences in sex.

One possible limitation surrounds how mouse 103821 had an underdeveloped right eye. This mouse had one usable injection into V2M without spill into ec, but when comparing to the other V2M injection the pattern when estimating the proportion of counted cells was not very different and the mouse was therefore included for analysis. The number of counted cells from this injection was however quite low (n = 24 cells across 8 sections), which might be partially due to the physical impairment of the animal as the injection hit secondary visual cortex (103821; Fig. 7B). The other V2M injection had a much higher number of counted cells (n =163 cells across 5 sections) which could imply that it is not due to V2M being weakly innervated by PER that the cell count is low for 103821, however this other V2M injection had notable spill into ec (104375; Fig. 7A) so it is difficult to say with certainty what the reason is for this low cell count number in mouse 103821.

4.5 Future work

Moving forward, one interesting project building upon the findings of this thesis would be to investigate what cell types in L6 of primary somatosensory cortex receive the FB innervation by PER. This would allow us to understand what circuits PER FB neurons partake in by elucidating the specific inhibitory interneuron and projection neuron types innervated. One possible way of assessing this would be in a similar way as Naskar et al. (2021), who investigated the cell-type-specific recruitment of GABAergic interneurons in the primary somatosensory cortex by long-range inputs (Naskar et al., 2021). One can use transgenic mouse lines expressing fluorescent markers for PV, SST, 5HT3aR VIP and non-VIP inhibitory neurons, and inject adeno-associated viruses expressing channelrhodopsin into PER. By performing whole-cell patch clamp recordings in ex-vivo preparations and identifying the various inhibitory cell types which have all been shown to exist in wS1 L6 (Perrenoud et al., 2013; Tremblay et al., 2016), measuring light-evoked responses in the various interneuron types when shining light onto PER would show which interneuron type receives innervation by PER. To elucidate what type of pyramidal neurons in wS1 L6 are targeted by PER, one could inject retrograde tracers into the thalamus and cortex. This would label corticothalamic neurons and corticocortical neurons of wS1 L6 respectively, and one could then record the labeled neurons when shining light onto PER.

Foroughi (2022) shows that various thalamic nuclei provide input to PER in mice (Foroughi, 2022). A future project could be to expand upon these findings by investigating PER efferents to relevant thalamic nuclei in mice. One could investigate whether the outputs from PER to sensory thalamus follows the same rostrocaudal distribution as outputs from PER to sensory cortices in mice. Furthermore, one could

investigate whether the outputs to thalamus from PER follow the inputs from thalamus to PER described by Foroughi (2022). Ways of doing this include injecting either anterograde tracers into PER or retrograde tracers into thalamic nuclei of interest. The first order thalamic nuclei of interest pertaining to the somatosensory modality include the ventral posteromedial nucleus and ventral posterolateral nucleus which are the main nuclei relaying somatosensory signals in rodents (O'Reilly et al., 2021), as well as the higher order posterior nucleus which also directly interfaces with the mouse barrel cortex (Casas-Torremocha et al., 2019). For the visual modality, the lateral posterior complex of the thalamus as well as the dorsal lateral geniculate nucleus are the main nuclei of which the visual cortex receives its input from (Evangelio et al., 2018).

5 Conclusion

Studies of PER interconnectivity has in later years mostly been focused on primates and rats, with little work done in mice despite the vast benefits of using this animal as a model for neuroscience. By injecting retrograde tracers into various rostrocaudal levels of wS1 L6 and V1, I provide novel findings in this thesis by showing that PER provides FB innervation to wS1 L6 and V1 in mice.

The PER FB efferents to wS1 originate in rostral PER which closely follows the input from wS1 to PER in mice (Foroughi, 2022) and is consistent with findings in rats on PER efferents (Agster & Burwell, 2009). Furthermore, PER FB efferents to wS1 slightly trend towards A36 which is consistent with findings in rats on PER efferents (Agster & Burwell, 2009), and primarily originate in deep layers which is consistent with literature on feedback efferents in primates (Markov et al., 2014). -

My results indicate the PER FB efferents to V1 to originate in a rostrocaudal level of PER that closely follows the rostrocaudal level of the injection site in V1, which is inconsistent with findings in rats on efferents of PER as well as input to PER from V1 in mice which indicate caudal PER as the region of PER interconnected with V1 (Agster & Burwell, 2009; Foroughi, 2022). I show that the PER FB neurons to V1 primarily originate in A36 which is consistent with findings in rats on efferents from PER to visual areas (Agster & Burwell, 2009), and primarily originate in deep layers.

Additional findings of this thesis include how the neurons of PER projecting to the primary somatosensory and visual cortices do not project to both simultaneously but are distinct populations within PER that project to only one of the primary sensory cortices. Furthermore, contralateral PER projects to wS1 L6 but were not indicated to project to V1 or superficial layers of wS1 based on my findings. The projections from contralateral PER to wS1 L6 were almost exclusively distributed to L5, and primarily originated in A35 over A36.

These findings will hopefully aid the investigation of PER in the future when using the mouse as a model. Investigating the multisensory nature of PER and functions such as object recognition in mice will be aided by the findings in this thesis surrounding cortical connectivity from PER to primary sensory cortices of the visuotactile modalities.

References

Agster, K. L., & Burwell, R. D. (2009). Cortical Efferents of the Perirhinal, Postrhinal, and Entorhinal Cortices of the Rat. *Hippocampus*, *19*(12), 1159-1186. https://doi.org/10.1002/hipo.20578

Agster, K. L., Pereira, I. T., Saddoris, M. P., & Burwell, R. D. (2016). Subcortical connections of the perirhinal, postrhinal, and entorhinal cortices of the rat. II. efferents. *Hippocampus*, *26*(9), 1213-1230. https://doi.org/10.1002/hipo.22600

Allen Reference Atlas - Mouse Brain. (2011). Allen Institute for Brain Science. atlas.brain-map.org

Angelucci, A., & Bressloff, P. C. (2006). Contribution of feedforward, lateral and feedback connections to the classical receptive field center and extra-classical receptive field surround of primate V1 neurons. *Prog Brain Res*, *154*, 93-120. https://doi.org/10.1016/S0079-6123(06)54005-1

Beaudin, S. A., Singh, T., Agster, K. L., & Burwell, R. D. (2013). Borders and Comparative Cytoarchitecture of the Perirhinal and Postrhinal Cortices in an F1 Hybrid Mouse. *Cerebral Cortex*, *23*(2), 460-476. https://doi.org/10.1093/cercor/bhs038

Bruce, C., Desimone, R., & Gross, C. G. (1981). Visual Properties of Neurons in a Polysensory Area in Superior Temporal Sulcus of the Macaque. *Journal of Neurophysiology*, *46*(2), 369-384. https://doi.org/DOI 10.1152/jn.1981.46.2.369

Burwell, R. D., & Amaral, D. G. (1998a). Cortical afferents of the perirhinal, postrhinal, and entorhinal cortices of the rat. *Journal of Comparative Neurology*, *398*(2), 179-205. https://doi.org/Doi 10.1002/(Sici)1096-9861(19980824)398:2<179::Aid-Cne3>3.0.Co;2-Y

Burwell, R. D., & Amaral, D. G. (1998b). Perirhinal and postrhinal cortices of the rat: Interconnectivity and connections with the entorhinal cortex. *Journal of Comparative Neurology*, *391*(3), 293-321. https://doi.org/Doi 10.1002/(Sici)1096-9861(19980216)391:3<293::Aid-Cne2>3.0.Co;2-X

Burwell, R. D., Witter, M. P., & Amaral, D. G. (1995). Perirhinal and postrhinal cortices of the rat: A review of the neuroanatomical literature and comparison with findings from the monkey brain. *Hippocampus*, *5*(5), 390-408. https://doi.org/DOI 10.1002/hipo.450050503

Casas-Torremocha, D., Porrero, C., Rodriguez-Moreno, J., Garcia-Amado, M., Lubke, J. H. R., Nunez, A., & Clasca, F. (2019). Posterior thalamic nucleus axon terminals have different structure and functional impact in the motor and somatosensory vibrissal cortices. *Brain Structure & Function*, *224*(4), 1627-1645. https://doi.org/10.1007/s00429-019-01862-4

Conte, W. L., Kamishina, H., & Reep, R. L. (2009). The efficacy of the fluorescent conjugates of cholera toxin subunit B for multiple retrograde tract tracing in the central nervous system. *Brain Structure & Function*, *213*(4-5), 367-373. https://doi.org/10.1007/s00429-009-0212-x

De Haan, L., & Hirst, T. R. (2004). Cholera toxin: a paradigm for multi-functional engagement of cellular mechanisms (Review). *Mol Membr Biol*, *21*(2), 77-92. https://doi.org/10.1080/09687680410001663267

Doron, G., Shin, J. N., Takahashi, N., Druke, M., Bocklisch, C., Skenderi, S., de Mont, L., Toumazou, M., Ledderose, J., Brecht, M., Naud, R., & Larkum, M. E. (2020). Perirhinal input to neocortical layer 1 controls learning. *Science*, *370*(6523). https://doi.org/10.1126/science.aaz3136

Eacott, M. J., Machin, P. E., & Gaffan, E. A. (2001). Elemental and configural visual discrimination learning following lesions to perirhinal cortex in the rat. *Behavioural Brain Research*, *124*(1), 55-70. https://doi.org/10.1016/s0166-4328(01)00234-0

Ennaceur, A., & Delacour, J. (1988). A New One-Trial Test for Neurobiological Studies of Memory in Rats .1. Behavioral-Data. *Behavioural Brain Research*, *31*(1), 47-59. https://doi.org/Doi 10.1016/0166-4328(88)90157-X

Evangelio, M., Garcia-Amado, M., & Clasca, F. (2018). Thalamocortical Projection Neuron and Interneuron Numbers in the Visual Thalamic Nuclei of the Adult C57BL/6 Mouse. *Front Neuroanat*, *12*, 27. https://doi.org/10.3389/fnana.2018.00027

Felleman, D. J., & Van Essen, D. C. (1991). Distributed hierarchical processing in the primate cerebral cortex. *Cerebral Cortex*, *1*(1), 1-47. https://doi.org/10.1093/cercor/1.1.1-a

Foroughi, A. (2022). *Organization of afferent sensory input onto the mouse perirhinal cortex* [Master's thesis, Norwegian University of Science and Technology]. NTNU Open. https://hdl.handle.net/11250/3052141

Frandolig, J. E., Matney, C. J., Lee, K., Kim, J., Chevee, M., Kim, S. J., Bickert, A. A., & Brown, S. P. (2019). The Synaptic Organization of Layer 6 Circuits Reveals Inhibition as a Major Output of a Neocortical Sublamina. *Cell Rep*, *28*(12), 3131-3143 e3135. https://doi.org/10.1016/j.celrep.2019.08.048

Franklin, K. B. J., & Paxinos, G. (2008). *The mouse brain in stereotaxic coordinates* (3rd compact ed.). London : Elsevier/Academic Press. http://bvbr.bib-bvb.de:8991/F?func=service&doc_library=BVB01&doc_number=016372855&line_number=0001&func_code=DB_RECORDS&service_type=MEDIA

Gogolla, N. (2017). The insular cortex. *Current Biology*, *27*(12), R580-R586. https://doi.org/DOI 10.1016/j.cub.2017.05.010

Gusel'nikova, V. V., & Korzhevskiy, D. E. (2015). NeuN As a Neuronal Nuclear Antigen and Neuron Differentiation Marker. *Acta Naturae*, *7*(2), 42-47. https://www.ncbi.nlm.nih.gov/pubmed/26085943

Higuchi, S., & Miyashita, Y. (1996). Formation of mnemonic neuronal responses to visual paired associates in inferotemporal cortex is impaired by perirhinal and entorhinal lesions. *Proc Natl Acad Sci U S A*, *93*(2), 739-743. https://doi.org/10.1073/pnas.93.2.739

Kealy, J., & Commins, S. (2011). The rat perirhinal cortex: A review of anatomy, physiology, plasticity, and function. *Progress in Neurobiology*, *93*(4), 522-548. https://doi.org/10.1016/j.pneurobio.2011.03.002

Kenworthy, A. K., Schmieder, S. S., Raghunathan, K., Tiwari, A., Wang, T., Kelly, C. V., & Lencer, W. I. (2021). Cholera Toxin as a Probe for Membrane Biology. *Toxins*, *13*(8). https://doi.org/ARTN 543

10.3390/toxins13080543

Lavenex, P., Suzuki, W. A., & Amaral, D. G. (2002). Perirhinal and parahippocampal cortices of the macaque monkey: Projections to the neocortex. *Journal of Comparative Neurology*, *447*(4), 394-420. https://doi.org/10.1002/cne.10243

Lavenex, P., Suzuki, W. A., & Amaral, D. G. (2004). Perirhinal and parahippocampal cortices of the macaque monkey: Intrinsic projections and interconnections. *Journal of Comparative Neurology*, *472*(3), 371-394. https://doi.org/10.1002/cne.20079

Markov, N. T., Vezoli, J., Chameau, P., Falchier, A., Quilodran, R., Huissoud, C., Lamy, C., Misery, P., Giroud, P., Ullman, S., Barone, P., Dehay, C., Knoblauch, K., & Kennedy, H. (2014). Anatomy of hierarchy: feedforward and feedback pathways in macaque visual cortex. *Journal of Comparative Neurology*, *522*(1), 225-259. https://doi.org/10.1002/cne.23458

Naskar, S., Qi, J., Pereira, F., Gerfen, C. R., & Lee, S. (2021). Cell-type-specific recruitment of GABAergic interneurons in the primary somatosensory cortex by long-range inputs. *Cell Rep*, *34*(8), 108774. https://doi.org/10.1016/j.celrep.2021.108774

Nwaneshiudu, A., Kuschal, C., Sakamoto, F. H., Anderson, R. R., Schwarzenberger, K., & Young, R. C. (2012). Introduction to confocal microscopy. *J Invest Dermatol*, *132*(12), e3. https://doi.org/10.1038/jid.2012.429

O'Reilly, C., Iavarone, E., Yi, J., & Hill, S. L. (2021). Rodent somatosensory thalamocortical circuitry: Neurons, synapses, and connectivity. *Neurosci Biobehav Rev*, *126*, 213-235. https://doi.org/10.1016/j.neubiorev.2021.03.015

Ohara, S., Blankvoort, S., Nair, R. R., Nigro, M. J., Nilssen, E. S., Kentros, C., & Witter, M. P. (2021). Local projections of layer Vb-to-Va are more prominent in lateral than in medial entorhinal cortex. *Elife*, *10*. https://doi.org/10.7554/eLife.67262

Pereira, I. T., Agster, K. L., & Burwell, R. D. (2016). Subcortical connections of the perirhinal, postrhinal, and entorhinal cortices of the rat. I. afferents. *Hippocampus*, *26*(9), 1189-1212. https://doi.org/10.1002/hipo.22603

Perrenoud, Q., Rossier, J., Geoffroy, H., Vitalis, T., & Gallopin, T. (2013). Diversity of GABAergic interneurons in layer VIa and VIb of mouse barrel cortex. *Cerebral Cortex*, *23*(2), 423-441. https://doi.org/10.1093/cercor/bhs032

Room, P., & Groenewegen, H. J. (1986). Connections of the Parahippocampal Cortex .1. Cortical Afferents. *Journal of Comparative Neurology*, *251*(4), 415-450. https://doi.org/DOI 10.1002/cne.902510402

Squire, L. R., Stark, C. E., & Clark, R. E. (2004). The medial temporal lobe. *Annu Rev Neurosci*, *27*, 279-306. https://doi.org/10.1146/annurev.neuro.27.070203.144130

Suzuki, W. A. (2009). Comparative analysis of the cortical afferents, intrinsic projections, and interconnections of the parahippocampal region in monkeys and rats. *The cognitive neurosciences*, 659-674.

Suzuki, W. A., & Amaral, D. G. (1994). Perirhinal and Parahippocampal Cortices of the Macaque Monkey - Cortical Afferents. *Journal of Comparative Neurology*, *350*(4), 497-533. https://doi.org/DOI 10.1002/cne.903500402

Suzuki, W. A., & Naya, Y. (2014). The perirhinal cortex. *Annu Rev Neurosci*, *37*, 39-53. https://doi.org/10.1146/annurev-neuro-071013-014207

Thomson, A. M. (2010). Neocortical layer 6, a review. *Front Neuroanat*, *4*, 13. https://doi.org/10.3389/fnana.2010.00013

Tremblay, R., Lee, S., & Rudy, B. (2016). GABAergic Interneurons in the Neocortex: From Cellular Properties to Circuits. *Neuron*, *91*(2), 260-292. https://doi.org/10.1016/j.neuron.2016.06.033

van Groen, T. (2001). Entorhinal cortex of the mouse: cytoarchitectonical organization. *Hippocampus*, *11*(4), 397-407. https://doi.org/10.1002/hipo.1054

van Groen, T., Kadish, I., & Wyss, J. M. (1999). Efferent connections of the anteromedial nucleus of the thalamus of the rat. *Brain Research Reviews*, *30*(1), 1-26. https://doi.org/Doi 10.1016/S0165-0173(99)00006-5

Wang, Q., Ng, L., Harris, J. A., Feng, D., Li, Y., Royall, J. J., Oh, S. W., Bernard, A., Sunkin, S. M., Koch, C., & Zeng, H. (2017). Organization of the connections between claustrum and cortex in the mouse. *Journal of Comparative Neurology*, *525*(6), 1317-1346. https://doi.org/10.1002/cne.24047

Wang, Q. X., & Burkhalter, A. (2007). Area map of mouse visual cortex. *Journal of Comparative Neurology*, *502*(3), 339-357. https://doi.org/10.1002/cne.21286

Winters, B. D., & Reid, J. M. (2010). A distributed cortical representation underlies crossmodal object recognition in rats. *J Neurosci*, *30*(18), 6253-6261. https://doi.org/10.1523/JNEUROSCI.6073-09.2010

Witter, M. P., & Groenewegen, H. J. (1986). Connections of the Parahippocampal Cortex in the Cat .3. Cortical and Thalamic Efferents. *Journal of Comparative Neurology*, *252*(1), 1-31. https://doi.org/DOI 10.1002/cne.902520102

Witter, M. P., Wouterlood, F. G., Naber, P. A., & Van Haeften, T. (2000). Anatomical organization of the parahippocampal-hippocampal network. *Ann N Y Acad Sci*, *911*, 1-24. https://doi.org/10.1111/j.1749-6632.2000.tb06716.x

Zagha, E. (2020). Shaping the Cortical Landscape: Functions and Mechanisms of Top-Down Cortical Feedback Pathways. *Front Syst Neurosci*, *14*, 33. https://doi.org/10.3389/fnsys.2020.00033

Appendix A

A1 Histology

A1.1 Histology of 66702 CtB647 injection site

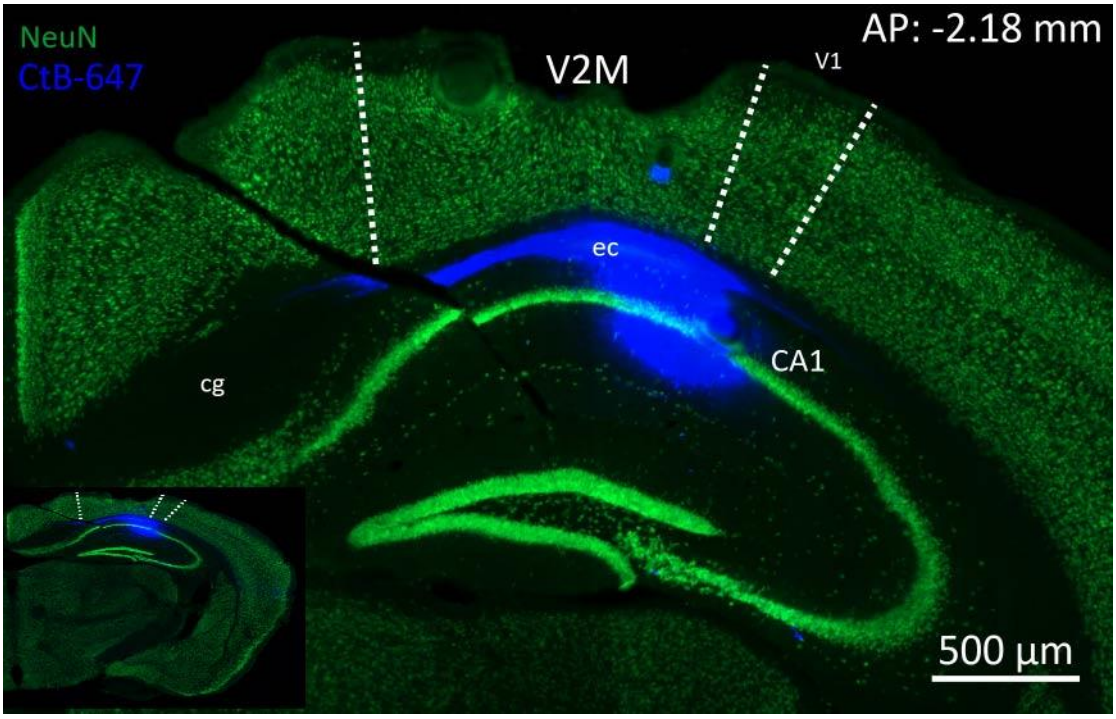

Figure 1: Histology of mouse 66702 CtB647 injection.

A1.2 Histology of 104380 CtB555 and CtB647 injection sites

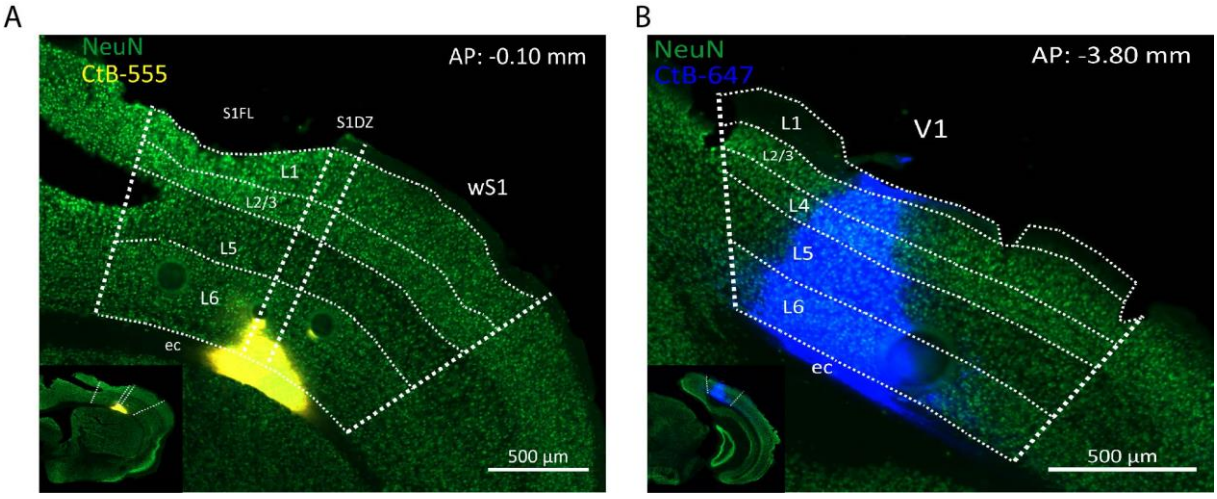

Figure 2: Histology of mouse 104380 CtB555 and CtB647 injections.

A1.3 Example histology image of damage to PER in mouse 104380

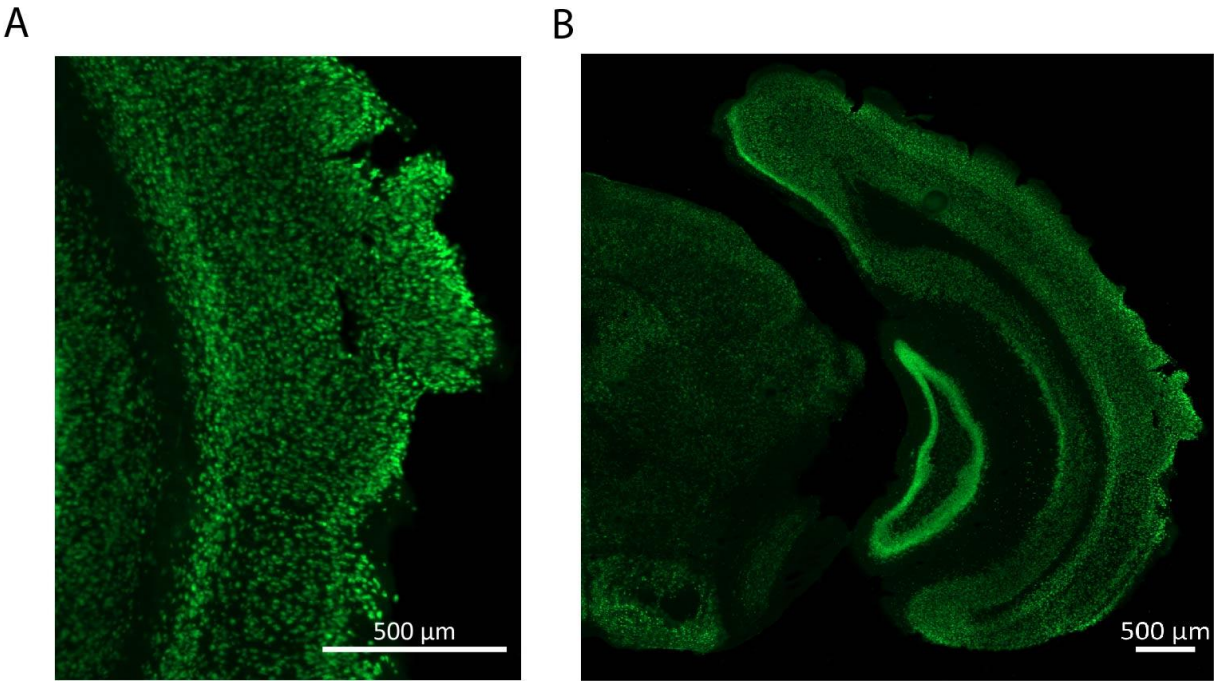

Figure 3: Histology of example section showing damage to PER for mouse 104380.

Appendix B

B1 PV Quantification

B1.1 Rostrocaudal distribution of PV cells for 103823, 103824 & 103825

AP	103823	103824	103825
-2.06	225	111	123
-2.18	167		
-2.3		137	180
-2.46	151		
-2.54		125	80
-2.8	137	104	22
-3.16			21
-3.28	86	67	
-3.52	70		25
-3.64		50	
-3.8			33
-3.88	43		
-4.04		71	11
-4.16	18		

Table 1: Rostrocaudal distribution of the number of counted PV+ cells in PER.

AP	103823	103824	103825
-2.06	326.2907	237.9934	239.4285
-2.18	326.5743		
-2.3		285.8033	264.3688
-2.46	352.1038		
-2.54		321.7553	173.6844
-2.8	307.3754	285.7087	58.90378
-3.16			58.44412
-3.28	242.8116	249.8193	
-3.52	189.1529		75.89912
-3.64		199.8685	
-3.8			120.937
-3.88	150.2394		
-4.04		275.0754	42.86307
-4.16	59.22507		

Table 2: Rostrocaudal distribution of the density of PV+ cells in PER. Density is given in mm^2.

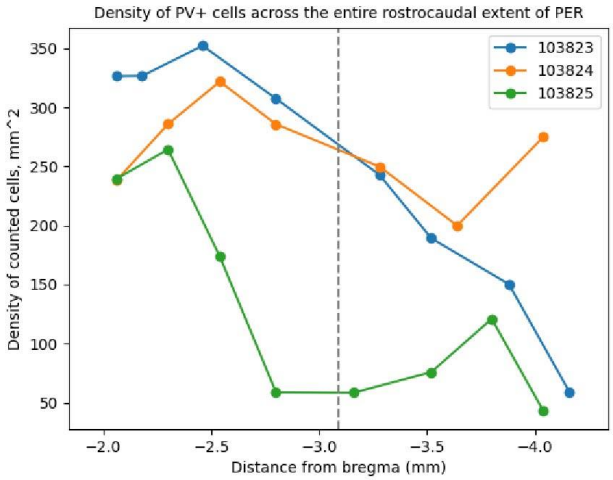

Figure 1: Rostrocaudal distribution of the density of PV+ cells in PER for three mice.

B1.2 KMeans cluster analysis

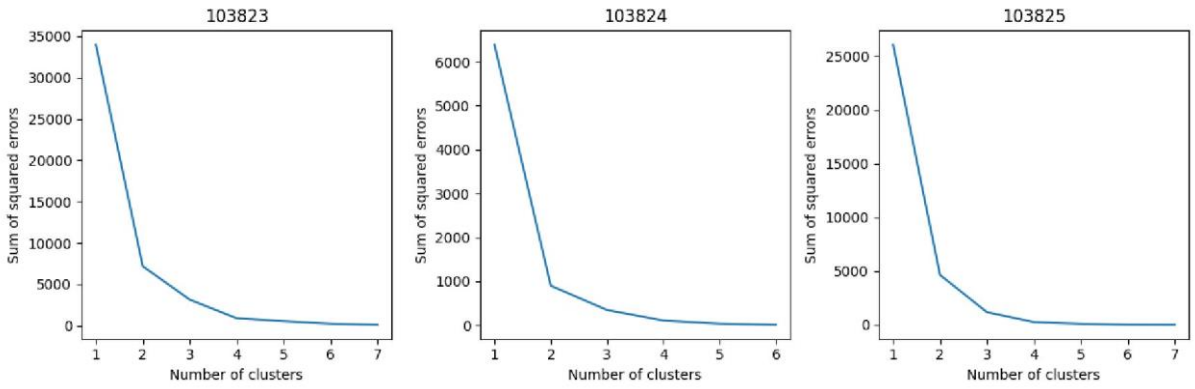

Figure 2: PV cell counts KMeans

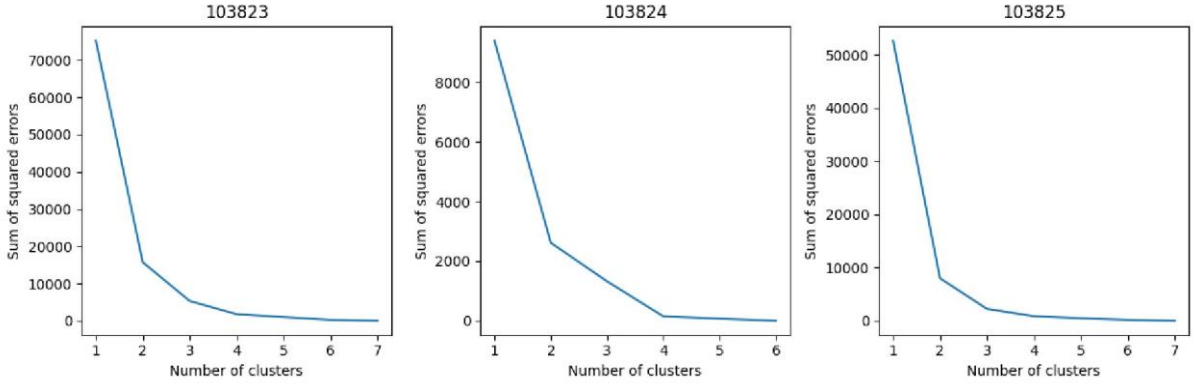

Figure 3: PV densities KMeans

B2 wS1 data

B2.1 wS1 rostrocaudal distribution

AP	66702	104375	104376	104379	103824	103825
-1.94	0.598361	0.5625	0.445313	0.568807		0.258427
-2.06					0.443709	
-2.18						0.52809
-2.3				0.243119	0.251656	
-2.46	0.254098	0.354167				0.078652
-2.54			0.296875	0.087156	0.112583	
-2.7						0.078652
-2.8					0.046358	
-2.92	0.065574	0.0625	0.078125			0.022472
-3.08				0.050459	0.033113	
-3.16						0
-3.4	0.02459			0.013761		0.011236
-3.52			0.078125		0.02649	
-3.64		0.020833				
-3.8						
-3.88			0.0625	0.027523	0.033113	0.011236
-4.04						
-4.16	0.057377	0	0.039063	0.009174	0.05298	0.011236
-4.24						
Sum cells	122	48	128	218	151	89

Table 3: Proportion of counted cells in PER at each section for wS1 injected mice. Total sum of counted cells per mouse for that injection listed at the end of table.

Bins	66702	104375	104376	104379	103824	103825	Mean	Std
(-1.94 -> -3.08):	0.918033	0.979167	0.820313	0.949541	0.887417	0.966292	0.924759	0.05023
(-3.16 -> -4.24):	0.081967	0.020833	0.179688	0.050459	0.112583	0.033708	0.075241	0.05023

Table 4: Proportion of counted cells in PER from wS1 injections when summing into two bins based on PV expression.

Bins	66702	104375	104376	104379	103824	103825	Mean	Std
(-1.94 -> -2.7):	0.852459016	0.916667	0.742188	0.899083	0.807947	0.9438202	0.8643	0.068248

(-2.8 -> -3.4):	0.090163934	0.0625	0.078125	0.06422	0.07947	0.0337079	0.068723	0.020219
(-3.52 -> -4.24):	0.057377049	0.020833	0.179688	0.036697	0.112583	0.0224719	0.066977	0.053685

Table 5: Proportion of counted cells in PER from wS1 injections when summing into three bins based on PV expression.

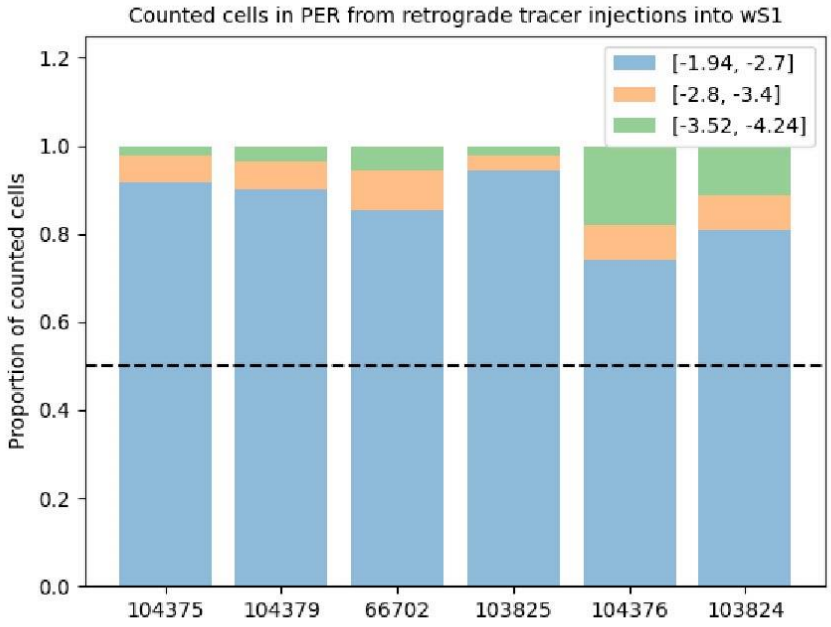

Figure 4: Stacked chart of rostrocaudal distribution of counted neurons in PER from wS1 injections. Three bins according to Table 5 above.

B2.2 wS1 laminar distribution

Mouse ID	L1	L2/3	L5	L6
66702	0	0.270492	0.672131	0.057377
104375	0	0.291667	0.583333	0.125
104376	0	0.390625	0.585938	0.023438
104379	0	0.192661	0.720183	0.087156
103824	0	0.112583	0.715232	0.172185
103825	0	0.044944	0.752809	0.202247

Table 6: Laminar distribution of proportion of counted cells in PER from wS1 injections.

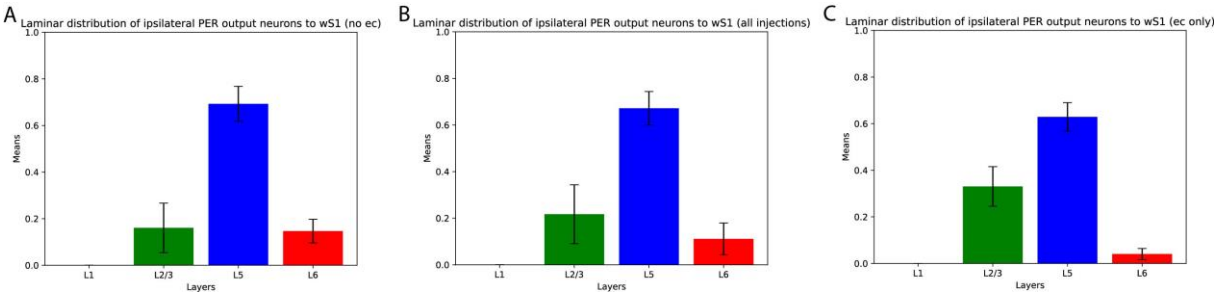

Figure 5: Laminar distribution of FB neurons in PER to wS1. A: Using injections without spill into ec. B: Using all injections into wS1. C: Using only the injections with spill into ec.

B2.3 wS1 dorsoventral distribution

Mouse ID	A36	A35
66702	0.532786885	0.467213
104375	0.520833333	0.479167
104376	0.5234375	0.476563
104379	0.541284404	0.458716
103824	0.562913907	0.437086
103825	0.617977528	0.382022
Mean	0.535361174	0.464639
Stdev	0.01788872	0.017889

Table 7: Dorsoventral distribution of counted cells in PER from wS1 injections.

B3 V1 data

B3.1 V1 rostrocaudal distribution

AP	103824	103823r	103825	104376	103823c
-1.94			0.013245	0.025735	
-2.06	0.428571	0.0379747			0
-2.18			0.07947		
-2.3	0.333333	0.3734177			0.0447761
-2.46			0.145695		
-2.54	0.095238	0.3544304		0.066176	0.1791045
-2.7			0.119205		
-2.8	0.047619	0.0949367			0.238806
-2.92			0.066225	0.154412	
-3.08	0.047619				
-3.16		0.0506329	0.112583		0.1641791
-3.28					
-3.4			0.086093		
-3.52	0	0.0506329		0.297794	0.2089552
-3.64					
-3.8					
-3.88	0	0.0379747	0.165563	0.305147	0.0746269
-4.04					
-4.16	0.047619	0	0.211921	0.150735	0.0895522
-4.24					
Sum	21	158	151	544	67

Table 8: Proportion of counted cells in PER at each section for V1 injected mice. Total sum of counted cells per mouse for that injection listed at the end of table.

Bins	103824	103823r	103825	104376	*103823c*	Mean	Std
(-1.94 -> -3.08):	0.952381	0.8607595	0.423841	0.246324	0.4626866	0.462686567	0.341789
(-3.16 -> -4.24):	0.047619	0.1392405	0.576159	0.753676	0.5373134	0.537313433	0.341789

Table 9: Proportion of counted cells in PER from V1 injections when summing into two bins based on PV expression.

Bins	103824	103823r	103825	104376	103823c	Mean	Std
(-1.94 -> -2.7):	0.857143	0.7658228	0.357616	0.091912	0.2238806	0.459899519	0.335665
(-2.8 -> -3.4):	0.095238	0.1455696	0.264901	0.154412	0.4029851	0.210958549	0.124155
(-3.52 -> -4.24):	0.047619	0.0886076	0.377483	0.753676	0.3731343	0.329141933	0.285502

Table 10: Proportion of counted cells in PER from V1 injections when summing into three bins based on PV expression.

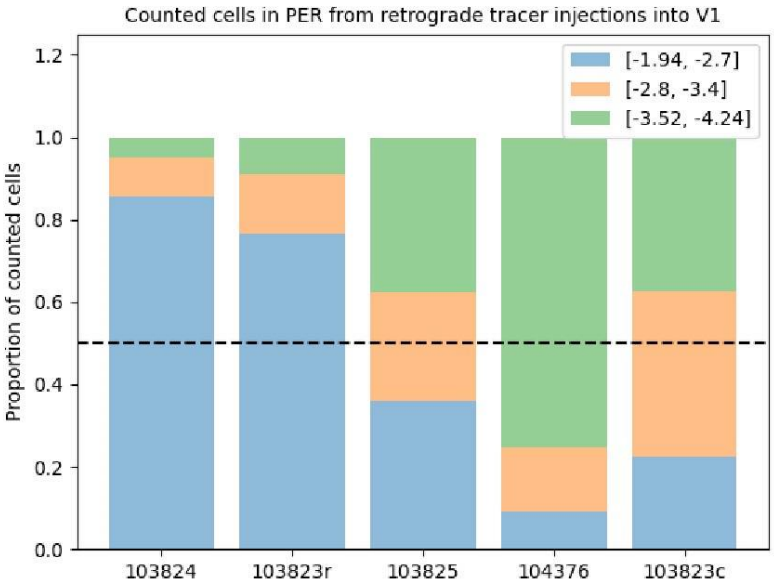

Figure 6: Stacked chart of rostrocaudal distribution of counted neurons in PER from V1 injections. Three bins according to Table 10 above.

B3.2 V1 laminar distribution

Mouse ID	L1	L2/3	L5	L6
103824	0	0.095238	0.619048	0.285714
103823r	0	0.310127	0.563291	0.126582
103825	0	0.072848	0.708609	0.218543
104376	0	0.28125	0.661765	0.056985
103823c	0	0	0.656716	0.343284

Table 11: Laminar distribution of proportion of counted cells in PER from V1 injections.

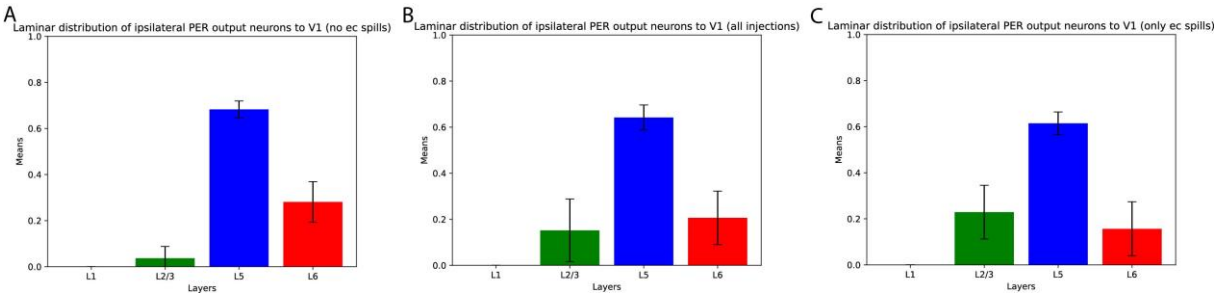

Figure 7: Laminar distribution of FB neurons in PER to V1. A: Using injections without spill into ec. B: Using all injections into V1. C: Using only the injections with spill into ec.

B3.3 V1 dorsoventral distribution

Mouse ID	A36	A35
103824	0.333333333	0.666667
103823r	0.759493671	0.240506
103825	0.59602649	0.403974
104376	0.733455882	0.266544
103823c	0.552238806	0.447761
Mean	0.596303566	0.403696
Stdev	0.172117165	0.172117

Table 12: Dorsoventral distribution of counted cells in PER from V1 injections.

B4 Contralateral PER to wS1 L6 data

B4.1 Contralateral PER to wS1 and V1 rostrocaudal distribution

AP	66702	104375	104376	104379	103824	103825
-1.94	0.487805	0.478261		0.373134		
-2.06					0.179487	1
-2.18			0.75	0.41791		
-2.3					0.205128	
-2.46	0.341463	0.391304		0.164179		0
-2.54						
-2.7	0.097561		0.083333	0	0.358974	0
-2.8						0
-2.92		0.086957	0.0625		0.076923	
-3.08						0
-3.16	0			0.014925		
-3.4		0				0
-3.52			0.03125	0.014925	0.076923	
-3.64						0
-3.8	0					
-3.88			0.0625	0.014925	0	
-4.04		0.043478				0
-4.16	0.073171		0.010417		0.102564	
-4.24						
Sum	41	23	96	67	39	3

Table 13: Proportion of counted cells in contralateral PER at each section for wS1 injected mice. Total sum of counted cells per mouse for that injection is listed at the end of table.

AP	103824	103823r	103825	104376	103823c
-1.94		21			0
-2.06	0				
-2.18		27		0.137698	0
-2.3	2				
-2.46		15			1
-2.54				0.167043	
-2.7	0	3			0
-2.8					
-2.92	0			0.200903	
-3.08		6			0
-3.16					
-3.28					

-3.4		5			1
-3.52	0			0.103837	
-3.64					
-3.8		6			1
-3.88	0			0.227991	
-4.04					
-4.16	1	4		0.162528	1
-4.24					
Sum	3	87	10	443	4

Table 14: Proportion of counted cells in contralateral PER at each section for V1 injected mice. Total sum of counted cells per mouse for that injection is listed at the end of table.

B4.2 Contralateral PER to wS1 L6 laminar distribution

Mouse ID	L1	L2/3	L5	L6
66702	0	0.121951	0.878049	0
104375	0	0	1	0
104376	0	0.302083	0.697917	0
104379	0	0.029851	0.970149	0
103824	0	0.051282	0.948718	0

Table 15: Laminar distribution of proportion of counted cells in contralateral PER from wS1 L6 injections.

B4.3 Contralateral PER to wS1 L6 dorsoventral distribution

Mouse ID	A36	A35
66702	0.390244	0.609756
104375	0.347826	0.652174
104376	0.75	0.25
104379	0.283582	0.716418
103824	0.487179	0.512821
Mean	0.451766	0.548234
Stdev	0.182395	0.182395

Table 16: Dorsoventral distribution of counted cells in PER from V2M and LPtA+PTPR injections.

B5 V2M and LPtA+PTPR data

B5.1 V2M and LPtA+PTPR rostrocaudal distribution

	V2M	V2M	LPtA+PTPR
AP	104375 CtB647	103821 CtB647	104379
-1.94	0.061349693		0.533333333
-2.06		0.083333333	
-2.18			
-2.3		0.291666667	
-2.46	0.595092025		
-2.54		0.041666667	0.108333333
-2.7			
-2.8			
-2.92	0.17791411	0.166666667	
-3.08			0.058333333
-3.16			
-3.28		0.166666667	
-3.4			0.025
-3.52		0.041666667	
-3.64	0.042944785		
-3.8			
-3.88		0.166666667	0.008333333
-4.04			
-4.16	0.122699387		0.041666667
-4.24		0.041666667	
Sum	163	24	120

Table 17: Proportion of counted cells in PER at each section for V2M and LPtA+PTPR injected mice. Total sum of counted cells per mouse for that injection listed at the end of table.

B5.2 V2M and LPtA+PTPR laminar distribution

Mouse ID (inj site)	L1	L2/3	L5	L6
104375 (V2M)	0	0.319018405	0.607361963	0.07362
103821 (V2M)	0	0	0.666666667	0.333333
104379 (LPtA+PTPR)	0.008333333	0.266666667	0.675	0.05

Table 18: Laminar distribution of proportion of counted cells in PER from V2M and LPtA+PTPR injections.

B5.3 V2M and LPtA+PTPR dorsoventral distribution

Mouse ID (inj site)	A36	A35
104375 (V2M)	0.82208589	0.17791411
103821 (V2M)	0.625	0.375
104379 (LPtA+PTPR)	0.833333333	0.166666667

Table 19: Dorsoventral distribution of counted cells in PER from V2M and LPtA+PTPR injections.

Appendix C

C1 Immunohistochemistry protocol for NeuN

Immunostaining protocol (Trondheim)

Investigator:

Start: **Mouse:**

End: **DOB:**

1. Wash in PB 3 X 10 minutes ☐ ☐ ☐
2. Blocking 1h ☐
3. Primary in incubating overnight ☐
4. Wash 3 X 20 min in PB ☐ ☐ ☐
5. Secondary in incubating overnight ☐
6. Wash 3 X 10 minutes in PB ☐ ☐ ☐
7. Mount in PB

Blocking:

Serum: 10 % NGS Triton: 0.1 %

4.5 ml PB, 0.5 ml NGS, 5 µl Triton

Incubating:

Serum: 1 % NGS Triton: 0.1 %

Primary: 4.95 ml PB, 50 µl NGS, 5 µl Triton, 5 µl GP α-NeuN

Secondary: 4.93 ml PB, 50 µl NGS, 5 µl Triton, 20 µl Goat α-GP A488

Primary 1:1000	**Secondary** 1:500
Guinea Pig anti-NeuN	Goat anti-Guinea Pig A488

C2 Immunohistochemistry protocol for PV

Immunostaining protocol (Trondheim)

Investigator: Erik Courcelles

Start: **Mouse:**

End: **DOB:**

1. Wash in PB 3 X 10 minutes ☐ ☐ ☐
2. Blocking 1h ☐
3. Primary in incubating overnight ☐
4. Wash 3 X 20 min in PB ☐ ☐ ☐
5. Secondary in incubating overnight ☐
6. Wash 3 X 10 minutes in PB ☐ ☐ ☐
7. Mount in PB

Blocking:

Serum: 10 % NGS Triton: 0.1 %

4.5 ml PB, 0.5 ml NGS, 5 µl Triton

Incubating:

Serum: 1 % NGS Triton: 0.1 %

Primary: 4.95 ml PB, 50 µl NGS, 5 µl Triton, 5 µl Rabbit α-PV

Secondary: 4.93 ml PB, 50 µl NGS, 5 µl Triton, 20 µl Donkey α-Rabbit A488

Primary 1:1000	**Secondary** 1:500
Rabbit anti-Parvalbumin	Donkey anti-Rabbit A488

Appendix D

D1 Neurolucida

D1.1 The code used for extraction of target cells from Microsoft Excel files produced by Neurolucida:

```
import os
import pandas as pd

# Set the path to the folder containing the Excel files
folder_path = "/file/path/here/"

# Initialize an empty list to hold the data from each sheet
data_list = []

# Initialize an empty list to hold the names of files without the sheet
files_without_sheet = []

# Loop through all the files in the folder
for file in os.listdir(folder_path):
    # Check if the file is an Excel file
    if file.endswith(".xlsx"):
        # Try to read the specific sheet into a DataFrame
        try:
            df = pd.read_excel(os.path.join(folder_path, file), sheet_name="Markers-Closed Contours")
            # Add the file name as a new row to the DataFrame
            file_row = pd.DataFrame([[f"{file}"]], columns=["File Name"])
            data_list.append(file_row)
            data_list.append(df)
        except ValueError:
            # If the sheet is not found, add the file name to the list of files without the sheet
            files_without_sheet.append(file)

# Concatenate the list of data frames into a single data frame
if data_list:
```

```
    summary_df = pd.concat(data_list, ignore_index=True)
else:
    summary_df = pd.DataFrame()


# Write the summary DataFrame to a new Excel file
writer = pd.ExcelWriter(os.path.join(folder_path, "summary.xlsx"),
engine="xlsxwriter")
summary_df.to_excel(writer, sheet_name="Summary", index=False)


# Write the list of files without the sheet to a new sheet in the summary
Excel file
if len(files_without_sheet) > 0:
    pd.DataFrame(files_without_sheet, columns=["Files Without
Sheet"]).to_excel(writer, sheet_name="Files Without Sheet", index=False)


# Save and close the Excel writer
writer.save()
```

D2 KMeans

D2.1 Example of the code used for KMeans analyses of PV data

```
import numpy as np
import matplotlib.pyplot as plt
from sklearn.cluster import KMeans

# define datasets
datasets = [
    {
        'x': np.array([2.06, 2.18, 2.46, 2.8, 3.28, 3.52, 3.88, 4.16]),
        'y': np.array([225, 167, 151, 137, 86, 70, 43, 18])
    },
    {
        'x': np.array([2.06, 2.3, 2.54, 2.8, 3.28, 3.64, 4.04]),
        'y': np.array([111, 137, 125, 104, 67, 50, 71])
    },
    {
        'x': np.array([2.06, 2.3, 2.54, 2.8, 3.16, 3.52, 3.8, 4.04]),
        'y': np.array([123, 180, 80, 22, 21, 25, 33, 11])
    }
]

# create subplots
fig, axs = plt.subplots(1, 3, figsize=(12, 4))

# loop over datasets
for i, data in enumerate(datasets):

    # concatenate x and y arrays
    X = np.column_stack((data['x'], data['y']))

    # calculate SSE for different values of K
    sse = []
    for k in range(1, len(data['x'])):
        kmeans = KMeans(n_clusters=k)
```

```
        kmeans.fit(X)
        sse.append(kmeans.inertia_)

    # plot SSE curve
    axs[i].plot(range(1, len(data['x'])), sse)
    axs[i].set_xlabel('Number of clusters')
    axs[i].set_ylabel('Sum of squared errors')

    # set custom title for each subplot
    if i == 0:
        axs[i].set_title('103823')
    elif i == 1:
        axs[i].set_title('103824')
    elif i == 2:
        axs[i].set_title('103825')

# show plots
plt.tight_layout()
plt.show()
```

D3 Example scripts for main figures

D3.1 Rostrocaudal axis line graph code

```
import matplotlib.pyplot as plt


# Define x and y values for each series

series_data = {

    '104375 L6b + S1DZ L5 (0.38)': {

        'x': [-1.94, -2.46, -2.92, -3.64, -4.16],

        'y': [0.5625, 0.354166667, 0.0625, 0.020833333, 0]

    },

    '104379 L4-6 (-0.70)': {

        'x': [-1.94, -2.3, -2.54, -3.08, -3.4, -3.88, -4.16],

        'y': [0.568807339, 0.243119266, 0.087155963, 0.050458716,
0.013761468, 0.027522936, 0.009174312]

    },

    '66702 L6b + ec (-1.22)': {

        'x': [-1.94, -2.46, -2.92, -3.4, -4.16],

        'y': [0.598360656, 0.254098361, 0.06557377, 0.024590164,
0.057377049]

    },

    '103825 L1-5a (-1.46)':{

        'x': [-1.94, -2.18, -2.46, -2.7, -2.92, -3.16, -3.4, -3.88, -4.16],

        'y': [0.258426966, 0.528089888, 0.078651685, 0.078651685,
0.02247191, 0, 0.011235955, 0.011235955, 0.011235955]

    },

    '104376 L6b + ec (-1.58)': {

        'x': [-1.94, -2.54, -2.92, -3.52, -3.88, -4.16],

        'y': [0.462025316, 0.303797468, 0.082278481, 0.069620253,
0.050632911, 0.03164557]

    },

    '103824 L6 (-1.82)': {

        'x': [-2.06, -2.3, -2.54, -2.8, -3.08, -3.52, -3.88, -4.16],

        'y': [0.468531469, 0.265734266, 0.118881119, 0.048951049,
0.034965035, 0.027972028, 0.034965035, 0.052980132]

    }

}
```

```
fig, ax = plt.subplots()


for series, data in series_data.items():
    ax.plot(data['x'], data['y'], marker='o', label=series)


ax.invert_xaxis() # invert the x-axis direction
ax.set_xlabel('Distance from bregma (mm)')
ax.set_ylabel('Proportion of counted cells')
ax.set_title('Counted cells in ipsilateral PER from retrograde tracer
injections into wS1', fontsize=10)
ax.axvline(x=-3.09, linestyle='--', color='grey') # add a vertical dotted
line at x=-3.09
ax.set_xlim(-1.84, -4.34)
ax.legend()
plt.show()
```

D3.2 Rostrocaudal axis stacked bar graph code

```
import matplotlib.pyplot as plt

import numpy as np


# Input data

categories = ['104375', '104379', '66702', '103825', '104376', '103824']

values1 = [0.979166667, 0.949541284, 0.918032787, 0.966292135, 0.848101266,
0.887417219]

values2 = [0.020833333, 0.050458716, 0.081967213, 0.033707865, 0.151898734,
0.112582781]


# Set up the bar chart

x_pos = np.arange(len(categories))

width = 0.8


fig, ax = plt.subplots()


# Plot the first set of data

ax.bar(x_pos, values1, width, align='center', alpha=0.5, label='[-1.94, -
3.08]')


# Plot the second set of data on top of the first

ax.bar(x_pos, values2, width, bottom=values1, align='center', alpha=0.5,
label='[-3.16, -4.24]')


# Customize the plot

ax.set_xticks(x_pos)

ax.set_xticklabels(categories)

ax.set_ylabel('Proportion of counted cells')

ax.set_title('Counted cells in PER from retrograde tracer injections into
wS1', fontsize=10)

ax.set_ylim(0.0, 1.25)

ax.axhline(y=0.5, linestyle='--', color='black') # add a vertical dotted
line at y=0.5

ax.legend()


plt.show()
```

D3.3 Contralateral PER rostrocaudal axis bar graph code

```
import matplotlib.pyplot as plt

import numpy as np


# Sample data

categories = ['[-1.94, -3.08]', '[-3.16, -4.24]']

means = [0.910984208, 0.089015792]

stds = [0.056339378, 0.056339378]


# Set up the bar chart

x_pos = np.arange(len(categories))

width = 0.8


fig, ax = plt.subplots()

ax.bar(x_pos, means, width, yerr=stds, align='center', alpha=0.5,
ecolor='black', capsize=10)

ax.set_xticks(x_pos)

ax.set_xticklabels(categories)

ax.set_xlabel('Distance from bregma (mm)')

ax.set_ylabel('Proportion of counted cells')

ax.set_title('Counted cells in contralateral PER from retrograde tracer
injections into wS1 L6', fontsize=10)


plt.show()
```

D3.4 Layers bar plot code

```
import matplotlib.pyplot as plt


means = [0, 0.160463455, 0.692889399, 0.146647146]

stds = [0, 0.106283082, 0.074915593, 0.05083099]

labels = ['L1', 'L2/3', 'L5', 'L6']


# Set up the bar chart

fig, ax = plt.subplots()

ax.bar(labels, means, yerr=stds, capsize=5, color=['yellow', 'green',
'blue', 'red'])

ax.set_xlabel('Layers')

ax.set_ylabel('Means')

ax.set_title('Laminar distribution of ipsilateral PER output neurons to wS1
(no ec)')

ax.set_ylim([0, 1.0])


plt.show()
```

D3.5 Dorsoventral distribution stacked bar chart code

```
import matplotlib.pyplot as plt

import numpy as np


# Input data

categories = ['104375', '104379', '66702', '103825', '104376',  '103824']

values1 = [0.520833333, 0.541284404, 0.532786885, 0.617977528, 0.518987342,
0.562913907]

values2 = [0.479166667, 0.458715596, 0.467213115, 0.382022472, 0.481012658,
0.437086093]


# Set up the bar chart

x_pos = np.arange(len(categories))

width = 0.8


fig, ax = plt.subplots()


# Plot the first set of data

ax.bar(x_pos, values1, width, align='center', alpha=0.5, label='A36',
color='red')


# Plot the second set of data on top of the first

ax.bar(x_pos, values2, width, bottom=values1, align='center', alpha=0.5,
label='A35', color='blue')


# Customize the plot

ax.set_xticks(x_pos)

ax.set_xticklabels(categories)

ax.set_ylabel('Proportion of counted cells')

ax.set_title('Dorsoventral distribution of ipsilateral PER output neurons
to wS1', fontsize=10)

ax.set_ylim(0.0, 1.25)

ax.axhline(y=0.5, linestyle='--', color='black') # add a horisontal dotted
line at y=0.5

ax.legend()


plt.show()
```

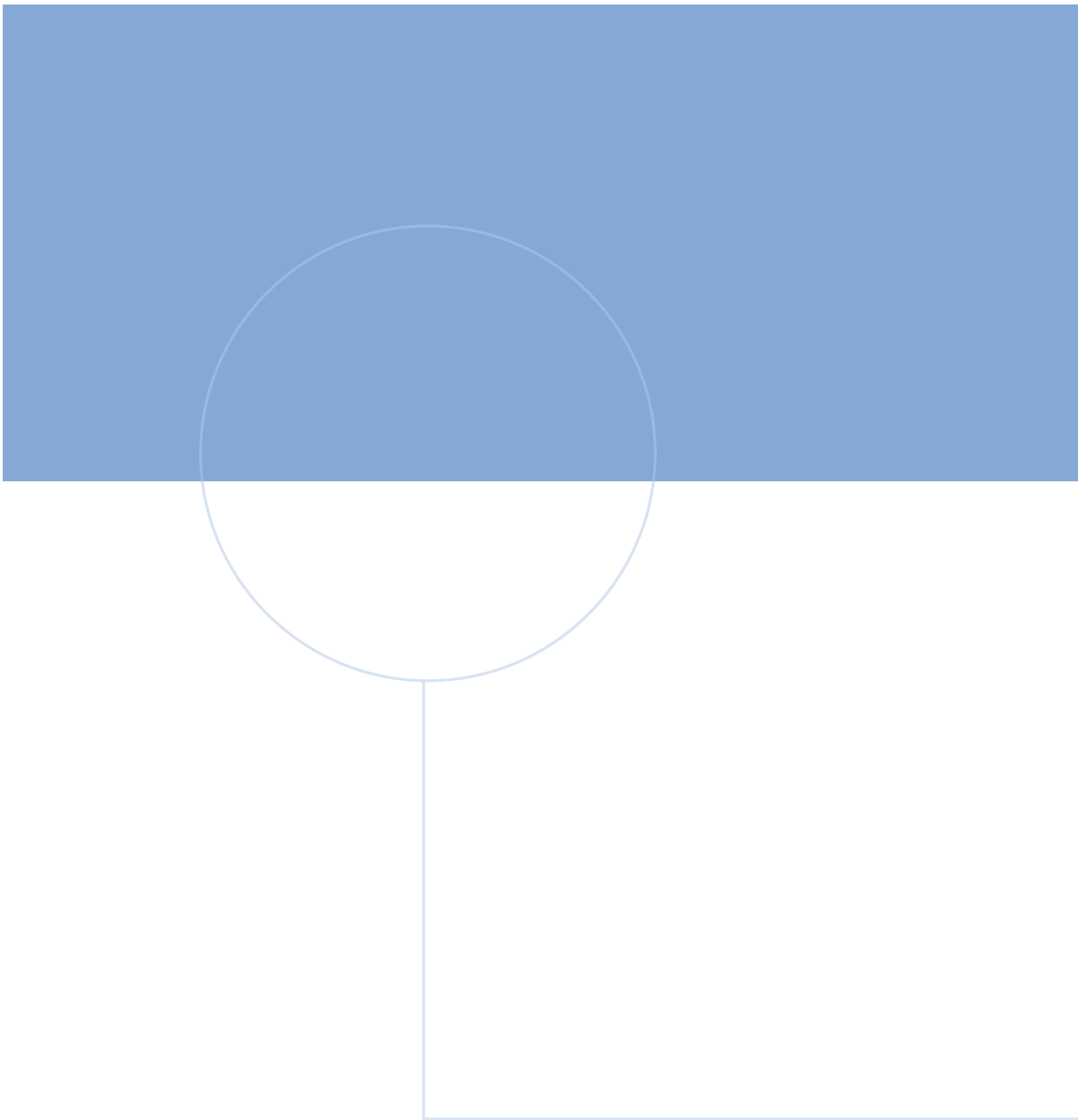

NTNU

Norwegian University of
Science and Technology